Gas sensing with field-effect transistors

Andringa, Anne-Marije

Gas sensing with field-effect transistors

Anne-Marije Andringa

Gas sensing with field-effect transistors

Anne-Marije Andringa
PhD thesis
University of Groningen, The Netherlands

Watch the movie of the sensor demonstrator on
www.youtu.be/YAQ5vCIKP1E

Zernike Institute PhD thesis series 2013-03
ISSN: 1570-1530
ISBN: 978-90-367-6014-0 (Printed version)
978-90-367-6015-7 (Electronic version)

Printed by Gildeprint Drukkerijen, Enschede
Cover design by OZIEZO vormgeving, Groningen

Netherlands Organisation for Scientific Research

Organic Nanomaterials for Electronics and Photonics

This PhD project was carried out in the group Molecular Electronics - Physics of Organic Semiconductors at the Zernike Institute for Advanced Materials according to the requirements of the Graduate School of Science (Faculty of Mathematics and Natural Sciences, University of Groningen) and in the group Photonic Materials and Devices at Philips Research, Eindhoven. The research was financially supported by the Netherlands Organisation for Scientific Research (NWO, Vidi Grant).

university of groningen / faculty of mathematics and natural sciences / zernike institute for advanced materials

RIJKSUNIVERSITEIT GRONINGEN

Gas sensing with field-effect transistors

Proefschrift

ter verkrijging van het doctoraat in de
Wiskunde en Natuurwetenschappen
aan de Rijksuniversiteit Groningen
op gezag van de
Rector Magnificus, dr. E. Sterken,
in het openbaar te verdedigen op
vrijdag 8 februari 2013
om 16.15 uur

door

Anne-Marije Andringa

geboren op 30 juli 1984
te Boornsterhem

Promotor:	Prof. dr. D.M. de Leeuw
Beoordelingscommissie:	Prof. dr. H.L. Gomes
	Prof. dr. E.P.A.M. Bakkers
	Prof. dr. ir. P.W.M. Blom

Contents

Chapter 1

Gas sensing with field-effect transistors

A general introduction into the use of field-effect transistors as gas sensors is presented. First, the need for NO_x sensors is highlighted, followed by an overview of existing sensors. The working principle of a transistor is introduced and the benefits of the transistor as gas sensor are explored. At the end of this chapter, the scope of this thesis is presented.

1.1 Introduction

Development of miniaturized, low-cost electronic sensor techniques is important to make gas sensors generally available for a broad range of applications. Especially for in- and outdoor air quality monitoring, medical diagnostics and food quality control, the demand for small and low-cost gas sensors is high. Carbon dioxide sensors can, for example, be used in air-conditioned buildings or vehicles interiors. Oxygen sensors can be used to optimize the combustion in engines and power plants, and methane sensors can be used to detect gas leaks. Sensors in intelligent food packaging can identify if the meat or fish is still fresh. Furthermore, several diseases can be detected by analyzing trace gases in exhaled breath. The use of electronic sensors in these applications has the advantage that the signal can easily be read and recorded via low-end supporting electronics.

The electronic sensor that is studied in this thesis is based on a field-effect transistor (FET), a three terminal device that acts as a micro-electronic switch. An interesting application area for field-effect transistor based sensors is the detection of nitrogen oxides, NO_x. Nitrogen oxides are released during the combustion of fossil fuels and play a major role in the formation of ozone, acid rain and smog. Nitrogen dioxide, NO_2, is used as the indicator for the larger group of NO_x and is the component of greatest concern. Inhalation of NO_2 has been linked to adverse respiratory effects such as airway inflammations. Real-time monitoring of NO_2 is therefore of utmost importance for public health and environmental safety. In this thesis, the operational mechanism of NO_x detection with field-effect transistors is investigated and the obtained insights are used to develop a sensitive real-time NO_2 sensor.

This chapter serves as a general introduction into gas sensing with field-effect transistors. First the impact of NO_x emission on public health and the environment is discussed. Then an overview of the existing NO_x sensors used to monitor and control the NO_x emission is presented. For very sensitive detection of NO_x, field-effect transistors have been investigated. The operation principle of a transistor is introduced and the benefits of the transistor as gas sensor are explored. The outline of this thesis will be presented at the end of this chapter.

1.2 Nitrogen oxides

Nitrogen oxides, NO_x, are dangerous air pollutants.[1,2] This group contains highly reactive gases such as nitric oxide (NO) and nitrogen dioxide (NO_2). Nitrogen oxides play an important role in the chemistry of the atmosphere. Under the influence of sunlight, NO_2 breaks down in NO and an oxygen radical. The oxygen radical reacts further with oxygen

to create ozone, which is a major cause for smog. The created NO reacts with oxygen, ozone or oxidized organic species and NO_2 is formed again. In this reaction cycle, the sum of the NO and NO_2 concentrations remains nearly constant. Furthermore, NO_x gases react in heat and sunlight with ammonia, moisture, hydrocarbons and other compounds to form tiny particles or acid rain.

Nitrogen oxides are released during the combustion of fossil fuels. In 2009, the most significant sources of NO_x emissions in Europe were the 'Road transport' sector (38 %), the 'Energy production and distribution' sector (22 %), the 'Commercial, institutional and households' sector (15 %) and the 'Energy use in industry' sector (13 %), as presented in the chart in Figure 1.1.[3]

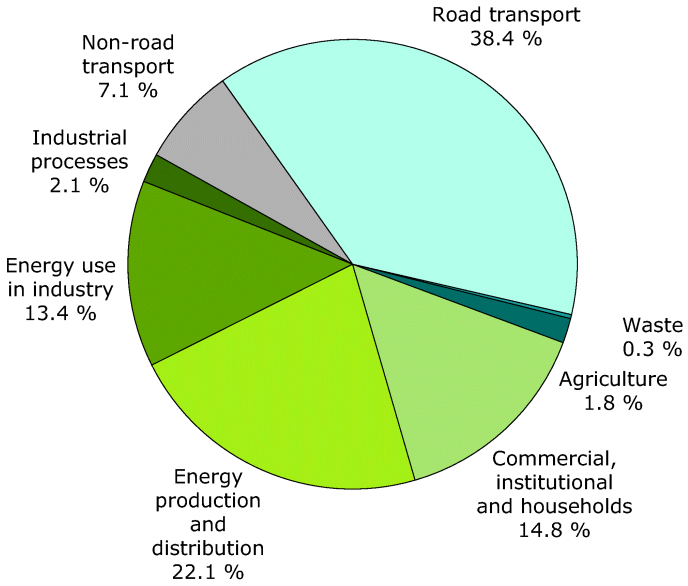

Figure 1.1: The contribution made by different sectors to emissions of nitrogen oxides in 2009 in Europe. Data obtained from the European Environment Agency (EEA).[3]

The huge amounts of NO_x released into the atmosphere everyday can cause fatal problems not only to human beings but also to animals and plants, both aquatic and terrestrial.[1] Inhalation of NO_x has been linked to adverse respiratory effects like airway inflammation in healthy people and to increased respiratory symptoms in people with asthma. For air quality monitoring, NO_2 is the most interesting compound as it can be used as the indicator for the larger group of nitrogen oxides. The U.S. Environmental Protection Agency has set the air-quality standard at a level of 53 ppb NO_2.

Another interesting application is the detection of nitric oxide for medical diagnostics. Detection of nitric oxide in exhaled breath can be used to identify an infection of lung

tissue.[4,5] The NO level in exhaled breath increases three to fivefold a few days before an asthma attack. When patients with asthma could monitor their NO level at home with a hand-held device, they could preventively take medicines.

1.3 Existing sensors

The huge impact of NO_x emission on public health and the environment has led to extensive scientific and technological progress in the field of NO_x sensors. For real-time monitoring and controlling air quality, sensitive, calibrated and reliable NO_2 sensors have been developed. There are a variety of monitoring methods commercially available, such as chemiluminescent, electrochemical, resistive and optical sensors.

In the detection method based on chemiluminescence, the light resulting from a chemical reaction is detected. The chemiluminescent sampler for the measurement of NO_2 relies on the reaction of NO with O_3 to produce an excited form of NO_2. As the excited molecule returns to its ground state, fluorescent radiation is emitted. The intensity of the light is proportional to the concentration of NO. A sensor based on this method is sold by Eco Physics and depicted in Figure 1.2a.[6]

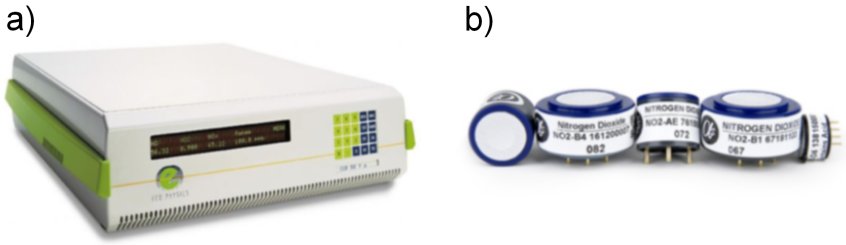

Figure 1.2: Commercially available NO_2 sensors. a) NO analyser Eco Physics based on chemiluminescence.[6] b) Electrochemical sensors Alphasense.[7]

A variety of portable samplers are available that are based on the use of electrochemical cells.[8] The operation principle depends on the electrochemical reduction of NO_2 between two electrodes immersed in an electrolyte reservoir. NO_2 present in the sample air passes through a capillary diffusion barrier into the reaction cell, where it is reduced at the electrode. The migration of electrons produced by the reaction results in a net current flow, which is proportional to the NO_2 concentration. Electrochemical NO_2 sensors are for example available from Alphasense (see Figure 1.2b) and Dräger. An electrochemical sensor is used as well for NO analysis in exhaled breath. In 2005, a hand-held device was developed by Aerocrine, the NIOX MINO, which is able to determine the NO concentration in exhaled breath accurately.[9]

The most common NO_2 sensors, however, are chemiresistors based on semiconducting metal oxides such as tin oxide, SnO_2, tungsten oxide, WO_3, or zinc oxide, ZnO.[10–12] Porous oxide layers with high specific surface area's are used. The gas diffuses into the oxide and modulates the grain boundary resistances by transfer of charge carriers from the semiconductor to the adsorbed surface species. Nowadays, many companies offer metal-oxide based gas sensors, like AppliedSensors and Synkera Technologies Inc.

1.4 Field-effect transistors

Because of the need for sensitive NO_2 sensors for air-quality monitoring, new strategies from material synthesis to new device technologies are being pursued. One of the approaches is the application of field-effect transistors as NO_2 sensors. The field-effect transistor is the basic building block for solid-state electronics. A FET acts as a micro-electronic switch. Here a brief introduction is given. For more information on (organic) field-effect transistors, the reader is encouraged to read several review articles.[13–15]

The basic lay-out of a field-effect transistor is presented in the inset of Figure 1.3. A semiconductor layer is contacted by two electrodes, the source and the drain. The third electrode, the gate, is electrically insulated from the semiconductor layer via an insulating oxide layer, creating a parallel plate capacitor with a capacitance per unit area, C_{ox}. By applying a gate bias, V_G, with respect to the source electrode, charge carriers can electrostatically be accumulated or depleted in the semiconductor at the semiconductor-insulator interface. Due to this field-effect the charge carrier density in the semiconductor can be varied. Therefore, the resistivity of the semiconductor, and hence the current through the semiconductor (upon application of a source-drain field), can be varied over orders of magnitude.

The semiconductor may consist of metal oxides,[16] carbon nanotubes,[17] small molecules,[18] or polymers[13] among other materials. Figure 1.3 shows a typical transfer curve of an *n*-type ZnO transistor, where the drain current is measured as a function of gate bias at a constant drain bias. At positive gate bias electrons are accumulated in the channel. Upon applying a source-drain bias, current flows. At negative gate bias all electrons in the *n*-type semiconductor are depleted. Holes cannot be injected and, furthermore, are immobile in an *n*-type semiconductor. Hence, as schematically depicted in the inset of Figure 1.3, in depletion no current flows. For a *p*-type semiconductor, the majority carriers are holes. The transfer curve is then mirrored. In Figure 1.3 the current starts to flow around zero gate bias. This onset is called the pinch-off voltage. The gate bias at which an accumulation channel starts to form is called the threshold voltage, V_{th}. The threshold voltage is determined by linearly plotting the source-drain current as a

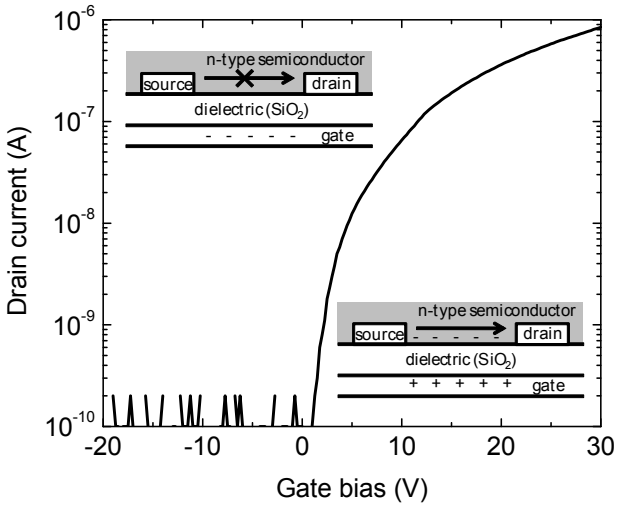

Figure 1.3: Typical transfer curve of an *n*-type field-effect transistor measured with a drain bias of 2 V. In the insets, schematic presentations of transistors in the off- and on-state are shown. At a negative gate bias the semiconductor is depleted and the transistor is off. At a positive bias electrons are accumulated in the semiconductor at the semiconductor-SiO_2 interface and current flows.

function of the gate bias and taking the intercept of the extrapolated transfer curve with the voltage axis. A threshold voltage shift is assumed to be due to trapped charges with surface density N_{tr}. The threshold voltage shift, ΔV_{th}, is then given by $\Delta V_{th} = eN_{tr}/C_{ox}$, where e is the elementary charge. Another transistor characteristic is the on-off ratio: the ratio of the current in the on-state and the current in the off-state.

The transistor is measured in the linear regime, where the drain bias, V_D, is much smaller than the gate bias, V_G. When the drain bias is equal to or larger than the bias on the gate, the transistor is driven in saturation. In both regimes, an expression can be derived for the absolute value of the current analogous to classical inorganic MOS modeling.[19] This expression does not take the gate voltage dependent mobility and contact resistance into account. In the linear regime ($|V_D| \ll |V_G - V_{th}|$) the source-drain current, I_D, can be approximately described by:

$$I_D^{lin} = -\mu_{lin}\frac{C_{ox}W}{L}(V_G - V_{th})V_D \tag{1.1}$$

in which W and L are the width and length of the transistor, and μ_{lin} the mobility of the charge carriers in the linear regime. The mobility of the charge carriers can be extracted from the current-voltage characteristics. The usual way to deduce the mobility is to take

the first derivative of the source-drain current to the gate bias, divide by the drain bias and correct for the geometrical parameters of the transistor:

$$\mu_{\text{lin}} = \frac{L}{V_{\text{D}} C_{\text{ox}} W} \frac{\partial I_{\text{D}}}{\partial V_{\text{G}}} \tag{1.2}$$

The source-drain current in the saturation regime, when $|V_{\text{D}}| \geq |V_{\text{G}} - V_{\text{th}}|$, equals:

$$I_{\text{D}}^{\text{sat}} = -\mu_{\text{sat}} \frac{C_{\text{ox}} W}{2L} (V_{\text{G}} - V_{\text{th}})^2 \tag{1.3}$$

The saturated mobility can then be obtained by taking the second derivative of the source-drain current to the gate bias and correct for the geometrical parameters of the transistor:

$$\mu_{\text{sat}} = -\frac{L}{C_{\text{ox}} W} \left(\frac{\partial I_{\text{D}}}{\partial V_{\text{G}}} \right)^2 \tag{1.4}$$

1.5 Field-effect transistors as gas sensors

The electrical characteristics of a transistor change upon exposure to a wide range of gases. The changes can be monitored using multiple transistor parameters, such as the bulk conductivity, the mobility and the threshold voltage.[20,21] In literature, several options for the underlying mechanisms have been suggested. The electrical response may be caused by bulk resistive changes arising from doping effects, local dipole screening effects, partial charge transfer between the materials or analyte-induced charge trapping. In general, a larger current change is observed upon exposure to higher analyte concentrations. An advantage of a transistor over a resistor is the amplified sensor response due to current modulation by the gate electrode. Furthermore, the control of charge carrier density in the semiconductor by the gate electrode can be exploited. Analyte-induced charge trapping can be fastened when a high charge carrier density is induced.

Field-effect transistors have attracted attention as gas sensors for a wide range of gases. Already in 1975, a hydrogen sensor based on a Pd-gated MOSFET was demonstrated.[22] This sensor exhibited a threshold voltage shift depending upon the gas concentration and was particularly sensitive to hydrogen down to the ppm level with maximum threshold voltage shift of about 0.5 V. In recent years, a wide variety of semiconductors has been used in transistors for gas sensing, such as carbon nanotubes,[23] organic[20,24–29] and oxidic[30] semiconductors.

For NO_2 detection, a range of sensing layers has been used, such as amorphous organic semiconductors,[31,32] porous silicon,[33] metal oxides,[34] carbon nanotubes[35–43] and

silicon[44] and metal oxide nanowires.[45] In all cases changes in current upon NO_2 exposure have been demonstrated; *i.e.* a current decrease for *n*-type semiconductors and a current increase for *p*-type semiconductors. The current change is in agreement with a threshold voltage shift towards positive gate biases. In addition, response to 10 ppb NO_2 has been reported.

1.6 Scope of this thesis

This thesis presents a thorough study on NO_x detection with field-effect transistors. The research comprises experimental measurements, modeling of the effect of NO_x on charge transport and characterization of trapped charges. Finally the thesis is complemented with the demonstration of a newly developed real-time NO_2 sensor that operates in ambient air.

In Chapter 2, a detailed overview is presented of the transistor fabrication and the semiconductors and characterization techniques used throughout this thesis. Additionally, the gas detection setups constructed for this research are discussed.

Chapter 3 describes a gas sensor based on a self-assembled monolayer field-effect transistor (SAMFET). A SAMFET based sensor is highly sensitive because the analyte and the active channel are separated by only one monolayer. The sensor is functionalized with porphyrin receptors to detect nitric oxide (NO), a biomarker for airway inflammations such as asthma. Upon exposure to NO, a threshold voltage shift towards positive gate biases is observed. It is argued that the threshold voltage shift is due to trapping of charges.

A change of the threshold voltage is observed as well in organic field-effect transistors with a specific self-assembled monolayer (SAM) on the gate dielectric. The sign of the threshold voltage depends on the chemical nature of the SAM. In Chapter 4, scanning Kelvin probe microscopy in combination with exfoliation of the semiconductor is used to reveal the origin of the threshold voltage shift.

The thesis is continued with the investigation of zinc oxide field-effect transistors as NO_2 sensors. In Chapter 5, a mechanism for NO_2 detection involving charge carrier trapping is proposed. It will be shown that upon application of a positive gate bias during NO_2 exposure, the threshold voltage shifts towards that gate bias. The dynamics of the shift under prolonged gate bias are evaluated at room temperature as a function of the NO_2 concentration and ZnO layer thickness. The sensor response is also investigated using other semiconductors to demonstrate the generic nature of the detection mechanism.

A requisite for a real-time sensor is reversibility. When the gate bias is turned off, the trapped electrons can be thermally released. Chapter 6 presents the dynamics of charge

trapping and recovery as a function of temperature. The extracted activation energy for recovery points to deep traps around 1.2 eV. The presence of trapped charge carriers and the trap depth are verified with thermally stimulated current measurements.

The location of the trapped electrons in NO_2 sensors based on organic field-effect transistors is studied in Chapter 7. Surface potential measurements before and after exfoliation of the semiconductor disclose that the charges are not in the semiconductor but at the gate dielectric.

In Chapter 8, the obtained insights into the detection mechanism are translated to an analytical model that predicts the sensors temporal behavior. Based on this phenomenological model, a sensor protocol will be developed for a functional NO_2 sensor that monitors the partial NO_2 pressure in real time. The model is experimentally verified and used to optimize the sensor protocol.

A functional NO_2 sensor demonstrator based on a ZnO field-effect transistor is presented in Chapter 9. The partial NO_2 pressure in ambient air is monitored in real-time for concentrations as low as 40 ppb. The sensor can be fabricated using standard IC technology, which can easily be miniaturized and used in handheld applications.

References

1. Environmental Protection Agency (EPA), Air Pollution, 2012 http://www.epa.gov/air/nitrogenoxides/ (accessed 18–07–2012).
2. Environmental Science Published for Everyone Round the Earth (ESPERE), http://www.epa.gov/air/nitrogenoxides/ (accessed 18–07–2012).
3. European Environment Agency (EEA), Nitrogen oxides (NOx) emissions (APE 002), http://www.eea.europa.eu/data–and–maps/figures/sector–share–of–nitrogen–oxides–emissions–eea–member–countries–2 (accessed 23–08–2012).
4. J. L. Puckett, S. C. George, *Respir. Physiol. Neurobiol.* **2008**, *163*, 166.
5. C. A. Bates, P. E. Silkoff, *J. Allergy Clin. Immunol.* **2003**, *111*, 256.
6. Eco Physics, www.ecophysics.com (accessed 14–11–2012).
7. Alphasense, www.alphasense.com/industrial–sensors/index.html (accessed 14–11–2012).
8. F. Opekar, K. Stulik, *Crit. Rev. Anal. Chem.* **2002**, *32*, 253.
9. NIOX Personalized asthma management, http://www.niox.com/en/ (accessed 14–11–2012).
10. N. Barsan, D. Koziej, U. Weimar, *Sens. Actuators B* **2007**, *121*, 18.
11. N. Barsan, U. Weimar, *J. Electroceram.* **2001**, *7*, 143.
12. T. Inoue, K. Ohtsuka, Y. Yoshida, Y. Matsuura, Y. Kajiyama, *Sens. Actuators B* **1995**, *25*, 388.
13. A. R. Brown, C. P. Jarrett, D. M. de Leeuw, M. Matters, *Synthetic Met.* **1997**, *88*, 37.
14. D. Braga, G. Horowitz, *Adv. Mater.* **2009**, *21*, 1473.
15. R. A. Street, *Adv. Mater.* **2009**, *21*, 2007.

16. E. Fortunato, P. Barquinha, R. Martins, *Adv. Mater.* **2012**, *24*, 2945.
17. M. Anantram, F. Leonard, *Rep. Prog. Phys.* **2006**, *69*, 507.
18. B. Lucas, T. Trigaud, C. Videlot-Ackermann, *Polym. Int.* **2012**, *61*, 374.
19. S. M. Sze, *Physics of Semiconductor Devices*, Wiley-Interscience, New York, **1981**.
20. L. Torsi, A. Dodabalapur, L. Sabbatini, P. G. Zambonin, *Sens. Actuators B* **2000**, *67*, 312.
21. L. Torsi, A. Dodabalapur, *Anal. Chem.* **2005**, *77*, 380A.
22. K. I. Lundstrom, M. S. Shivaraman, C. M. Svensson, *J. Appl. Phys.* **1975**, *46*, 3876.
23. A. Goldoni, L. Petaccia, S. Lizzit, R. Larciprete, *J. Phys. Condens. Mat.* **2010**, *22*, 8.
24. M. Bouvet, *Anal. Bioanal. Chem.* **2006**, *384*, 366.
25. B. Li, D. N. Lambeth, *Nano Lett.* **2008**, *8*, 3563.
26. K. C. See, A. Becknell, J. Miragliotta, H. E. Katz, *Adv. Mater.* **2007**, *19*, 3322.
27. J. Huang, J. Miragliotta, A. Becknell, H. E. Katz, *J. Am. Chem. Soc.* **2007**, *129*, 9366.
28. H. E. Katz, *Electroanalysis* **2004**, *16*, 1837.
29. J. T. Mabeck, G. G. Malliaras, *Anal. Bioanal. Chem.* **2006**, *384*, 343.
30. S. Dutta, A. Dodabalapur, *Sens. Actuators B* **2009**, *143*, 50.
31. A. Das, R. Dost, T. Richardson, M. Grell, J. J. Morrison, M. L. Turner, *Adv. Mater.* **2007**, *19*, 4018.
32. F. Marinelli, A. Dell'Aquila, L. Torsi, J. Tey, G. P. Suranna, P. Mastrorilli, G. Romanazzi, C. F. Nobile, S. G. Mhaisalkar, N. Cioffi, F. Palmisano, *Sens. Actuators B* **2009**, *140*, 445.
33. G. Barillaro, A. Diligenti, A. Nannini, L. M. Strambini, E. Comini, G. Sberveglieri, *IEEE Sens. J.* **2006**, *6*, 19.
34. A. Afzal, N. Cioffi, L. Sabbatini, L. Torsi, *Sens. Actuators B* **2012**, *171-172*, 25.
35. J. Kong, N. R. Franklin, C. W. Zhou, M. G. Chapline, S. Peng, K. J. Cho, H. J. Dai, *Science* **2000**, *287*, 622.
36. M. Mattmann, T. Helbling, L. Durrer, C. Roman, C. Hierold, R. Pohle, M. Fleischer, *Appl. Phys. Lett.* **2009**, *94*, 183502.
37. T. Helbling, R. Pohle, L. Durrer, C. Stampfer, C. Roman, A. Jungen, A. Fleischer, C. Hierold, *Sens. Actuators B* **2008**, *132*, 491.
38. S. Peng, K. J. Cho, P. F. Qi, H. J. Dai, *Chem. Phys. Lett.* **2004**, *387*, 271.
39. T. Helbling, C. Hierold, L. Durrer, C. Roman, R. Pohle, M. Fleischer, *Phys. Status Solidi B* **2008**, *245*, 2326.
40. O. Kuzmych, B. L. Allen, A. Star, *Nanotechnology* **2007**, *18*, 7.
41. J. Li, Y. J. Lu, Q. Ye, M. Cinke, J. Han, M. Meyyappan, *Nano Lett.* **2003**, *3*, 929.
42. P. Qi, O. Vermesh, M. Grecu, A. Javey, Q. Wang, H. Dai, S. Peng, K. J. Cho, *Nano Lett.* **2003**, *3*, 347.
43. J. Zhang, A. Boyd, A. Tselev, M. Paranjape, P. Barbara, *Appl. Phys. Lett.* **2006**, *88*, 3.
44. M. C. McAlpine, H. Ahmad, D. W. Wang, J. R. Heath, *Nat. Mater.* **2007**, *6*, 379.
45. D. H. Zhang, Z. Q. Liu, C. Li, T. Tang, X. L. Liu, S. Han, B. Lei, C. W. Zhou, *Nano Lett.* **2004**, *4*, 1919.

Chapter 2

Materials & methods

The performance of a field-effect transistor highly depends on the choice of semiconductor. The processing technology to apply the semiconductor and the fabrication of the transistor substrate also influence the device characteristics. In this chapter, the materials and processing methods used to prepare the transistors that are studied in this thesis will be described, as well as the main characterization methods. Furthermore, the gas detection setups constructed for this research will be discussed.

2.1 Transistor substrate fabrication

This thesis presents a study on gas sensing with field-effect transistors. The transistors were manufactured using pre-fabricated test substrates. The substrates contain a gate dielectric and source and drain contacts, the substrate itself acts as the gate electrode. Standard IC process standardization guarantees reproducible transistor substrates.

The substrates were fabricated on 150-mm silicon wafers acquired from Siltronic AG. The wafers are 675 μm thick and heavily *n*-type doped with arsenic implantation. The SiO_2 gate dielectric of typically 200 nm thick was formed by wet oxidation in an H_2O vapor at 1000 °C. The gate capacitance depends on the thickness of the dielectric and its dielectric constant, which is 3.9 for SiO_2. Gold source and drain electrodes with a thickness of 30 nm were sputtered and patterned using conventional photolithography. A 2 nm titanium layer was used as an adhesion layer for the gold on SiO_2. The wafer was diced by sawing to about two third of the wafer thickness. To prevent silicon particles on the wafer, a protective layer of photoresist was applied. Acetone and subsequently fuming HNO_3 were used to remove the photoresist and to clean the wafer. The SiO_2 surface was passivated by applying the primer hexamethyldisilazane (HMDS) from the gas phase. This passivation reduces the amount of traps, ensuring a higher mobility and an increased stability under gate bias stress.[1] A photograph of a 150-mm wafer containing multiple test substrates together with a detailed photograph of a single substrate is depicted in Figure 2.1.

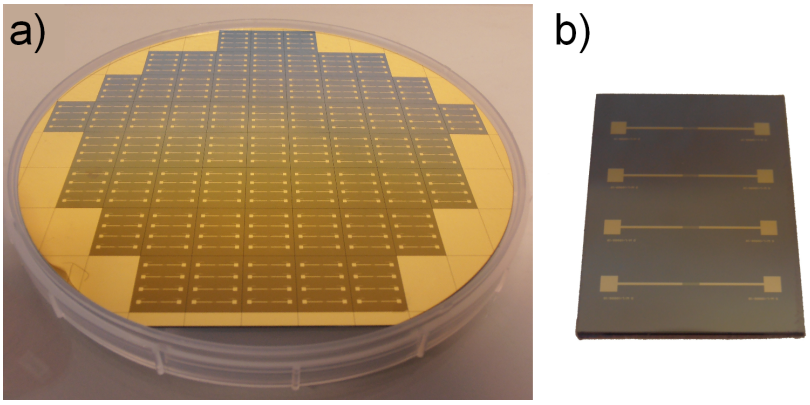

Figure 2.1: a) Photograph of a 150-mm monitor wafer containing multiple test substrates. b) Photograph of a single test substrate of 1.3 x 1.7 cm, containing four interdigitated gold transistor structures, with a channel length and width of 10 and 10,000 μm, respectively.

2.2 Semiconductor properties and processing

In this thesis, a selection of carbon based organic semiconductors and the oxidic semiconductor zinc oxide (ZnO) are used. The electrical properties and material processing will be discussed here.

Organic semiconductors

Organic materials such as polymers (*plastics*) or small molecules are usually electrical insulators. In conventional electronics, plastics are therefore applied to prevent short circuits between electrical components or wires. Plastics consist of high molecular mass chains of repeating monomer units. They are widely used for inexpensive and disposable products due to their ease of manufacturing, low cost and versatility.

A special class of organic materials is not insulating but exhibits semiconducting properties. The conductivity originates from conjugation, *i.e.* the presence of alternating single and double bonds. Three out of four electrons in the outer shell of the carbon atom are located in sp^2 hybridized orbitals, that form the σ bonds in the polymer backbone. The fourth electron in a conjugated system is delocalized on the connected p_z orbitals. The interaction between neighboring p_z orbitals is either bonding or antibonding. The bonding π orbital is of lower energy and is called the HOMO (highest occupied molecular orbital) and the anti-bonding π orbital is called the LUMO (lowest unoccupied molecular orbital). The HOMO and LUMO levels can be compared to the valence and conduction bands of inorganic semiconductors. Additional electrons added to the system occupy states in the LUMO, leading to *n*-type transport. Electron vacancies in the HOMO, also called holes, lead to *p*-type transport.

The charge transport in organic semiconductors is different than in inorganic semiconductors. The transport is affected by structural disorder, which limits the conjugation length and broadens the energy levels. Due to the presence of disordered localized states, the charge carrier transport occurs via a hopping process. A measure for the speed of the charge carriers through the semiconductor is the mobility. The mobility is not just a material parameter but also a device parameter. The exact value is influenced by for example the gate bias (charge density), trap states on the gate dielectric, chemical impurities, and the device geometry.[2]

Semiconducting polymers benefit from the same processing advantages as regular polymers. Many polymers and small molecules are soluble in organic solvents. Therefore, established process techniques like spin coating or inkjet printing can be applied. The ability to process on large areas at low temperatures makes organic semiconductors suit-

able as active materials in optoelectronic applications such as displays, LEDs and flexible solar cells. Additionally, the solubility allows for self-assembly of organic molecules.[3]

The chemical structures of the organic semiconductors used in this thesis are depicted in Figure 2.2. The corresponding HOMO and LUMO levels are presented in Table 2.1. In Chapter 3, a monolayer thick semiconductor layer is applied by self-assembly. The monolayer consists of T5-silane molecules with a *p*-type semiconducting quinquethiophene core and an aliphatic spacer that is attached to the gate dielectric with a monofunctional anchoring group.[4] Transistor substrates with HF activated SiO_2 were left for two days in a solution of chloro[11-(5''''-ethyl-5,2':5',2'':5'',2''':5''',2''''-quinquethien-5-yl)undecyl] dimethylsilane in dry toluene. A nucleophilic substitution reaction with the silanol surface groups attaches the molecules to the SiO_2 interface. The SAM forms a close-packed 2D nano-crystal on the SiO_2 interface, facilitated by the π-π stacking of the conjugated T5-groups. The resulting self-assembled monolayer field-effect transistor (SAMFET) had a mobility of about 0.01 cm^2/Vs and a current modulation of 6 decades.

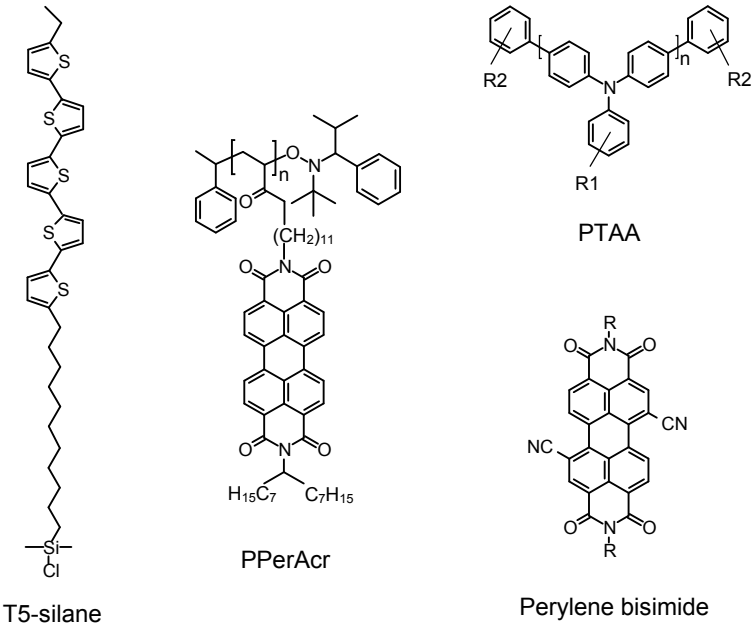

Figure 2.2: Chemical structures of the organic semiconductors used in this thesis.

A second unipolar *p*-type semiconducting polymer, polytriarylamine (PTAA), was applied by spincoating. PTAA is a well-established air-stable semiconductor that exhibits charge carrier mobilities of 10^{-3} - 10^{-2} cm^2/Vs. PTAA was obtained from Merck-UK (batch no. S1124) and is commercially available under the brand name Lisicon®.[5]

As *n*-type semiconductors, the small molecule N,N-dialkylsubstituted-(1,7&1,6)-dicyanoperylene-3,4:9,10-bis(dicarboximide) derivative (Perylene bisimide, Polyera Activ-Ink™ N1400)[6] and the polymer poly(perylene bisimide acrylate) (PPerAcr, Mw 30,900 g/mol, PDI 1.86)[7] were applied by spincoating. ActivInk™ N1400 is an air-stable semiconductor with charge carrier mobilities of 0.01-0.4 cm^2/Vs, while the mobility of PPerAcr is approximately 4 x 10^{-4} cm^2/Vs.

Table 2.1: HOMO and LUMO levels of the semiconductors used in this thesis.

	HOMO (eV)	LUMO (eV)
T5-silane[8]	5.0	∼2.4
PTAA[9]	5.2	-
ActivInk N1400[6]	6.4	4.3
PPerAcr[7,10]	6.0	3.7-3.9
ZnO[11]	7.6	4.3

Zinc oxide

ZnO is an attractive material for applications in electronics, photonics and sensing. ZnO is non toxic, has a high electron mobility and a high optical transparency. Zinc oxide is a II-VI material with a wide bandgap of ∼3.3 eV. Oxygen vacancies in the hexagonal crystal structure act as an *n*-type donor. ZnO layers can be grown with a diverse range of techniques including sputtering, pulsed-laser deposition, metal-organic chemical vapor deposition, as well as solution processing methods such as dip coating, spin coating, and spray pyrolysis.

Here the ZnO layers were applied using spray pyrolysis at a substrate temperature of 400 °C in ambient atmosphere. The prefabricated substrates were placed on a hotplate and an aerosol of a solution of zinc acetate dihydrate [$Zn(CH_3COO)_2{\cdot}2H_2O$] (0.1 M, Sigma Aldrich) in methanol was sprayed onto them using a conventional airbrush, as reported by, for example, Bashir *et al.*[12] The growth of ZnO from zinc acetate and is based on the reaction:[13]

$$Zn(CH_3COO)_2\ (ads) + H_2O\ (g) \longrightarrow ZnO\ (s) + 2\ CH_3COOH\ (g)$$

The growth rate was approximately 0.5 nm per second. The spray pyrolysis setup is shown in Figure 2.3.

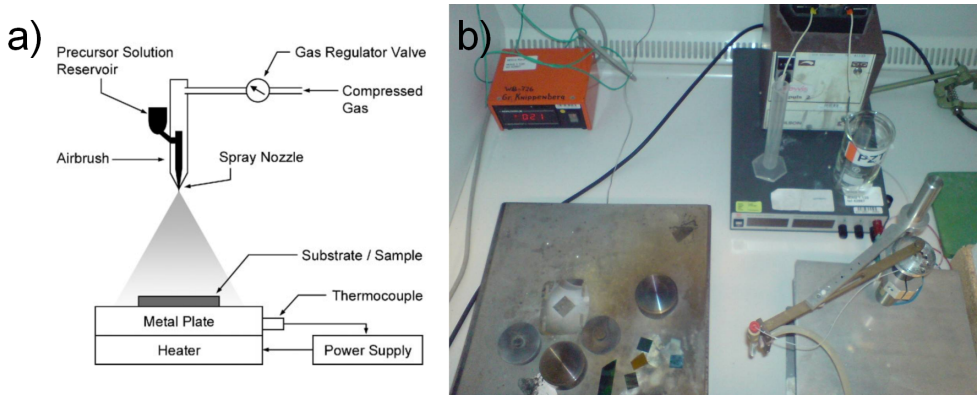

Figure 2.3: a) Schematical drawing of the spray pyrolysis setup.[12] b) Experimental spray pyrolysis setup used for deposition of ZnO.

This simple deposition technique yielded high-performance *n*-channel transistors with negligible hysteresis and a field-effect mobility of 0.1-2 cm^2/Vs. The current modulation exceeded 6 orders of magnitude and the threshold voltage was 0 V. The layer thickness was modified by varying the spray time and measured with X-ray fluorescence (XRF). The film thickness was typically only 10 nm to ensure permeability for NO_2. The ZnO layer was further characterized using X-ray diffraction (XRD) and atomic force microscopy (AFM). A SEM image is shown in Figure 2.4. The mirror-like ZnO films exhibited a microcrystalline morphology with a surface rms roughness of 1 nm. XRD measurements showed that the ZnO films exhibited a (102) textured microstructure.

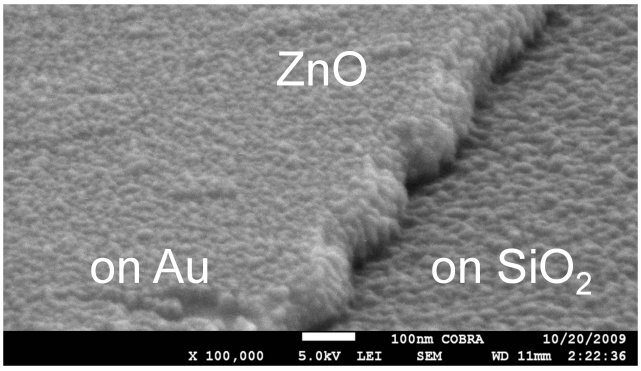

Figure 2.4: SEM image of ZnO layer on top of gold and SiO_2 after 20 seconds spray pyrolysis.

2.3 Transistor characterization

The fabricated transistors were investigated using numerous characterization techniques. Here the main characterization methods are presented.

Electrical characterization

The transistors were electrically characterized by measuring the transfer and output curves with an Agilent 4155B/C semiconductor parameter analyzer. This analyzer was also used for the charge trapping measurements during NO_2 exposure described in Chapter 5 and 7 and the thermally stimulated current measurements in Chapter 6. A Keithley 2602A System Source Meter controlled by in-house developed Labview programs was used for charging and recovery measurements in NO_2 atmosphere (Chapter 6) and the real-time NO_2 sensor demonstrator (Chapter 8 and 9).

Scanning Kelvin probe microscopy (SKPM)

In Chapter 4 and 7, SKPM is performed to visualize trapped charge carriers. SKPM is able to map the local surface potential with a resolution down to approximately 100 nm. SKPM is based on the well-known technique atomic force microscope.[14] AFM collects topological information of a sample surface by scanning it with a mechanical probe. The probe consists of a cantilever with a sharp tip at the end. The tip is brought in close proximity of the sample surface. Due to van der Waals-forces between the tip and the sample the resonance frequency, amplitude and phase of the cantilever are changed. While scanning the surface, a feedback mechanism is used to adjust the tip-to-sample distance to maintain a constant force between the tip and the sample. The displacement needed to keep a constant force provides the topography of the surface.

SKPM[15] is performed in lift mode; the tip is raised approximately 25 nm and the sample is scanned at a constant tip-to-sample distance. An alternating bias with a frequency ω is applied on the tip. The surface potential is obtained by nullifying the frequency component of the electrostatic force, F_ω, on the tip: $F_\omega = \partial C/\partial z[(V_{\text{sample}} - V_{\text{dc}})V_{\text{ac}}\sin(\omega t)]$, in which C is the capacitance between tip and sample, z the distance of the tip to the sample surface and V_{ac} the amplitude of the applied alternating voltage signal. When the electrostatic potential applied to the tip, V_{dc}, is equal to the electrostatic potential on the surface, V_{sample}, the electrostatic force is zero. Therefore, the surface potential between the tip and sample can be deduced directly from the applied potential on the tip, using $V_{\text{dc}} = V_{\text{sample}}$. The potential on the surface can result from a difference in work function between tip and sample, aligned dipoles, charge accumulation or an

applied bias on metals for instance. The combination of charge transport measurements together with the local surface potential profile provides new insights on charge carrier trapping in field-effect transistors.

2.4 Gas detection setups

Several gas detection setups were constructed to investigate the sensor response. A large closed chamber of 20 L was used in Chapter 3 and 5 to detect NO or NO_2. The stainless steel chamber was equipped with feed-throughs for electrical contacts, several gas inlets, a vacuum pump and a manometer. Inside the chamber, the sample was mounted on a hot stage and contacted with probes. Cylinders containing 5 ppm NO and 3 ppm NO_2 in N_2 as a carrier gas and pure N_2 (Praxair) were used. The chamber could also be filled with compressed dry air or ambient air. Photographs of the probe station and the gas cylinders are shown in Figure 2.5.

Figure 2.5: a) Stationary gas detection setup, equipped with feed-throughs for electrical contacts, several gas inlets, a vacuum pump and a manometer. b) Gas cylinders in the safety closet.

The gas response of the field-effect transistors in this static system was tested by admitting small amounts of gas into the closed chamber. The gas pressure was then used to calculate the partial NO or NO_2 concentration at 1 bar. The NO_2 concentration however, dropped with time due to a conversion of NO_2 to NO at the stainless steel surface.[16] Therefore this setup could only be used to perform measurements at high NO_2 concentration, above 0.5 ppm, within half an hour.

Reliable measurements at lower NO_2 concentrations, as described in Chapter 5, 6 and 8, were performed in a flow cell. The front side of the stainless steel chamber was closed with the sample holder flange. The sample holder was mounted on a stick connected

to the flange, placing the transistor in the middle of the flow chamber. The transistor substrate was placed onto a ceramic plateau fitting around a UHV Substrate Heater (HeatWave Labs, Inc.). The temperature of the heater, electrically insulated from the transistor substrate by a thin ceramic sheet, was regulated using a type K thermocouple, a Eurotherm 2416 controller and a Delta power supply. Four transistors were contacted simultaneously with nickel plated steel pins that exactly fitted onto the gold source and drain pads of the test substrate. An air tight electrical connector, power supply connector for the heater and thermocouple opening were embedded in the flange. A photograph of the gas detection flow setup and the sample holder is presented in Figure 2.6.

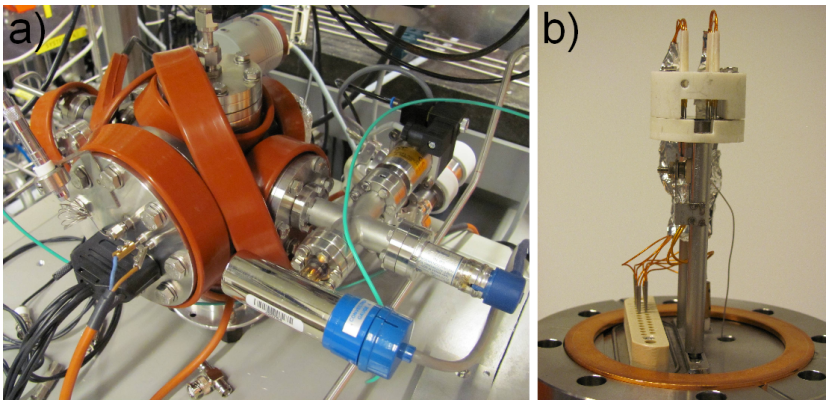

Figure 2.6: a) Photograph of the gas detection flow setup. The cell is closed with the sample holder flange. The system contains gas cylinders, an air inlet and outlet, mass flow controllers and a vacuum pump. b) Photograph of the sample holder flange, consisting of a ceramic table with electrical probes, an electrical connector for contacting, a heater and a thermocouple.

As NO_2 source, a cylinder containing 3 ppm NO_2 in N_2 was used. The concentration was diluted with pure N_2. Two digital mass flow controllers (SEC-Z512X, HORIBA STEC) were used to produce the desired NO_2 concentrations. The diluted gas was flushed through the chamber at a constant total flow rate of 500 sccm. A stabilized concentration was reached after 30 minutes flow. The NO_2 concentration was calibrated inline using an Eco Physics CLD 88p NO sensor based on chemiluminescence. A gas converter (series CG, M&C TechGroup) was used to convert NO_2 catalytically to NO at 330 °C with a carbon molybdenum mixture.

A portable gas detection setup was constructed for the SKPM measurements described in Chapter 7 and the sensor demonstrator described in Chapter 9. The sensor cell of 0.4 L was fabricated from Teflon and equipped with feed-throughs for electrical contacts. Teflon is a suitable material at lower temperatures as it is inert to NO_2.[16] In the SKPM experiment, the NO_2 was supplied from a 3 ppm cylinder. Additional N_2 was

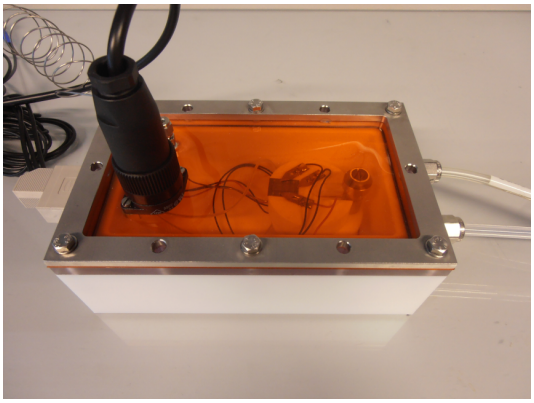

Figure 2.7: Photograph of the Teflon sensor cell in demonstrator mode containing a ZnO field-effect transistor mounted on a heater. The lid of the flow cell was covered with an orange foil filtering UV light.

used to further dilute the mixture. The concentration was regulated using two mass flow controllers. The transistor substrate was placed on a polycarbonate plate with electrical probes, constructed to fit under the SKPM. A Teflon lid was used. The sensor demonstrator was fabricated with a sample heater and a transparent polycarbonate lid, covered with an orange foil filtering UV light. A photograph is presented in Figure 2.7.

References

1. S. G. J. Mathijssen, M. Kemerink, A. Sharma, M. Coelle, P. A. Bobbert, R. A. J. Janssen, D. M. de Leeuw, *Adv. Mater.* **2008**, *20*, 975.
2. T. Richards, H. Sirringhaus, *Appl. Phys. Lett.* **2008**, *92*, 023512.
3. G. M. Whitesides, B. Grzybowski, *Science* **2002**, *295*, 2418.
4. E. C. P. Smits, S. G. J. Mathijssen, P. A. van Hal, S. Setayesh, T. C. T. Geuns, K. Mutsaers, E. Cantatore, H. J. Wondergem, O. Werzer, R. Resel, M. Kemerink, S. Kirchmeyer, A. M. Muzafarov, S. A. Ponomarenko, B. de Boer, P. W. M. Blom, D. M. de Leeuw, *Nature* **2008**, *455*, 956.
5. http://www.merck–performance–materials.com/en/display/lisicon/lisicon.html, (accessed 27–08–2012).
6. http://www.polyera.com/downloads/Product_Info/InfoSheet–N1400.pdf, (accessed 27–08–2012).
7. S. Hüttner, M. Sommer, M. Thelakkat, *Appl. Phys. Lett.* **2008**, *92*, 093302.
8. J. van Haare, *Redox states of pi-conjugated oligomers and polymers*, PhD thesis, Eindhoven University of Technology, **1997**.
9. W. Zhang, J. Smith, R. Hamilton, M. Heeney, J. Kirkpatrick, K. Song, S. E. Watkins, T. Anthopoulos, I. McCulloch, *J. Am. Chem. Soc.* **2009**, *131*, 10814.

10. S. M. Lindner, S. Hüttner, A. Chiche, M. Thelakkat, G. Krausch, *Angew. Chem. Int. Edit.* **2006**, *45*, 3364.

11. G. Adamopoulos, A. Bashir, P. H. Wobkenberg, D. D. C. Bradley, T. D. Anthopoulos, *Appl. Phys. Lett.* **2009**, *95*, 133507.

12. A. Bashir, P. H. Wobkenberg, J. Smith, J. M. Ball, G. Adamopoulos, D. D. C. Bradley, T. D. Anthopoulos, *Adv. Mater.* **2009**, *21*, 2226.

13. M. Tammenmaa, T. Koskinen, L. Hiltunen, L. Niinisto, M. Leskela, *Thin Solid Films* **1985**, *124*, 125.

14. E. Meyer, *Prog. Surf. Sci.* **1992**, *41*, 3.

15. V. Palermo, M. Palma, P. Samori, *Adv. Mater.* **2006**, *18*, 145.

16. A. White, L. Beddows, *J. Appl. Chem. Biotechnol.* **1973**, *23*, 759.

Chapter 3

Gas sensing with self-assembled monolayer field-effect transistors

A new sensitive gas sensor based on a self-assembled monolayer field-effect transistor (SAMFET) was used to detect the biomarker nitric oxide (NO). A SAMFET based sensor is highly sensitive because the analyte and the active channel are separated by only one monolayer. SAMFETs were functionalized for direct NO detection using iron porphyrin as a specific receptor. Upon exposure to NO, a threshold voltage shift towards positive gate biases was observed. The sensor response was examined as a function of NO concentration. High sensitivity has been demonstrated by detection of ppb concentrations of NO.

Published as:
A. Andringa, M. Spijkman, E. C. P. Smits, S. G. J. Mathijssen, P. A. van Hal, S. Setayesh, N. P. Willard, O. V. Borschev, S. A. Ponomarenko, P. W. M. Blom, D. M. de Leeuw, *Organic Electronics*, **2010**, *11*, 895.

3.1 Introduction

Human noses can perceive hundreds of thousands of different odor molecules.[1] The olfactory system consists of an array of receptors, each of which detects a limited number of substances. This complex system warns us about dangers such as fire, air pollutants or spoiled food. In the past decades electronic noses have been developed that mimic the human olfactory system.[2] An electronic nose comprises a gas sampling unit and an array of chemical sensors. Various transducers can be used like carbon black or conducting polymer based chemiresistors, metal oxide semiconductor field-effect transistors, and surface or bulk acoustic wave resonators.[3] The sensors themselves are not selective; a fingerprint of the smell is obtained and a neural network is incorporated for pattern recognition.

An emerging application is the detection of the biomarker nitric oxide (NO). NO plays an important role in biological functions by acting as a neurotransmitter and by regulating the relaxation of blood vessels.[4] Furthermore NO is a marker for airway inflammations such as asthma.[5] Measurement of the NO concentration in exhaled breath is applied to diagnose and monitor the inflammation and the obtained information is used as a tool to manage the asthma treatment. NO detection is based on electrochemical, optical or electrical techniques.[6,7] Typically, NO is detected indirectly since NO is first converted into NO_2 by *e.g.* CrO_3 or ozone.[8] Although NO sensors are commercially available,[9] there is a demand for small, sensitive NO transducers for point of care use.[10,11]

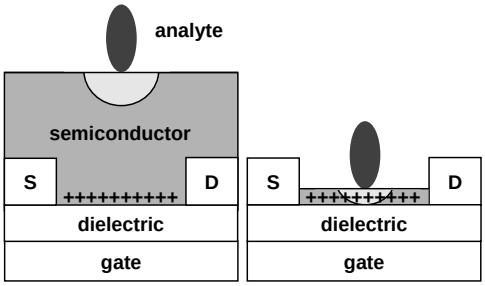

Figure 3.1: Schematic representation of the operation principle of a SAMFET sensor. In the transistor, a conducting channel is formed at the semiconductor gate dielectric interface. On the left side, analyte molecules are absorbed on top of a thick semiconductor layer. The current modulation is limited by the thickness of the semiconductor. The electrostatic interactions are stronger when the distance between the analyte and the channel is decreased. Hence a monolayer thick semiconductor (right) yields the ultimate sensing performance.

Here, a new sensitive gas sensor based on self-assembled monolayer field-effect transistors (SAMFET) is introduced. The proof-of-principle is demonstrated by direct detec-

tion of NO. The operation principle is elucidated in Figure 3.1. The left side shows a standard organic field-effect transistor. Upon applying a bias to the gate, charge carriers are accumulated at the gate dielectric-semiconductor interface. A conducting channel is formed with a thickness of approximately 1 - 2 nm.[12] Analyte molecules absorbed on top of the semiconductor can modulate the charge transport in the channel by electrostatic interactions. However, it has been demonstrated by Huang *et al.*[13] that the sensitivity of such a sensor is dependent on the thickness of the active layer. The response of organic transistors to nerve agent simulants increased dramatically with decreasing layer thickness, due to the strong distance dependence of the electrostatic interactions. Torsi *et al.*[14] have reported chiral sensors and argue that the sensing is restricted to the conducting channel. Then the sensitivity did not increase with decreasing layer thickness, but this could be due to the granular nature of the semiconducting films. Finally, sensitivity enhancement of up to an order of magnitude has been reported in transistors by using ultra thin semiconducting films.[15] Hence a semiconductor of only one monolayer thickness should yield the most sensitive gas sensor, as shown in Figure 3.1 on the right.

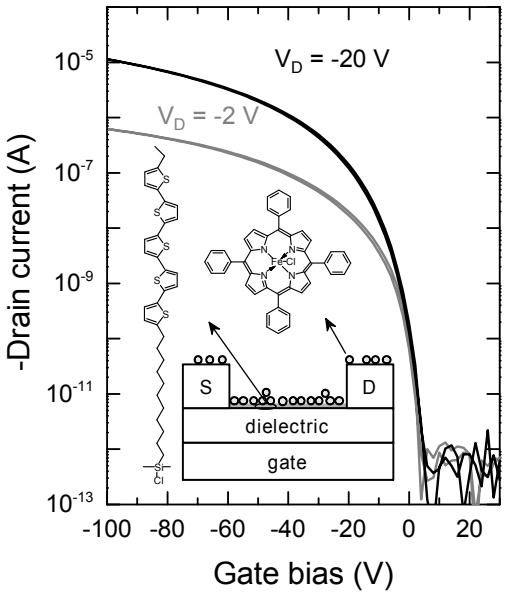

Figure 3.2: Transfer characteristics of a typical SAMFET in vacuum with a 1 μm SiO_2 gate dielectric in the linear and saturated regime. The device exhibited *p*-type behavior with a pinch off voltage around 0 V. The inset shows a schematic cross-section of the SAMFET sensor. The chemical structures of the SAM molecule (left) and the NO receptor Fe(TPP)Cl (above) are shown.

3.2 Preparation of self-assembled monolayer field-effect transistor

A SAMFET has recently been reported by Smits *et al.*[16] The monolayer consists of molecules with a semiconducting quinquethiophene core and an aliphatic spacer that is attached to the gate dielectric with a monofunctional anchoring group. The chemical structure of chloro[11-(5''''-ethyl-5,2':5',2'':5'',2''':5''',2''''-quinquethien-5-yl)undecyl] dimethylsilane is shown in the inset of Figure 3.2. The SAMFETs were manufactured on prefabricated transistor substrates (fabrication is described in Chapter 2), with a 1000 nm thermally oxidized SiO_2 layer as gate dielectric. Ring transistors with a channel length of 10 μm and a width of 2500 μm were used. Semiconducting monolayers were self-assembled from a toluene solution on a HF activated SiO_2 dielectric. The SAMFETs were annealed in vacuum at 110 °C for one hour to remove residual water and solvents. Electrical measurements were performed under vacuum. Possible gate bias stress effects in the electrical measurements were prevented by using a short integration time of less than 1 ms per step. Typical transfer curves in the linear and saturated regime are presented in Figure 3.2. The mobility is about 0.01 cm^2/Vs and the current modulation 6 decades, in good agreement with previous reports.

3.3 Nitric oxide detection

The response of the SAMFETs was measured by admitting small amounts of NO, diluted in nitrogen carrier gas, to the closed chamber. The gas pressure in this static system was used to calculate the partial NO concentration at 1 bar. The response of the SAMFET itself to NO is indistinguishable from random drift of the threshold voltage. To make the SAMFET specific for NO, a porphyrin receptor was used. Porphyrins are known to bind NO in *e.g.* biological systems.[17] Here iron(III) tetraphenylporphyrin chloride (Fe(TPP)Cl, Sigma Aldrich) was applied, that was previously used to detect NO in solution with a molecular controlled semiconductor resistor.[18] In the ideal case this receptor is grafted on, or incorporated into, the monolayer. Here, to demonstrate the concept, a thin spin coated film was used. The porphyrin receptor was dissolved in toluene, 1.6 mg/ml, and thin layers were spin coated at 800 rpm. The films are only 10 nm thick and contain a lot of pinholes. Therefore the diffusion of the nitric oxide is not limiting the detection rate. The addition of porphyrin on the SAMFET had no significant influence on the performance of the SAMFET. The chemical structure and the device lay-out are schematically depicted in the inset of Figure 3.2.

The transfer curve of the SAMFET with the porphyrin shifts upon exposure to NO. The field-effect mobility remains unaffected; the only effect is a change in the threshold

voltage towards positive gate bias. This clearly points to an increase of fixed negative interface charges upon exposure to NO. However, the reaction is not instantaneous, the threshold voltage shifts with time. A typical example is presented in Figure 3.3. The threshold voltage shift takes about half an hour to saturate. A possible reason might be the slow supply of negatively charged minority carriers needed to convert NO into NO_x^-. The dynamics of charge carrier trapping will be extensively studied in Chapter 5 and 6. In order to arrive at a dose response curve, the transfer curves were measured 30 minutes after NO exposure. To exclude any influence of competing charging effects, the threshold voltage of the SAMFET was monitored in the absence of NO. This measurement did not reveal a change of threshold voltage in time. The response to NO of the SAMFET without porphyrin was also investigated. These reference measurements are shown in Figure 3.3. Only the combination of the SAMFET and the receptor in NO atmosphere yields a shift in threshold voltage.

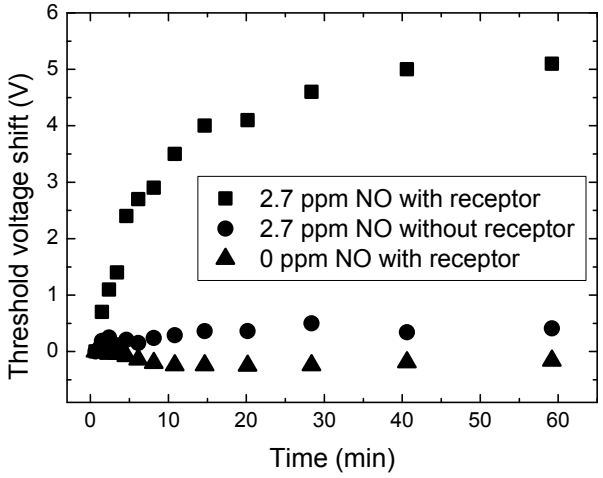

Figure 3.3: The response of the SAMFET sensor as a function of time for a fixed NO concentration (2.7 ppm). The threshold voltage shifts towards more positive voltages and saturates after approximately 30 minutes. Reference measurements of the SAMFET without the porphyrin in NO (2.7 ppm) and the SAMFET with porphyrin in absence of NO are included. Only the combination of the SAMFET and the receptor in NO shows a threshold voltage shift that stands out over random drift.

Many sensors were made and their response to NO was investigated. Figure 3.3 discussed above showed a typical measurement for 2.7 ppm NO. Concentrations in the ppm regime can reproducibly be detected. In exceptional cases however, a much higher sensitivity has been measured. An example is presented in Figure 3.4 where the transfer

curves measured in the linear regime are presented on a linear scale as a function of the NO concentration. The transfer curve systematically shifts to positive gate biases with increasing NO content. The relative threshold voltage shift was determined by taking the gate biases yielding a fixed source drain current of 60 nA, as indicated by the arrow in Figure 3.4. The shifts are used to construct a dose response curve. The inset shows the threshold voltage shift as a function of the NO concentration. The dose response curve shows that with the SAMFET sensor ppb concentrations of NO can be detected. The achieved sensitivity compares favorably with an earlier reported detection limit of an NO sensor based on a field-effect transistor.[19]

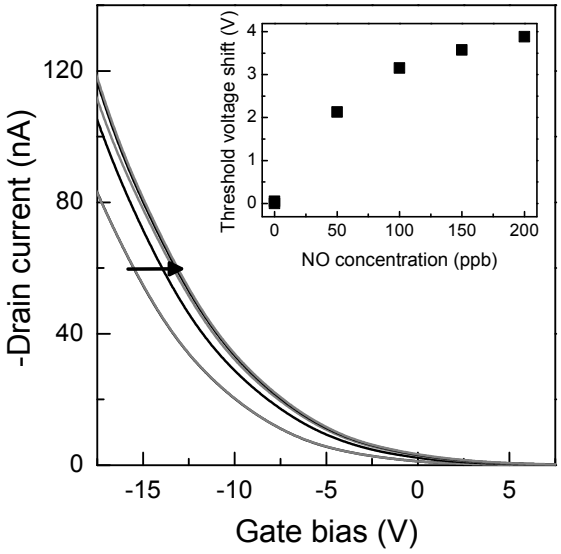

Figure 3.4: Linear plot of the transfer characteristics of the SAMFET sensor. The measurements performed in vacuum and nitrogen were identical. The transfer curve measured 30 minutes after exposure is shifted towards positive values for increasing NO concentrations. The inset shows the corresponding threshold voltage shift as a function of NO concentration. The detection limit is as low as sub 100 ppb NO.

The magnitude of the shift and the functional dependence such as the apparent saturation at high NO content are not yet quantitatively understood. Various operation mechanisms have been reported. For instance Fe(TPP)Cl has been attached to functionalized GaAs surfaces.[18] The current was measured upon exposure to NO in aqueous buffer solution. The current did increase with NO content. The change in current was

explained as originating from a change in dipole moment of the Fe(TPP)Cl complex. However a large threshold voltage shift in a field-effect transistor cannot be explained with only a change in surface dipole moment.[20] A different reaction mechanism was proposed by Lin and Farmer.[21] In solution NO forms a complex with Fe(TPP), NO-Fe(TPP). Catalytic reaction of this nitrosyl-complex with free NO then yields amongst others NO_2 which is known to cause a shift in threshold voltage[22] presumably by formation of negative surface charges. Recently, ZnO chemiresistors have been functionalized with a comparable iron(III)porphyrin, *viz.* ferriprotoporphyrin IX chloride.[23] NO could be detected down to the ppm range. The operation is reported to be due to electron transfer from ZnO to the receptor. In summary, iron porphyrins could selectively react towards NO, but the microscopic mechanism is unknown.

The selectivity of the SAMFET sensor versus other vapors was investigated. Preliminary experiments show that the sensor is not sensitive to a variety of gases. No threshold voltage shift was observed for non-oxidizing agents as toluene (8 ppm), methanol (%) and ammonia (2 ppm). Even for oxidizing agents as O_2 and SO_2 the threshold voltage shift is negligible showing the selectivity of the porphyrin towards these gases. Reversibility of the sensor after NO detection was also examined. Full recovery of the sensor is achieved by annealing under vacuum condition at 110 °C for 1 hour. Under those conditions the threshold voltage returns to its pristine value. The threshold voltage shift upon NO exposure is due to the formation of NO_x^-. The reversibility at elevated temperature is explained by detrapping of the electrons. The equilibrium shifts then to neutral nitrogen oxides that subsequently desorb from the surface. A major problem still to be resolved is that a significant spread in the NO response was found for the numerous investigated SAMFET sensors. The differences can be due to imperfections in the monolayer, variations in the porphyrin converter deposition, or parasitic reactions with residual water. The latter becomes more important at lower NO content.

3.4 Conclusions

The response of a field-effect sensor is dominated by the electrostatic interactions between the analyte and the conducting channel. In a self-assembled monolayer field-effect transistor the semiconductor is only one molecule thick, making it highly suited for sensing applications. SAMFET sensors were fabricated using iron porphyrin as a specific receptor for the biomarker NO. The transfer curve systematically shifts to positive gate biases with increasing NO content. Dose response curves were obtained by plotting the threshold voltage shift as a function of NO concentration. High sensitivity was demonstrated by detecting parts per billion concentrations NO.

References

1. I. Gaillard, S. Rouquier, D. Giorgi, *Cell. Mol. Life Sci.* **2004**, *61*, 456.
2. F. Rock, N. Barsan, U. Weimar, *Chem. Rev.* **2008**, *108*, 705.
3. K. J. Albert, N. S. Lewis, C. L. Schauer, G. A. Sotzing, S. E. Stitzel, T. P. Vaid, D. R. Walt, *Chem. Rev.* **2000**, *100*, 2595.
4. B. I. Jugdutt, *The Role of Nitric Oxide in Heart Failure*, Kluwer Academic Publishers, Boston, Massachusetts, **2004**.
5. J. L. Puckett, S. C. George, *Respir. Physiol. Neurobiol.* **2008**, *163*, 166.
6. T. Nagano, T. Yoshimura, *Chem. Rev.* **2002**, *102*, 1235.
7. A. Ciszewski, G. Milczarek, *Talanta* **2003**, *61*, 11.
8. O. Kuzmych, B. L. Allen, A. Star, *Nanotechnology* **2007**, *18*, 375502.
9. M. Gill, G. R. Graff, A. J. Adler, R. A. Dweik, *J. Asthma* **2006**, *43*, 731.
10. J. T. Mabeck, G. G. Malliaras, *Anal. Bioanal. Chem.* **2006**, *384*, 343.
11. L. Torsi, A. Dodabalapur, *Anal. Chem.* **2005**, *77*, 380A.
12. C. Tanase, E. J. Meijer, P. W. M. Blom, D. M. de Leeuw, *Org. Electron.* **2003**, *4*, 33.
13. J. Huang, J. Sun, H. E. Katz, *Adv. Mater.* **2008**, *20*, 2567.
14. L. Torsi, G. M. Farinola, F. Marinelli, M. C. Tanese, O. H. Omar, L. Valli, F. Babudri, F. Palmisano, P. G. Zambonin, F. Naso, *Nat. Mater.* **2008**, *7*, 412.
15. R. D. Yang, T. Gredig, C. N. Colesniuc, J. Park, I. K. Schuller, W. C. Trogler, A. C. Kummel, *Appl. Phys. Lett.* **2007**, *90*, 263506.
16. E. C. P. Smits, S. G. J. Mathijssen, P. A. van Hal, S. Setayesh, T. C. T. Geuns, K. Mutsaers, E. Cantatore, H. J. Wondergem, O. Werzer, R. Resel, M. Kemerink, S. Kirchmeyer, A. M. Muzafarov, S. A. Ponomarenko, B. de Boer, P. W. M. Blom, D. M. de Leeuw, *Nature* **2008**, *455*, 956.
17. J. A. McCleverty, *Chem. Rev.* **2004**, *104*, 403.
18. D. G. Wu, G. Ashkenasy, D. Shvarts, R. V. Ussyshkin, R. Naaman, A. Shanzer, D. Cahen, *Angew. Chem. Int. Ed.* **2000**, *39*, 4496.
19. F. Marinelli, A. Dell'Aquila, L. Torsi, J. Tey, G. P. Suranna, P. Mastrorilli, G. Romanazzi, C. F. Nobile, S. G. Mhaisalkar, N. Cioffi, F. Palmisano, *Sens. Actuators B* **2009**, *140*, 445.
20. S. K. Possanner, K. Zojer, P. Pacher, E. Zojer, F. Schuerrer, *Adv. Funct. Mater.* **2009**, *19*, 958.
21. R. Lin, P. J. Farmer, *J. Am. Chem. Soc.* **2001**, *123*, 1143.
22. A. Das, R. Dost, T. Richardson, M. Grell, J. J. Morrison, M. L. Turner, *Adv. Mater.* **2007**, *19*, 4018.
23. C. C. Liu, J. H. Li, C. C. Chang, Y. C. Chao, H. F. Meng, S. F. Horng, C. H. Hung, T. C. Meng, *J. Phys. D: Appl. Phys.* **2009**, *42*, 155105.

Chapter 4

Charge trapping by self-assembled monolayers as the origin of the threshold voltage shift in organic field-effect transistors

Crucial for any application of organic transistors is control of the threshold voltage. The value has been tuned by applying a self-assembled monolayer (SAM) on the gate dielectric. The microscopic origin however is under debate. In this chapter, the semiconductor is delaminated after electrical characterization. The surface potentials of the revealed SAM perfectly agree with the threshold voltages. This demonstrates that the shift is not due to the dipolar contribution of the SAM molecules but due to charge trapping at the SAM.

Published as:
F. Gholamrezaie, A. Andringa, W. S. C. Roelofs, A. Neuhold, M. Kemerink, P. W. M. Blom, D. M. de Leeuw, *Small*, **2012**, *8*, 241.

4.1 Introduction

Application of organic thin film transistors is envisioned in pixel engines, in active matrix displays and in integrated circuits for contactless radio-frequency identification transponders.[1–3] A key device parameter of a transistor is the threshold voltage, V_{th}. This voltage should be set at a given value and, furthermore, be identical for all devices in a circuit. Any deviation yields a reduced gain of logic gates, a decreased noise margin of integrated circuits or an inhomogeneously emitting display.[4,5] For standard silicon transistors, the threshold voltage can be accurately set by the amount of doping applied by ion implantation.[6,7] In organic transistors, however, local doping of individual transistors is not an option. To get around this constraint and to externally set V_{th}, several options have been published, such as the incorporation of level shifters in integrated circuits,[2] the use of a gate metal with a specific work function,[8,9] or the use of dual-gate transistors.[10] As an alternative method, the application of a self-assembled monolayer (SAM) at the gate dielectric interface has been reported.[11–15] The threshold voltage can be set by varying the chemical composition of the SAM. The change in V_{th} has tentatively been explained as being due to the dipole moment of the composing molecules. Device simulations, however, have indicated that the dipolar contribution is too small.[16] Alternatively, trapped interface charges have been suggested. The mechanism is under debate; as mentioned in a recent publication direct experimental evidence to accurately explain the voltage shifts is still lacking.[15]

Here, organic field-effect transistors with various self-assembled monolayers on the gate dielectric were fabricated. The value of the threshold voltage varied over tens of volts, depending on the chemical nature of the SAM. To elucidate the origin of the significant differences, the semiconductor was peeled off, and the surface potential of the SAM-modified gate dielectric was measured by scanning Kelvin probe microscopy (SKPM).[17,18] In this chapter, it is unambiguously shown that the origin of the threshold voltage shifts is charge trapping induced by the SAM. The temporal behavior of the surface potential after removing the semiconductor is discussed.

4.2 Fabrication of transistors with SAM-modified gate dielectric

Transistor test devices were fabricated as described in Chapter 2. The test devices were treated for 10 minutes with UV-ozone to remove all organic compounds.Three types of organosilane molecules with ethoxy end groups were used, *viz.* $(CF_3)(CF_2)_7(CH_2)_2Si(OC_2H_5)_3$, $(CH_3)(CH_2)_9Si(OC_2H_5)_3$, and $(NH_2)(CH_2)_3Si(OC_2H_5)_3$. The corresponding SAMs will be referred to as F-, CH_3- and NH_2-SAM, respectively. The chemical structures

are presented as insets in Figure 4.1. The SAMs were grown by vapor deposition at 120 °C for the NH_2-SAM and 150 °C for the F-SAM and the CH_3-SAM. The treated test devices were rinsed with iso-propanol to remove non-covalently bound molecules.

The microstructure of the SAMs was investigated with X-ray reflectivity, contact angle, and atomic force microscopy (AFM) measurements. Figure 4.1 shows the reflected X-ray intensity as a function of incidence angle. The black curves are a fit to the data, based on the recursive algorithm of Parratt and the roughness model of Nevot and Croce. The resulting measured and the calculated values of the SAM thickness are presented in Table 4.1. The values agree with the calculated lengths of the molecules. Only in case of the NH_2-SAM the numbers deviate, which could be due to formation of a double layer. The hydrophobicity of the SAMs was investigated by water contact angle measurements using the Contact Angle System OCA 30. The static contact angles presented in Table 4.1 correspond to literature values.[11,19,20] The morphology of the SAMs was investigated with AFM. A typical topographical image is presented in the inset of Figure 4.1. The monolayer is homogeneous without microscopic defects.

Table 4.1: Thickness of the SAMs derived from X-ray reflectivity measurements and calculated length of the molecules. Static contact angles of the SAMs before and after exfoliation of the PTAA semiconductor are presented.

	F-SAM	CH_3-SAM	NH_2-SAM
SAM thickness (nm)	1.3	1.1	0.88
SAM thickness calculated (nm)	1.2	1.2	0.36
Water contact angle (°)	108	91	67
Water contact angle after exfoliation (°)	105	90	64

Polytriarylamine (PTAA) was used as a *p*-type amorphous semiconductor. The chemical structure is presented as inset in Figure 4.3. Saturated transfer curves of the polytriarylamine transistors with three different SAMs are presented in Figure 4.2a. The major difference between the transistors is the value of the threshold voltage, here approximated by the pinch-off voltage. The offset between the pinch-off voltage and the threshold voltage can be disregarded for the discussion. The threshold voltage of transistors with a CH_3-SAM is around 0 V; with a NH_2-SAM the threshold voltage is negative, and with a F-SAM the threshold voltage is positive. For the example of Figure 4.2a, the numbers are about 0, -16, and +20 V, respectively, in agreement with threshold voltages reported for corresponding pentacene transistors.[11]

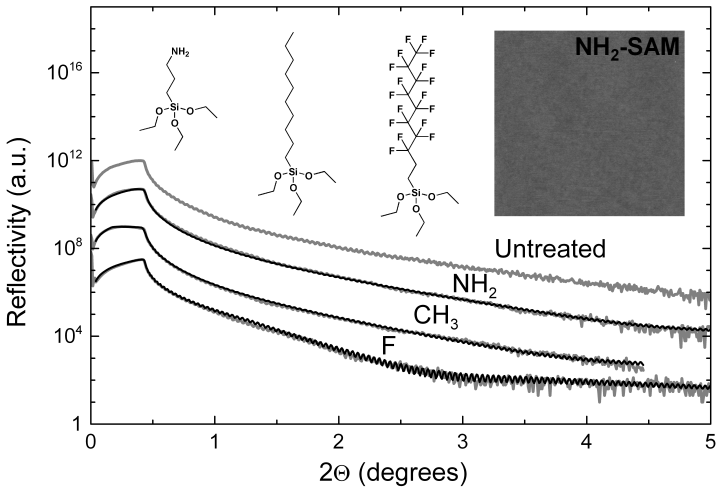

Figure 4.1: X-ray reflection as a function of the diffracted angle for the SAMs. The solid black lines are fits to the experimental data. Inset: Chemical structures of the SAM molecules: NH_2-SAM, CH_3-SAM, F-SAM (from left to right). AFM topography image of 20 μm $\times$ 20 μm of NH_2-SAM (right).

4.3 Delamination of the semiconductor

The change in threshold voltage can be the result of the following mechanisms: the macroscopic dipole moment of the SAM, charge trapping at the gate dielectric semiconductor interface, or doping of the semiconductor. To disentangle the mechanisms, the local potential is probed with SKPM. The bulk semiconductor however electrically shields the buried SAM, which prevents the SAM from being probed directly; therefore the semiconductor has to be removed. With a piece of adhesive tape, the PTAA semiconductor layer is completely removed as a continuous film from the gate dielectric. After peeling off the polymer, the source-drain current is zero. The exfoliation is facilitated by the SAM, which lowers the interfacial energy. The complete removal is supported by X-ray photoelectron spectroscopy (XPS) measurements, a well-established technique to identify the chemical composition of the top-most surface layers. Nitrogen is a marker for the presence of the semiconductor PTAA. Figure 4.3 presents the N 1s peak with a binding energy around 399 eV before and after exfoliation of the PTAA. For the F-SAM and the CH_3-SAM, the signal has completely disappeared as checked on various spots on the surface, indicating the complete removal of PTAA. For the NH_2-SAM, XPS is not an appropriate technique because nitrogen is present in both the polymer and monolayer.

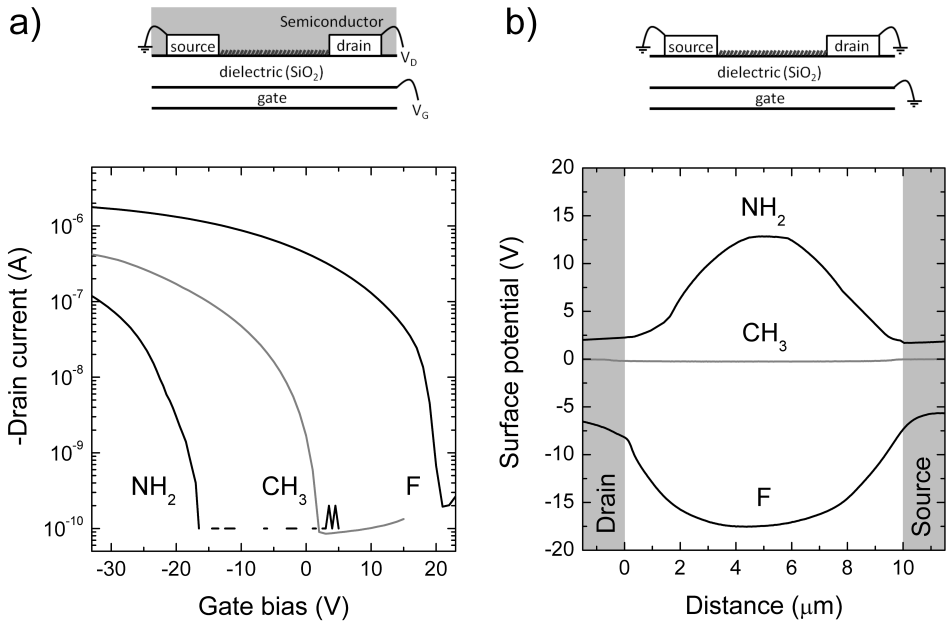

Figure 4.2: a) Saturated transfer characteristics of field-effect transistors modified with an F-SAM, a CH_3-SAM, and an NH_2-SAM on the gate dielectric. The channel length and width are 10 and 10 000 μm, respectively, and the source-drain bias is -30 V. At the top the transistor layout is depicted schematically. b) Local surface potentials of the SAMs after peeling off the PTAA semiconductor for the F-SAM, CH_3-SAM, and NH_2-SAM. The transistor layout after delamination is schematically presented at the top. During SKPM measurements all electrodes are grounded.

Contact angle measurements on the SAM confirm that the SAM itself is not affected by exfoliation. Table 4.1 shows that the static contact angles after peeling off the semiconductor resemble the contact angles of the freshly prepared SAMs. A photograph of the CH_3-SAM contact angle measurement after exfoliation is presented as an inset in Figure 4.3.

4.4 Linking the threshold voltage shift to trapped charges

To prove that the shift in threshold voltage is due to trapping of charges, the surface potential of the area between the source and drain was measured as quickly as possible after measuring the transfer curve (Figure 4.2a) and peeling off the PTAA layer. During the SKPM measurement, all electrodes were grounded. The potential profiles were scanned in ambient atmosphere in non-contact lift mode 20 nm above the surface. The local surface potentials are presented in Figure 4.2b. The offset at the source and drain contacts

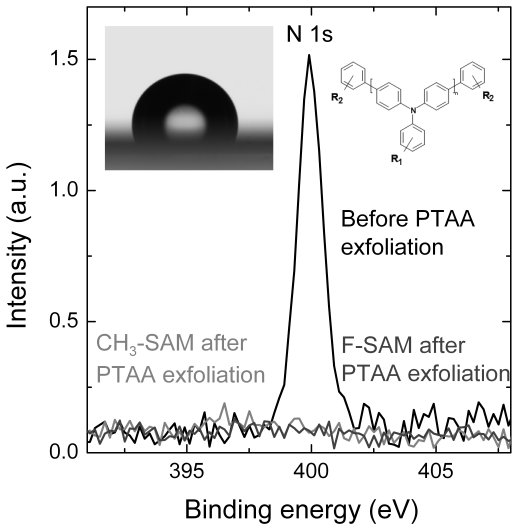

Figure 4.3: X-ray photoelectron spectra before and after peeling off the PTAA semiconductor. The black line shows the PTAA N 1s peak before peeling off. The light and dark grey lines are measured after peeling off the PTAA semiconductor from the CH_3-SAM and F-SAM, respectively. The insets show the chemical structure of the PTAA semiconductor and a picture of a water droplet on the pristine CH_3-SAM.

is due to the capacitive coupling between the AFM cantilever and the transistor channel region. The surface potential in the channel region depends on the type of SAM. For the CH_3-SAM the surface potential is zero. In the case of the F-SAM, a negative surface potential of -18 V is observed while the NH_2-SAM shows a positive surface potential of $+14$ V.

The surface potentials have been measured as fast as possible after peeling off because their amplitude decreases with time. As an example the temporal behavior of the surface potential of the F-SAM is presented in Figure 4.4a. The value of the maximum potential is plotted as a function of time in Figure 4.4b. The potential decreases about exponentially with time. The time constant depends on the relative humidity of the air. At 60 % relative humidity, the decay constant is a factor of five smaller than in dry air. The temporal behavior is not well understood. The trapped charges in the channel region become compensated, which might be caused by surface conduction through absorbed water.[21]

The threshold voltage of a field-effect transistor is equal to the flat band voltage, V_{FB}, corrected for fixed oxide charges, Q_f, trapped interface charges, Q_i,[22] and the dipolar contribution due to SAM, V_{SAM}:

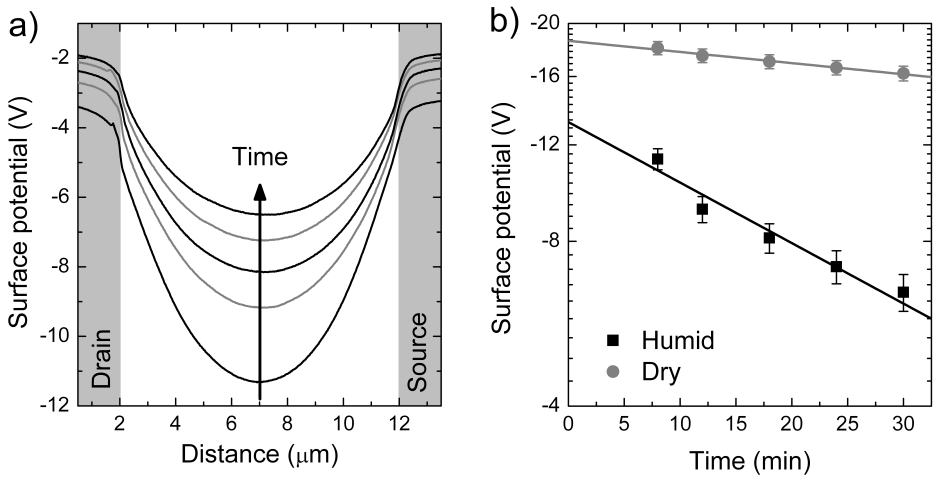

Figure 4.4: a) Surface potential profiles measured with SKPM on the F-SAM after peeling off the PTAA semiconductor. The potentials decrease with time. The time interval between the measurements amounted to 6 minutes. The relative humidity was 60 %. b) Maximum local surface potentials as a function of time. The grey and black points were measured in a relative humidity of 30 % and 60 %, respectively. The solid lines are an exponential fit to the data.

$$V_{\mathrm{th}} = V_{\mathrm{FB}} + V_{\mathrm{SAM}} - \frac{Q_{\mathrm{f}} + Q_{\mathrm{i}}}{C_{\mathrm{ox}}} \tag{4.1}$$

where C_{ox} is the dielectric capacitance. Flat band voltages are typically on the order of 0.1 V. The dipolar potential follows from the Helmholtz equation:

$$V_{\mathrm{SAM}} = \frac{\mu_{\mathrm{zSAM}}}{A\epsilon_{\mathrm{r}}\epsilon_0} \tag{4.2}$$

where μ_{zSAM} is the net vertical component of the molecular dipole moment, A is the lateral area per molecule, ϵ_{r} is the relative permittivity of the molecule and ϵ_0 is the vacuum permittivity.[23] The values of the observed threshold voltages are too big to be a result of the dipole moment of the SAM. Reported device simulations calculate a small dipolar contribution of less than 1 V for molecules with comparable dipole moments.[16] SKPM measurements on the bare SAMs before applying the PTAA semiconductor confirm the small dipolar potential; the differences in surface potential between SiO_2 surfaces covered with different SAMs are at most 1 V. Also, the observed variations in threshold voltage can not be due to fixed oxide charges. All SAMs bind in the same manner to the SiO_2 surface. Fixed oxide charges are highly unlikely, since the transfer curve of the CH_3-SAM exhibits a threshold voltage around 0 V. Hence the changes in threshold voltage of the NH_2-SAM and F-SAM are due to trapped interface charges. This assignment is

confirmed by the SKPM measurements. The contributions to the surface potential of the dipole moment of the molecules, the flat band voltage, and the fixed charges can be neglected with respect to the contribution of the interface charges. Therefore the surface potential when using grounded electrodes is given by $V_{SKPM} \approx Q_i/C_{ox}$; *i.e.* it is largely dominated by trapped interface charges.

In dry air the maximum surface potential of the stripped device extrapolated back to time zero perfectly matches with the corresponding threshold voltages (Figure 4.4b). In humid air the changes are too fast to reliably estimate the extrapolated starting potential. The agreement between extrapolated potential and threshold voltage unambiguously shows that the threshold voltage shift originates from trapped charges by the SAM. The CH_3-SAM is inactive while the NH_2-SAM traps positive charges and the F-SAM traps negative charges. The presence of the negative charges could be due to surface conduction of the SiO_2,[21] but it is not completely clear yet.

4.5 Exfoliation process

It is well known that exfoliation of two insulating materials can yield static charges by contact electrification or tribo-charging. A review on space-charge electrets that exhibit a net macroscopic electrostatic charge has been presented in the literature.[24] The classical example is the charging of adhesive tape by unrolling. Peeling off ordinary sticky tape in vacuum can even yield individual X-ray pulses, typically a few nanoseconds long, of up to 15 kV.[25] However, the potentials measured here are not generated by the peeling process.

Firstly, the one-to-one correspondence between the threshold voltage shifts due to application of SAMs on the gate dielectric with the surface potentials as measured by SKPM would be a rare coincidence. The measured surface potentials are highly reproducible. That is not expected when the charges are generated by peeling off. Then a large spread in the amount of static charges is expected. Secondly, in separate series of experiments, the surface potentials were measured with KPM before and after peeling off adhesive tape from a variety of substrates. Unrolling tape itself yields potentials higher than experimentally could be measured. Peeling off tape from a bare metal substrate does not lead to any static charges, as expected. Repetitive experiments on bare back-gated SiO_2 transistor substrates showed potential differences before and after exfoliation of at most 0.5 V. The measurements agree with literature data. Surface potentials of only 0.95 V were measured after peeling off Alq_3 with adhesive tape.[26] Thirdly, the exact same exfoliation procedure has been used previously to locate trapped charges in PTAA field-effect transistors generated upon prolonged application of the gate bias.[18]

After stressing the threshold voltage was measured. Subsequently the semiconductor was peeled off with adhesive tape, and the surface potential of the revealed interface was measured using SKPM. A one-to-one correlation of the threshold voltage shift with the measured surface potential was found, ruling out that the static charges are generated in the peeling process. Finally, depending on the nature of the SAM the transistor is either normally-on or normally-off, meaning that at 0 V bias, the semiconductor is either conducting or insulating. In a normally-on transistor, exfoliation cannot generate stable static charges, and therefore, the experimental procedure cannot be the cause of the negative threshold voltage shift. In short, generation of static charges by the exfoliation process can be disregarded. The measured threshold voltage shifts are due to charges trapped by the SAM.

4.6 Conclusions

In this chapter, organic field-effect transistors with different self-assembled monolayers on the gate dielectric were fabricated. The threshold voltage depends on the type of SAM. In agreement with literature data, the threshold voltage of CH_3-SAM was about 0 V, while the values for F-SAM and NH_2-SAM were at $+20$ and -16 V, respectively. To elucidate the origin of the large differences, the semiconductor was peeled off after electrical characterization, and the surface potential of the SAM modified gate dielectric was measured by SKPM. The surface potentials agree with the corresponding threshold voltage, which unambiguously shows that the surface potential shift is due to the charge trapping by the SAM.

References

1. G. H. Gelinck, H. E. A. Huitema, E. Van Veenendaal, E. Cantatore, L. Schrijnemakers, J. Van der Putten, T. C. T. Geuns, M. Beenhakkers, J. B. Giesbers, B. H. Huisman, E. J. Meijer, E. M. Benito, F. J. Touwslager, A. W. Marsman, B. J. E. Van Rens, D. M. De Leeuw, *Nat. Mater.* **2004**, *3*, 106.
2. E. Cantatore, T. C. T. Geuns, G. H. Gelinck, E. van Veenendaal, A. F. A. Gruijthuijsen, L. Schrijnemakers, S. Drews, D. M. de Leeuw, *IEEE J. Solid St. Circ.* **2007**, *42*, 84.
3. K. Myny, S. Steudel, P. Vicca, M. J. Beenhakkers, N. van Aerle, G. H. Gelinck, J. Genoe, W. Dehaene, P. Heremans, *Solid State Electron.* **2009**, *53*, 1220.
4. S. De Vusser, J. Genoe, P. Heremans, *IEEE Trans. Elect. Dev.* **2006**, *53*, 601.
5. J. R. Hauser, *IEEE Trans. Educ.* **1993**, *36*, 363.
6. M. R. Mac Pherson, *Appl. Phys. Lett.* **1971**, *18*, 502.
7. T. Mizuno, J. Okamura, A. Toriumi, *IEEE Trans. Elect. Dev.* **1994**, *41*, 2216.
8. I. Nausieda, K. K. Ryu, D. Da He, A. I. Akinwande, V. Bulovic, C. G. Sodini, *IEEE Trans. Elect. Dev.* **2010**, *57*, 3027.

9. H. W. Zan, W. T. Chen, C. C. Yeh, H. W. Hsueh, C. C. Tsai, H. F. Meng, *Appl. Phys. Lett.* **2011**, *98*, 153506.
10. M. Spijkman, E. C. P. Smits, P. W. M. Blom, D. M. de Leeuw, Y. B. Saint Come, S. Setayesh, E. Cantatore, *Appl. Phys. Lett.* **2008**, *92*, 143304.
11. S. Kobayashi, T. Nishikawa, T. Takenobu, S. Mori, T. Shimoda, T. Mitani, H. Shimotani, N. Yoshimoto, S. Ogawa, Y. Iwasa, *Nat. Mater.* **2004**, *3*, 317.
12. K. P. Pernstich, S. Haas, D. Oberhoff, C. Goldmann, D. J. Gundlach, B. Batlogg, A. N. Rashid, G. Schitter, *J. Appl. Phys.* **2004**, *96*, 6431.
13. Y. Jang, J. H. Cho, D. H. Kim, Y. D. Park, M. Hwang, K. Cho, *Appl. Phys. Lett.* **2007**, *90*, 132104.
14. J. Takeya, T. Nishikawa, T. Takenobu, S. Kobayashi, Y. Iwasa, T. Mitani, C. Goldmann, C. Krellner, B. Batlogg, *Appl. Phys. Lett.* **2004**, *85*, 5078.
15. Y. Chung, E. Verploegen, A. Vailionis, Y. Sun, Y. Nishi, B. Murmann, Z. A. Bao, *Nano Lett.* **2011**, *11*, 1161.
16. S. K. Possanner, K. Zojer, P. Pacher, E. Zojer, F. Schuerrer, *Adv. Funct. Mater.* **2009**, *19*, 958.
17. V. Palermo, M. Palma, P. Samori, *Adv. Mater.* **2006**, *18*, 145.
18. S. G. J. Mathijssen, M. J. Spijkman, A. Andringa, P. A. van Hal, I. McCulloch, M. Kemerink, R. A. J. Janssen, D. M. de Leeuw, *Adv. Mater.* **2010**, *22*, 5105.
19. H. Sugimura, K. Ushiyama, A. Hozumi, O. Takai, *Langmuir* **2000**, *16*, 885.
20. A. Hozumi, Y. Yokogawa, T. Kameyama, H. Sugimura, K. Hayashi, H. Shirayama, O. Takai, *J. Vac. Sci. Technol. A* **2001**, *19*, 1812.
21. S. G. J. Mathijssen, M. Kemerink, A. Sharma, M. Coelle, P. A. Bobbert, R. A. J. Janssen, D. M. de Leeuw, *Adv. Mater.* **2008**, *20*, 975.
22. S. M. Sze, *Physics of Semiconductor Devices*, Wiley-Interscience, New York, **1981**.
23. D. J. Ellison, B. Lee, V. Podzorov, C. D. Frisbie, *Adv. Mater.* **2011**, *23*, 502.
24. L. S. McCarty, G. M. Whitesides, *Angew. Chem. Int. Ed.* **2008**, *47*, 2188.
25. C. G. Camara, J. V. Escobar, J. R. Hird, S. J. Putterman, *Nature* **2008**, *455*, 1089.
26. Y. Okabayashi, E. Ito, T. Isoshima, H. Ito, M. Hara, *Thin Solid Films* **2009**, *518*, 839.

Chapter 5

Gate-bias controlled charge trapping as a mechanism for NO_2 detection with field-effect transistors

Detection of nitrogen dioxide, NO_2, is required to monitor the air-quality for human health and safety. Commercial sensors are typically chemiresistors, however field-effect transistors are being investigated. Although numerous investigations have been reported, the NO_2 sensing mechanism is not clear. In this chapter, the detection mechanism is investigated using ZnO field-effect transistors. The current gradually decreases upon NO_2 exposure and application of a positive gate bias. The current decrease originates from the trapping of electrons, yielding a shift of the threshold voltage towards the applied gate bias. The shift is observed for extremely low NO_2 concentrations down to 10 ppb and can phenomenologically be described by a stretched-exponential time relaxation. NO_2 detection has been demonstrated with n-type, p-type, and ambipolar semiconductors. In all cases, the threshold voltage shifts due to gate bias induced electron trapping. The description of the NO_2 detection with field-effect transistors is generic for all semiconductors and can be used to improve future NO_2 sensors.

Published as:
A. Andringa, J. R. Meijboom, E. C. P. Smits, S. G. J. Mathijssen, P. W. M. Blom, D. M. de Leeuw, *Advanced Functional Materials*, **2011**, *21*, 100.

5.1 Introduction

NO_2 is one of the most dangerous air pollutants affecting human health and the environment. The gas is released during the combustion of fossil fuels and plays a major role in the formation of ozone and acid rain. The control and improvement of the air quality is of great importance to modern society. The U.S. Environmental Control Agency has set the air-quality standard at a level of 53 ppb NO_2. The need for sensitive sensors for air-quality monitoring has led to extensive research in the field. Many sensors are commercially available, ranging from electrochemical to optical sensors.

The most common NO_2 sensors are chemiresistors based on semiconducting metal oxides such as tin oxide (SnO_2), tungsten oxide (WO_3), or zinc oxide (ZnO).[1–3] Porous oxide layers with high specific surface areas are used. The gas diffuses into the oxide and modulates the grain boundary resistances by the transfer of charge carriers from the semiconductor to the adsorbed surface species. Nowadays, many companies offer metal-oxide-based gas sensors. The lack of selectivity can be addressed by combining a number of sensors in an array. The sensors are selected for a specific application, such as bacteria growth[4] or car seat foams.[5] Challenges are reduction of the power consumption due to the high operating temperature and improvement of the sensitivity, which is typically about 1 ppm. To this end, other semiconductors, such as phthalocyanines[6–8] and carbon nanotubes films,[9] are being investigated in two terminal devices.

Field-effect transistors (FETs) have emerged as an alternative sensing technology. In 1975, a hydrogen sensor based on a Pd-gate FET was demonstrated.[10] In recent years, a wide variety of semiconductors has been used in transistors to detect a wide range of gases. Examples are carbon nanotubes[11] or organic[12–18] and oxidic[19] semiconductors. The key advantage of a transistor over a resistor is the reported amplified sensor response due to current modulation by the extra gate electrode.[13] The sensitivity can be enhanced by operating the sensor in the subthreshold regime. Apart from the current modulation, changes in other transistor parameters, such as mobility and threshold voltage, can be used for sensing. The idea of exploiting FETs as multiparameter gas sensors was suggested by Torsi *et al.*[20]

A wide variety of semiconductors has been investigated in transistors for NO_2 detection. A range of sensing layers, such as amorphous organic semiconductors,[21,22] porous silicon,[23] silicon nanowires,[24] carbon nanotubes,[25–33] and metal oxide nanowires,[34] were used. In all cases changes in current upon NO_2 exposure have been demonstrated. In addition, a high sensitivity down to 10 ppb NO_2 has been reported. The detection mechanism however is not clear and several possible sensing mechanism have been suggested. The adsorbed NO_2 is a strong electron acceptor that can influence the charge carrier

density in the channel. The change in current can then be explained by doping of the semiconductor by the oxidizing NO_2[17,21,22] or by depleting the electrons from the conduction channel.[31,34] For carbon nanotubes sensors Zhang *et al.*[32] postulated that the NO_2 molecules change the metal workfunction, leading to a change in the Schottky barrier height at the carbon nanotubemetal interface. Finally, Kong *et al.*[33] proposed molecular gating of the nanotubes by the polar NO_2 molecules as the sensing mechanism.

In this chapter, the NO_2 detection mechanism is elucidated using transistors with ZnO as a model semiconductor. ZnO was selected because it has been widely investigated in resistive sensors.[35–37] The sensor response was also investigated using other semiconductors to demonstrate the generic nature of the detection mechanism. The charge transport upon NO_2 exposure was measured. The current decreased with time, but only in combination with a positive gate bias. The decrease is due to charge trapping mediated by NO_2, yielding a shift in the threshold voltage. It is shown that for any positive gate bias, the threshold voltage shifts towards that applied gate bias. The dynamics of the shift under prolonged gate bias are evaluated at room temperature as a function of the NO_2 concentration and ZnO layer thickness. The kinetics of the threshold voltage shift can phenomenologically be described by a stretched-exponential time dependence. The functional dependence on the ZnO layer thickness and NO_2 concentration is discussed and a generic interpretation based on charge trapping is presented.

5.2 ZnO transistor fabrication and characterization

Field-effect transistors test substrates were fabricated as described in Chapter 2. Finger transistors were used with a channel length and width of 10 and 10,000 μm, respectively. The ZnO layer was applied using spray pyrolysis in ambient atmosphere. A solution of 0.1 M zinc acetate Sigma Aldrich, 99.99 %) in methanol was nebulized on the prefabricated transistor substrates heated at 400 °C, as reported by, for example, Bashir *et al.*[38] The *n*-type ZnO transistors showed negligible hysteresis and a field-effect mobility of 0.1-2 cm^2/Vs. The current modulation exceeded 6 orders of magnitude and the threshold voltage was 0 V. The layer thickness was varied by varying the spray time and measured by X-ray fluorescence (XRF). The film thickness was typically only 10 nm to ensure permeability for NO_2. The ZnO layer was further characterized using X-ray diffraction (XRD) and atomic force microscopy (AFM). The mirror-like ZnO films exhibited a microcrystalline morphology with a surface roughness of 1 nm (root mean square (rms)). XRD measurements showed that the ZnO films exhibited a (102) textured microstructure.

The sensor response in NO_2 atmosphere was tested in a stationary and a flow system as described in Chapter 2. Cylinders containing 3 ppm NO_2 in N_2 as a carrier gas

and pure N_2 were supplied by Praxair. The NO_2 concentration was calibrated in both setups using an Eco Physics CLD 88p NO sensor based on chemiluminescence. A gas converter (series CG, M&C TechGroup) was used to convert NO_2 catalytically to NO at 330 °C with a carbon molybdenum mixture. In the closed static gas system, the NO_2 concentration dropped with time due to a surface reaction with the interior of the closed chamber. Therefore this setup could only be used to perform measurements at high NO_2 concentration, above 0.5 ppm, within half an hour. Reliable measurements at lower NO_2 concentrations, in the range of 0-1200 ppb, were performed in a dynamic flow cell. Two mass flow controllers were used to produce the desired NO_2 concentrations. The gases were flushed through the chamber at a constant total flow rate of 500 sccm. Electrical measurements were performed in a stabilized concentration that is reached after 30 minutes flow.

All electrical characterization was done at 40 °C. Prior to use, the ZnO transistors were annealed in vacuum or air at 150 °C in order to make the pinch-off voltage 0 V. As the pinch-off voltage, the gate bias was taken at which the source drain current was 1 nA. The semiconductor parameter analyser was programmed to perform a complete measurement in less than one second. The state of the transistor was determined to be practically unaffected by the measurement. Because the transistors were stable when no bias was applied, the NO_2 concentration could be stabilized before starting the electrical measurements.

5.3 Chemiresistors versus transistors

In a metal-oxide-based gas sensor, the resistance is monitored as a function of the concentration of the target gas. The operation mechanism is well established.[1,2,39,40] Conventional metal oxide sensors are operated in air, at temperatures between 200 and 400 °C. The partial oxygen pressure is fixed and therefore the amount of oxygen absorbed on the metal oxide grains is constant. At the temperature used, the oxygen thermally dissociates. Due to the large electronegativity of oxygen atoms, charge transfer occurs. Electrons are removed from the metal oxide semiconductor, the free charge carrier concentration is reduced, and a depletion layer is formed. The resistance in air is therefore larger than in vacuum. Exposure to, for instance, a reducing gas leads to the removal of the oxygen atoms, thereby reinjecting electrons into the conduction band. Both the thickness of the depletion layer and the resistance decrease. The sensitivity of the sensor depends on the size of the depletion layer relative to the thickness of the bulk semiconductor. Commercial sensors therefore typically consist of thick porous films. Schottky contacts at the grain boundaries then dominate the electrical transport.

Commercial metal oxide sensors are two terminal chemiresistors. The change in resistance is due to a change in the charge carrier density. A field-effect transistor, discussed in Chapter 1, is a three terminal device in which an additional gate electrode modulates the charge carrier density in the semiconductor. Here, the influence of the gate field on the sensitivity is investigated.

In a transistor, the resistivity of the semiconductor, and hence the current through the semiconductor, can be varied over orders of magnitude. A typical transfer curve of a ZnO transistor, where the current is measured as a function of gate bias at a constant drain bias, is presented in Figure 5.1. ZnO is an intrinsic undoped *n*-type semiconductor. At zero gate bias there are no charges accumulated and the current is negligible. At positive gate bias electrons are accumulated in the channel and at negative gate bias all electrons in ZnO are depleted. Hence, as schematically depicted in the insets of Figure 5.1, the current switches from the off-state in depletion to the on-state in accumulation. The transistor is measured in the linear regime, where the drain bias is much smaller than the gate bias. Figure 5.1 shows that the current starts to flow around zero gate bias. This onset is the pinch-off voltage, which is assumed to be equal to the threshold voltage.

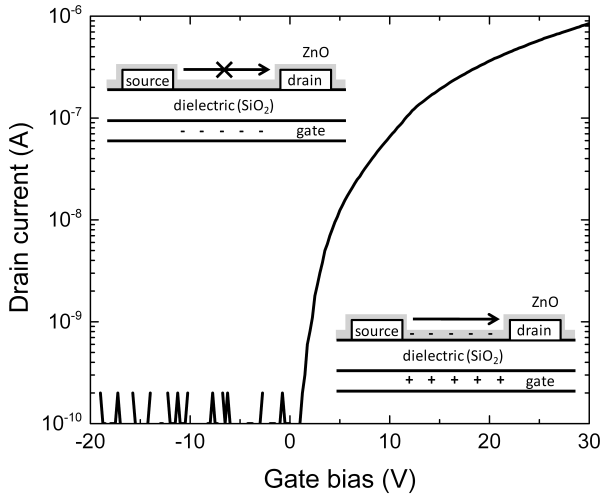

Figure 5.1: Typical transfer curve of a ZnO field-effect transistor measured with a drain bias of 2 V. In the insets, a schematic presentation of a transistor in the off- and the on-state is shown.

The ZnO transistors were characterized in an NO_2 ambient at room temperature. The gate was grounded and there were no charges in the semiconductor. The current was low for all drain biases and did not change with NO_2 content. Large changes occured, however, when a gate bias was applied. Figure 5.2a serves as an illustration. A ZnO

transistor kept in vacuum was turned on by applying a positive gate bias. A small source drain bias was applied and the current was measured as a function of time. The current was stable, there was only a small drift due to residual gate bias stress.[41] After 4 minutes of measuring, NO_2 gas was admitted. The current immediately dropped and within 10 minutes the current decreased by more than three orders of magnitude. To elucidate the origin of the current drop, the transfer curves were measured a few times during the transient current measurement. Figure 5.2b shows that in vacuum the transistor switches on at 0 V gate bias (left curve). After NO_2 exposure and upon continuously applying a positive gate bias, the transfer curve shifts towards the applied gate bias (middle and right curves). The shape however remains unaffected, implying that the field-effect mobility remains the same. The main effect of NO_2 exposure is a shift of the threshold voltage, V_{th}. At room temperature the recovery can be disregarded.

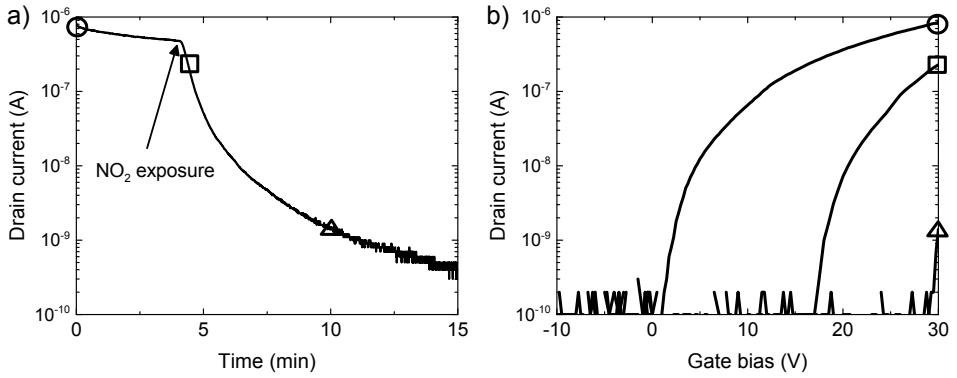

Figure 5.2: a) Drain current of a ZnO field-effect transistor as a function of time using an applied gate bias of 30 V and a drain bias of 2 V. The measurement starts in vacuum and after 4 minutes 250 ppb NO_2 was admitted. b) Transfer characteristics corresponding to the indicated times during the measurement in (a). The left curve was measured in vacuum, the middle and right curves were measured during NO_2 exposure.

In summary, at zero gate bias the electrical transport did not change; the ZnO transistors were chemically stable in NO_2. The transport only changed when a positive gate bias was applied in NO_2 ambient. The measurement of the transfer curve should not influence the state of the transistor. Hence it is crucial to keep the time to measure a transfer curve as short as possible.

5.4 Threshold voltage dynamics

The applied gate bias dominates the threshold voltage shift. When a ZnO transistor is kept in NO_2 atmosphere, with all contacts grounded, and at certain times quick transfer curves are measured, then the threshold voltage hardly changes. Hence doping of the ZnO semiconductor by oxidizing NO_2 can be disregarded.

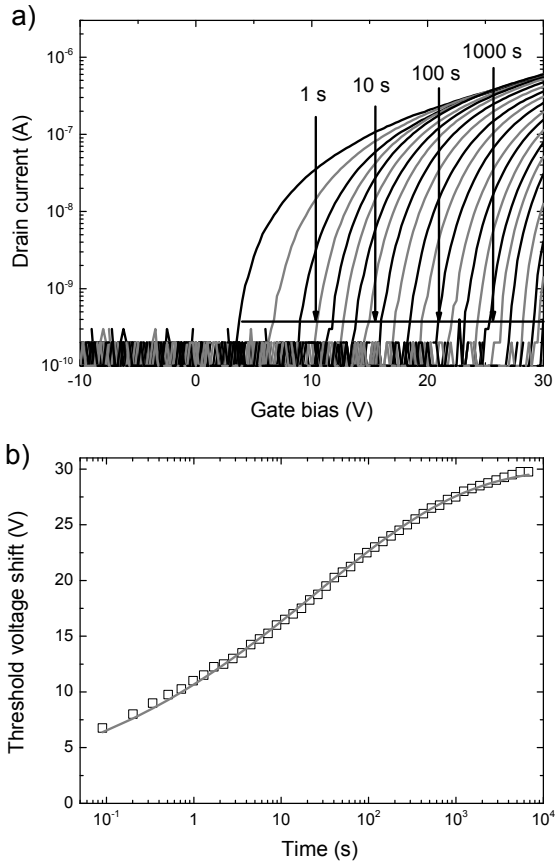

Figure 5.3: a) Transfer curves of a ZnO transistor under exposure of 320 ppb NO_2 as a function of time under a continuously applied gate bias of 30 V. The arrows indicate transfer curves measured after 1 to 1000 seconds. b) The threshold voltage shift obtained from (a) presented as a function of time on a semilogarithmic scale. The solid line is a fit to a stretched-exponential time dependence.

To elucidate the role of a finite gate field, a continuous gate bias was applied for a longer time, with grounded source-drain electrodes. The resulting threshold voltage shift was monitored by measuring the transfer curves as a function of time. In Figure 5.3a,

the linear transfer curves measured at a 2 V drain bias are presented as a function of stress time, the time at which the gate bias is applied. Figure 5.3a shows that the transfer curve shifts with stress time towards the applied gate bias, in this case 30 V. The arrows indicate transfer curves measured after 1 to 1000 seconds. The shape of the curves does not change. Therefore the shift in threshold voltage is similar to the shift in pinch-off voltage. The threshold voltage shift, with respect to the reference value measured in vacuum, is presented in Figure 5.3b as a function of time on a semilogarithmic scale. Initially a fast change is observed, while at longer times the threshold voltage shift saturates at the value of the applied gate bias. This rate of change resembles the temporal behavior of a stretched-exponential relaxation. Hence the threshold voltage shift was fitted to:

$$\Delta V_{\mathrm{th}}(t) = V_0 \left\{ 1 - \exp\left[-\left(\frac{t}{\tau} \right)^{\beta} \right] \right\} \tag{5.1}$$

where τ is a relaxation time, β is a dispersion parameter equal to T/T_0, and $V_0 = V_{\mathrm{G}} - V_{\mathrm{th0}}$, where V_{G} is the applied gate bias and V_{th0} is the threshold voltage at the start of the experiment. Figure 5.3b shows that a good agreement is obtained with a characteristic relaxation time of 26 seconds and a dispersion parameter β of 0.25.

The shift was determined for various gate biases. Figure 5.4a shows the threshold voltage as a function of time for various gate biases of 0, +10, +20, and +30 V. When the gate is grounded, the threshold voltage does not shift and the transfer curve does not change. Only when a finite positive gate bias is applied the threshold voltage shift towards the applied gate bias. The solid lines show that each measurement can be fitted with a stretched-exponential time dependence. The fit constants τ and β are independent of the gate bias as can be inferred from the inset of Figure 5.4a, which shows the threshold voltage shift normalized to the applied gate bias. Equation 5.1 describes the threshold voltage shifts for all gate biases.

Figure 5.4a can qualitatively be understood as follows. Upon application of a positive gate bias, electrons accumulate in the channel. Some are trapped at defect sites or acceptor molecules. The trapped charges do not contribute to the current but they shift the threshold voltage. When the trapped charges fully compensate the applied gate bias, there is no driving force left for charge accumulation. The threshold voltage shift saturates at the applied gate bias and a steady-state is reached. The charge trapping process is schematically depicted in Figure 5.4b. With time, mobile electrons are continuously trapped until the steady-state is reached where the gate bias is completely compensated by immobile trapped charges.

The threshold voltage shifts only when the gate bias is applied; the drain bias in the

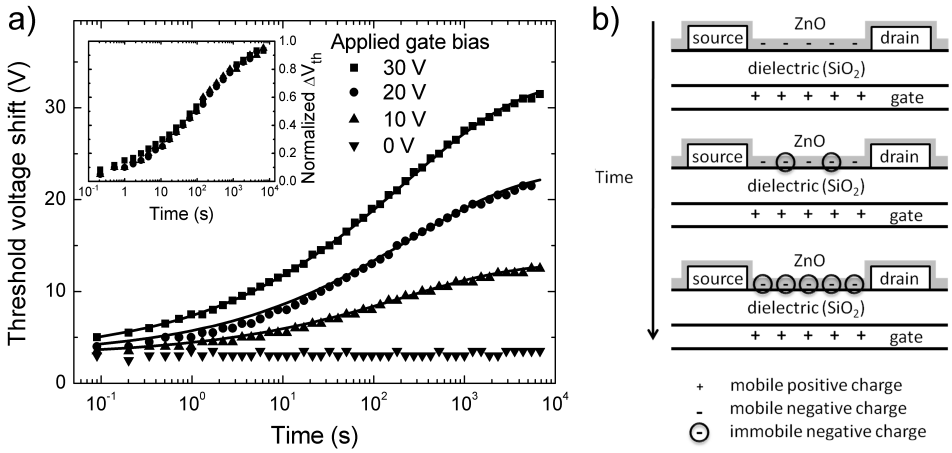

Figure 5.4: a) Threshold voltage shift as a function of time for various applied gate biases. The NO_2 concentration was 300 ppb. The data points were fitted to a stretched-exponential time dependence, Equation 5.1, as shown by the solid lines. The inset shows the threshold voltage shifts normalized to the applied gate bias. b) Schematic representation of the charge trapping process in a transistor. With time, mobile electrons are continuously trapped until the steady-state is reached and the gate bias is completely compensated by immobile trapped charges.

linear regime has no influence, in contrast with classical chemiresistors. A ZnO transistor was kept in NO_2 atmosphere and, as above, the current was measured as a function of time. At certain times the drain bias was grounded. Figure 5.5 shows a continuous current decrease, irrespective of the time that the drain bias was grounded, demonstrating that the drain bias can be disregarded. Implicitly it also shows that current itself is not the origin of the current decay. Therefore, contact degradation[42] can be ruled out as the sensing mechanism.

The temporal behavior was measured for various NO_2 concentrations using a single ZnO transistor. After each series of measurements the transistor was annealed at 150 °C in vacuum for 1 hour to recover the original 0 V threshold voltage. For each NO_2 concentration the threshold voltage shift was determined as a function of the stress time. Figure 5.6a shows the extracted threshold voltage shifts as a function of time and NO_2 concentration. For all concentrations, the threshold voltage shifts to the applied gate bias of 30 V. The main effect of exposing the transistor to different concentrations is the time dependence. The solid lines are a stretched-exponential fit to the data. For all concentrations a good agreement is obtained. The dispersion parameter β is almost unchanged. Figure 5.6b shows that the main change is in the characteristic relaxation time, which varies over orders of magnitude by changing the NO_2 concentration. The slope of

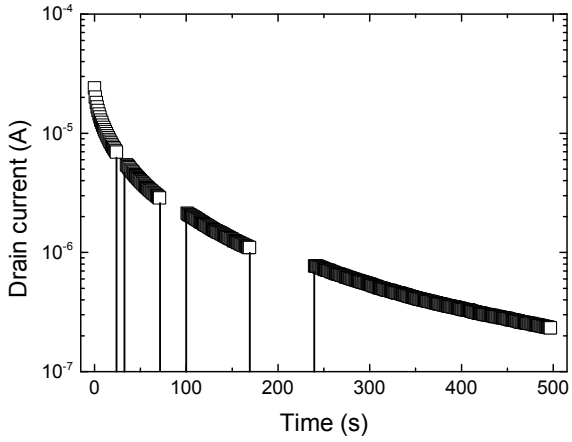

Figure 5.5: Drain current of a ZnO field-effect transistor under an applied gate bias of 30 V and drain bias of 2 V as a function of time. The NO_2 concentration was approximately 800 ppb. At certain times the drain bias was grounded.

the fit is unity; the relaxation time is inversely proportional to the NO_2 concentration. Finally it is noted that Figure 5.6 shows that extremely low NO_2 concentrations, down to the ppb level, can be detected.

Experimentally, a shift of the threshold voltage is found that can phenomenologically be described. To investigate the vast parameter space of field-effect transistors, the ZnO layer thickness was varied. For each thickness, the shift in threshold voltage was extracted and plotted in Figure 5.7a as a function of stress time. The solid lines are a fit to the data. A good agreement is obtained for all thicknesses. Again the change in dispersion parameter is negligible; the main effect is a change in relaxation time. Figure 5.7b shows that, within experimental accuracy, the relaxation time increases exponentially with layer thickness.

5.5 Rationalization of the temporal behavior

The experimental data can be summarized as follows. Without applied gate bias the transistors are stable in an NO_2 ambient. Hence doping of the ZnO semiconductor by oxidizing NO_2 can be disregarded. The current drops only when a positive gate bias is applied in an NO_2 ambient, regardless of the applied drain bias. The origin of the current drop is a shift in the threshold voltage. The shape of the transfer curve does not change, the mobility remains constant, and hence the material properties remain unaffected. Also

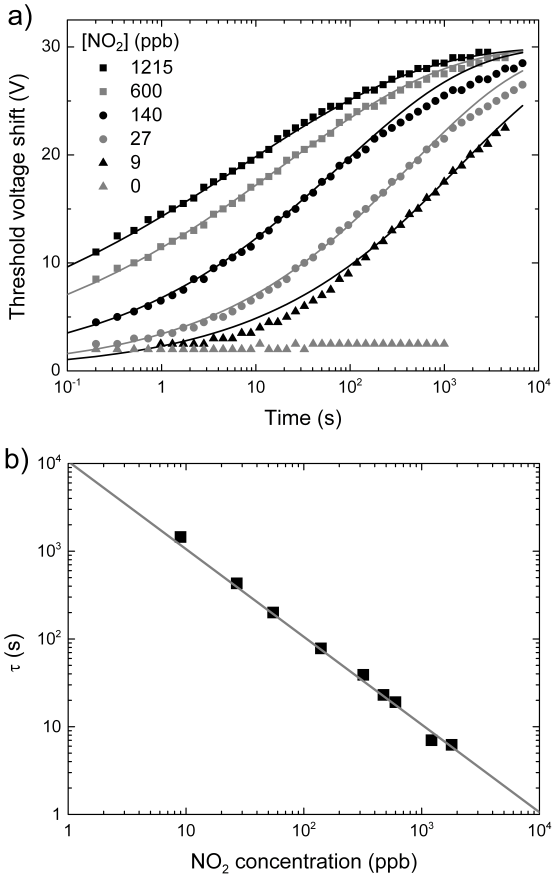

Figure 5.6: a) Threshold voltage shift of a ZnO transistor as a function of time upon exposure to different concentrations of NO_2. The continuously applied gate bias was 30 V. The extracted shifts were fitted to a stretched-exponential time dependence. b) Relaxation time, τ, as a function of the NO_2 concentration. The slope of the fit is unity.

contact degradation can be ruled out as the sensing mechanism because the current itself is not the origin for the current decay.

The threshold voltage shift is due to charge trapping mediated by the NO_2. The threshold voltage in a transistor is set by the flat band voltage, the difference in work function between the electrodes and the semiconductor. When a ZnO transistor is turned on electrons are accumulated. Some of them are trapped; the trapped charge themselves do not contribute to the current but are still part of the electrostatic charge that shield the gate voltage. The threshold voltage shifts by eQ_f/C_{ox} where e is the elementary charge, C_{ox} is the gate dielectric capacitance, and Q_f are the fixed charges.[43,44] A shift

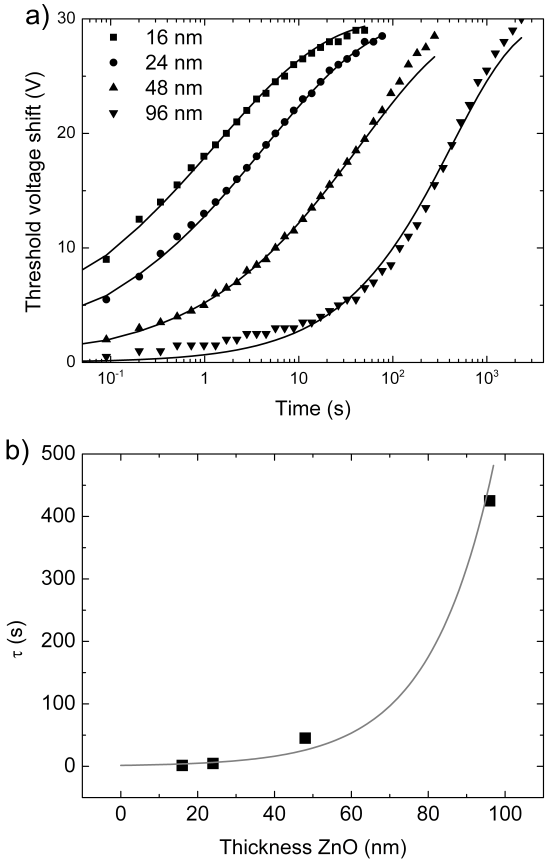

Figure 5.7: a) Threshold voltage shift as a function of time upon exposure to 3 ppm NO_2 for different ZnO layer thicknesses. The continuously applied gate bias was 30 V. The time dependence was fitted with a stretched-exponential. b) Relaxation times, τ, as a function of ZnO layer thickness. The solid line is an exponential fit to the data points.

of the threshold voltage with time is due to an increase of the fixed charges, Q_f. With time the effective gate field decreases and the threshold voltage saturates at the applied gate bias; no current flows and a steady-state is reached. It is tempting to assign the microscopic nature of the charged trap state directly to oxidized NO_2, but this requires further investigation and is irrelevant for the forthcoming description.

Experimentally it was determined that the threshold voltage shift as a function of time and partial NO_2 pressure can phenomenologically be described by a stretched-exponential time dependence. This stretched-exponential decay, called William-Watts or Kohlrausch relaxation, is observed in a wide class of disordered systems, such as relaxation of glasses

toward equilibrium, dielectric relaxation in a charge density wave system, and dispersive transport in photoconductors.[45] It holds for all dispersive transport processes in an exponential distribution of trap states.[46]

The measurement protocol used to determine the threshold voltage shift resembles that to determine the operational stability of amorphous semiconductors due to gate bias stress.[47,48] When a transistor is turned on for a long time, the threshold voltage shifts to the applied gate bias according to a stretched-exponential time dependence. Without NO_2, the ZnO transistor shift is small; the operational stability does not hinder the experiment. With NO_2 however, a dramatic shift of the threshold voltage was observed. The shift was orders of magnitude faster, but the functional dependence was the same. The microscopic mechanism for the operational stability in amorphous semiconductors is heavily debated, the origin could, for instance, be due to hydrogen diffusion.[49] That microscopic origin obviously does not apply here; hydrogen is absent. However, the formalism developed to describe the threshold voltage instability is generic and independent of the nature of the trap site.

Hydrogenated amorphous silicon contains metastable defect sites with a density, N_s. Upon stressing, metastable states are transformed into charged defects. The rate of defect formation is proportional to the rate of hydrogen diffusion. The conversion from metastable to charged defect states is large at the beginning of the experiment and zero at infinite time, $t \rightarrow \infty$. Consequently the change in defect density from equilibrium, ΔN_s, is given by:

$$\frac{d\Delta N_s}{dt} = -A\,D(t)\,\Delta N_s \tag{5.2}$$

where A is a proportionality constant and $D(t)$ is a time-dependent diffusion constant. Diffusion by trapping and detrapping of hydrogen atoms is usually modeled by a dispersive diffusion coefficient given by:[49]

$$D(t) = D_{00}(\omega t)^{-\alpha} \tag{5.3}$$

in which D_{00} is the microscopic diffusion constant, α is the temperature dependent dispersion parameter given by $\alpha = 1 - \beta$, and $\omega = 1/\tau$ is an attempt frequency. Solving Equation 5.2 with the boundary condition that the threshold voltage at infinite time is equal to the applied gate bias yields a stretched-exponential time relaxation for the threshold voltage shift in amorphous silicon transistors similar to Equation 5.1.

The analysis presented above can be applied to detection of NO_2 with ZnO transistors. Experimentally it was determined that the temporal behavior of the threshold voltage as a function of partial NO_2 pressure can phenomenologically be described by a stretched-

exponential decay as well. The characteristic relaxation time, τ, is inversely proportional to the partial NO_2 pressure and scales exponentially with the ZnO layer thickness. Both dependencies can be rationalized by assuming that the NO_2 mechanism relies on charge trapping with an anomalously wide distribution of trapping times due to a time-dependent diffusion coefficient. The dispersive diffusion coefficient is dominated by the density of NO_2 at the gate dielectric-ZnO interface. The partial NO_2 pressures are low (in the ppb range). Assuming a Langmuir isotherm for the NO_2 absorption, the density of absorbed NO_2 is then proportional to the partial vapor pressure. Simultaneously the density of absorbed NO_2 decreases exponentially with the ZnO layer thickness, with a decay constant determined by the morphology.[35] These realistic assumptions are sufficient to explain the experimentally observed dependencies of the characteristic time scale, τ on pressure and layer thickness, *i.e.*, $\tau \approx 1/p_{NO_2}$ and $\tau \approx \exp d_{ZnO}$.

Experimentally, a constant dispersion parameter, β, is observed that is given by T/T_0, in which T is the temperature and T_0 the isokinetic temperature characterizing the width of the density of trap states. The constant value of β might indicate that a single species is responsible for the charge trapping. The derivation above predicts an exponential dependence of τ on temperature and a linear dependence of β on T. Preliminary experimental results show, however, nearly temperature-independent parameters. The temperature dependence will be further investigated in Chapter 6.

5.6 Extension to organic semiconductors

The shift of the transfer curve for the ZnO field-effect transistors is towards the positive applied gate bias. ZnO is an *n*-type semiconductor. The shift originates from trapping of the majority charge carriers, *i.e.*, electrons, and therefore allows for a quantitative description of the trapping dynamics. To eliminate the possibility of a specific interaction between the NO_2 and ZnO as the sensing mechanism the semiconductor was varied. For completeness, air-stable *n*-type (perylene derivative ActivInk N1400, Polyera Corporation),[50] *p*-type (polytriarylamine Lisicon S1124, Merck Chemicals Ltd.),[51] and ambipolar (NiDT, bis[4-dimethylaminodithiobenzyl]-nickel, Sensient GmbH.)[52] organic semiconductors were studied. Layers were spin-coated on transistors test substrates. The shift of the transfer curves, as measured for the *n*-type and ambipolar semiconductors, shows that electrons are trapped. The temporal behavior is again in good agreement with a stretched-exponential decay, indicating that the same microscopic mechanism operates. For the *p*-type semiconductor the threshold voltage shifts to positive gate biases as well. Consequently the current at a fixed gate bias increases upon measuring in an NO_2 ambient. The shift in threshold voltage is again due to trapping of electrons and not

due to chemical doping. However, in a *p*-type semiconductor electrons are the minority carriers,[53] which hampers a quantitative interpretation of trapping dynamics.

Numerous investigations on the use of transistors with a large variety of semiconductors as potential NO_2 sensors have been reported. In all cases changes in current upon NO_2 exposure have been demonstrated, *i.e.*, a decrease for *n*-type semiconductors and an increase for *p*-type semiconductors. Many detection mechanisms have been reported, such as chemical doping of the bulk semiconductor, modulating the injection by varying the contact barrier, and depleting electrons from the charge transport layer. A detailed study of the dynamics of the threshold voltage shift has not yet been reported. The insights presented here rationalize previous results, yielding a generic description of the NO_2 detection mechanism in transistors. Furthermore, the detection mechanism and the derived measurement protocol can be used as a guideline to improve future NO_2 sensors.

5.7 Conclusions

NO_2 sensors are required to monitor and control the air-quality standards. Commercial sensors are typically chemiresistors, which monitor change in grain boundary resistances. In recent years, field-effect transistors have been suggested as an alternative sensing technology. In order to elucidate the NO_2 sensing mechanism, transistors with ZnO as a semiconductor were used. The electrical transport does not change when the transistor is exposed to NO_2. The transport only changes when in an NO_2 ambient a positive gate bias is applied. The current drops with time.

The current decrease of the transistor originates from a gradual shift of the threshold voltage. The temporal behavior can phenomenologically be described by a stretched-exponential time relaxation. The characteristic relaxation time is inversely proportional to the partial NO_2 pressure and scales exponentially with the ZnO layer thickness. NO_2 absorption is assumed to follow a Langmuir isotherm. A trapping and detrapping process of electrons can explain the stretched-exponential decay and the dependences on ZnO layer thickness and NO_2 concentration. NO_2 detection has been demonstrated with *n*-type, *p*-type, and ambipolar semiconductors. In all cases, a shift of the threshold voltage is obtained that is due to trapping of electrons. Hence, the description of the NO_2 detection in field-effect transistors is generic and can be used to improve future NO_2 sensors.

References

1. N. Barsan, D. Koziej, U. Weimar, *Sens. Actuators B* **2007**, *121*, 18.
2. N. Barsan, U. Weimar, *J. Electroceram.* **2001**, *7*, 143.

3. T. Inoue, K. Ohtsuka, Y. Yoshida, Y. Matsuura, Y. Kajiyama, *Sens. Actuators B* **1995**, *25*, 388.
4. J. W. Gardner, M. Craven, C. Dow, E. L. Hines, *Meas. Sci. Technol.* **1998**, *9*, 120.
5. M. Morvan, T. Talou, J. F. Beziau, *Sens. Actuators B* **2003**, *95*, 212.
6. S. Capone, S. Mongelli, R. Rella, P. Siciliano, L. Valli, *Langmuir* **1999**, *15*, 1748.
7. N. Kilinc, D. Atilla, S. Ozturk, A. G. Gurek, Z. Z. Ozturk, V. Ahsen, *Thin Solid Films* **2009**, *517*, 6206.
8. S. Paul, M. Joseph, *Sens. Actuators B* **2009**, *140*, 439.
9. C. Cantalini, L. Valentini, L. Lozzi, I. Armentano, J. M. Kenny, S. Santucci, *Sens. Actuators B* **2003**, *93*, 333.
10. I. Lundstrom, C. Svensson, A. Spetz, H. Sundgren, F. Winquist, *Sens. Actuators B* **1993**, *13*, 16.
11. A. Goldoni, L. Petaccia, S. Lizzit, R. Larciprete, *J. Phys. Condens. Mat.* **2010**, *22*, 8.
12. M. Bouvet, *Anal. Bioanal. Chem.* **2006**, *384*, 366.
13. L. Torsi, A. Dodabalapur, *Anal. Chem.* **2005**, *77*, 380A.
14. B. Li, D. N. Lambeth, *Nano Lett.* **2008**, *8*, 3563.
15. K. C. See, A. Becknell, J. Miragliotta, H. E. Katz, *Adv. Mater.* **2007**, *19*, 3322.
16. J. Huang, J. Miragliotta, A. Becknell, H. E. Katz, *J. Am. Chem. Soc.* **2007**, *129*, 9366.
17. H. E. Katz, *Electroanalysis* **2004**, *16*, 1837.
18. J. T. Mabeck, G. G. Malliaras, *Anal. Bioanal. Chem.* **2006**, *384*, 343.
19. S. Dutta, A. Dodabalapur, *Sens. Actuators B* **2009**, *143*, 50.
20. L. Torsi, A. Dodabalapur, L. Sabbatini, P. G. Zambonin, *Sens. Actuators B* **2000**, *67*, 312.
21. A. Das, R. Dost, T. Richardson, M. Grell, J. J. Morrison, M. L. Turner, *Adv. Mater.* **2007**, *19*, 4018.
22. F. Marinelli, A. Dell'Aquila, L. Torsi, J. Tey, G. P. Suranna, P. Mastrorilli, G. Romanazzi, C. F. Nobile, S. G. Mhaisalkar, N. Cioffi, F. Palmisano, *Sens. Actuators B* **2009**, *140*, 445.
23. G. Barillaro, A. Diligenti, A. Nannini, L. M. Strambini, E. Comini, G. Sberveglieri, *IEEE Sens. J.* **2006**, *6*, 19.
24. M. C. McAlpine, H. Ahmad, D. W. Wang, J. R. Heath, *Nat. Mater.* **2007**, *6*, 379.
25. M. Mattmann, T. Helbling, L. Durrer, C. Roman, C. Hierold, R. Pohle, M. Fleischer, *Appl. Phys. Lett.* **2009**, *94*, 183502.
26. T. Helbling, R. Pohle, L. Durrer, C. Stampfer, C. Roman, A. Jungen, A. Fleischer, C. Hierold, *Sens. Actuators B* **2008**, *132*, 491.
27. S. Peng, K. J. Cho, P. F. Qi, H. J. Dai, *Chem. Phys. Lett.* **2004**, *387*, 271.
28. T. Helbling, C. Hierold, L. Durrer, C. Roman, R. Pohle, M. Fleischer, *Phys. Status Solidi B* **2008**, *245*, 2326.
29. O. Kuzmych, B. L. Allen, A. Star, *Nanotechnology* **2007**, *18*, 375502.
30. J. Li, Y. J. Lu, Q. Ye, M. Cinke, J. Han, M. Meyyappan, *Nano Lett.* **2003**, *3*, 929.
31. P. Qi, O. Vermesh, M. Grecu, A. Javey, Q. Wang, H. Dai, S. Peng, K. J. Cho, *Nano Lett.* **2003**, *3*, 347.

32. J. Zhang, A. Boyd, A. Tselev, M. Paranjape, P. Barbara, *Appl. Phys. Lett.* **2006**, *88*, 3.

33. J. Kong, N. R. Franklin, C. W. Zhou, M. G. Chapline, S. Peng, K. J. Cho, H. J. Dai, *Science* **2000**, *287*, 622.

34. D. H. Zhang, Z. Q. Liu, C. Li, T. Tang, X. L. Liu, S. Han, B. Lei, C. W. Zhou, *Nano Lett.* **2004**, *4*, 1919.

35. R. Ferro, J. A. Rodriguez, P. Bertrand, *Thin Solid Films* **2008**, *516*, 2225.

36. C. Liewhiran, S. Phanichphant, *Sensors* **2007**, *7*, 185.

37. Z. H. Jing, J. H. Zhan, *Adv. Mater.* **2008**, *20*, 4547.

38. A. Bashir, P. H. Wobkenberg, J. Smith, J. M. Ball, G. Adamopoulos, D. D. C. Bradley, T. D. Anthopoulos, *Adv. Mater.* **2009**, *21*, 2226.

39. N. Barsan, U. Weimar, *J. Phys. Condens. Mat.* **2003**, *15*, R813.

40. D. Wilson, S. Hoyt, J. Janata, K. Booksh, L. Obando, *IEEE Sens. J.* **2001**, *1*, 256.

41. H. Sirringhaus, *Adv. Mater.* **2009**, *21*, 3859.

42. T. Richards, H. Sirringhaus, *Appl. Phys. Lett.* **2008**, *92*, 023512.

43. S. M. Sze, *Physics of Semiconductor Devices*, Wiley-Interscience, New York, **1981**.

44. K. P. Pernstich, S. Haas, D. Oberhoff, C. Goldmann, D. J. Gundlach, B. Batlogg, A. N. Rashid, G. Schitter, *J. Appl. Phys.* **2004**, *96*, 6431.

45. J. Kakalios, R. A. Street, W. B. Jackson, *Phys. Rev. Lett.* **1987**, *59*, 1037.

46. Y. F. Chen, S. F. Huang, *Phys. Rev. B* **1991**, *44*, 13775.

47. S. G. J. Mathijssen, M. Colle, H. Gomes, E. C. P. Smits, B. de Boer, I. McCulloch, P. A. Bobbert, D. M. de Leeuw, *Adv. Mater.* **2007**, *19*, 2785.

48. H. L. Gomes, P. Stallinga, F. Dinelli, M. Murgia, F. Biscarini, D. M. de Leeuw, M. Muccini, K. Mullen, *Polym. Adv. Technol.* **2005**, *16*, 227.

49. W. B. Jackson, J. M. Marshall, M. D. Moyer, *Phys. Rev. B* **1989**, *39*, 1164.

50. C. Piliego, D. Jarzab, G. Gigli, Z. H. Chen, A. Facchetti, M. A. Loi, *Adv. Mater.* **2009**, *21*, 1573.

51. J. Veres, S. D. Ogier, S. W. Leeming, D. C. Cupertino, S. M. Khaffaf, *Adv. Funct. Mater.* **2003**, *13*, 199.

52. E. C. P. Smits, T. D. Anthopoulos, S. Setayesh, E. van Veenendaal, R. Coehoorn, P. W. M. Blom, B. de Boer, D. M. de Leeuw, *Phys. Rev. B* **2006**, *73*, 205316.

53. A. Hepp, H. Heil, W. Weise, M. Ahles, R. Schmechel, H. von Seggern, *Phys. Rev. Lett.* **2003**, *91*, 157406.

Chapter 6

Dynamics of charge carrier trapping in NO_2 sensors based on ZnO field-effect transistors

Nitrogen dioxide (NO_2) detection with ZnO field-effect transistors is based on charge carrier trapping, as described in the previous chapter. In this chapter, the dynamics of charge trapping and recovery as a function of temperature are investigated by monitoring the threshold voltage shift. The threshold voltage shifts follow a stretched-exponential time dependence with thermally activated relaxation times. Activation energies of 0.1 eV for trapping and 1.2 eV for detrapping have been found. The attempt-to-escape frequency and characteristic temperature have been determined as 1 Hz and 960 K for charge trapping and 10^{11} Hz and 750 K for recovery, respectively. Thermally stimulated current measurements confirm the presence of trapped charge carriers with a trap depth of around 1 eV.

Published as part of:
A. Andringa, N. Vlietstra, E. C. P. Smits, M. Spijkman, H. L. Gomes, J. H. Klootwijk, P. W. M. Blom, D. M. de Leeuw, *Sensors and Actuators B: Chemical*, **2012**, *171-172*, 1172.

6.1 Introduction

NO_2 sensors are required to monitor and control air-quality. Commercial sensors are typically chemiresistors, which monitor changes in grain boundary resistances.[1–3] In recent years, field-effect transistors have been suggested as an alternative sensing technology.[4,5] A wide variety of semiconductors has been investigated for NO_2 sensing, such as amorphous organic semiconductors,[6,7] porous silicon,[8,9] silicon nanowires,[10] carbon nanotubes,[11–13] and metal oxide nanowires.[14] In all cases changes in current upon NO_2 exposure have been demonstrated. In addition, a high sensitivity down to 10 ppb NO_2 has been reported.

In the previous chapter, the detection mechanism has been elucidated using ZnO as a semiconductor.[15] Here a short summary will be given. The electrical transport does not change when the transistor is exposed to NO_2. However, the transport changes in an NO_2 ambient when a gate bias is applied. A current decrease in time is observed, originating from a shift of the threshold voltage towards the applied gate bias. The rate of the threshold voltage shift depends on the partial NO_2 pressure. Concentrations as low as 10 ppb can be detected.

A typical response of a ZnO transistor exposed to an NO_2 ambient is presented in the 3D plot of Figure 6.1. A constant gate bias was applied and after certain times the linear transfer curves were measured. The transfer curves shift with stress time in the direction of the applied gate bias. As a result, the source-drain current decreases and eventually becomes equal to the leakage current. The complete transfer curve shifts without changing shape, indicating that the mobility is not affected. The main effect of NO_2 exposure is a shift of the threshold voltage, V_{th}, here empirically defined as the onset of current flow.[16] In Figure 6.1, the grey line shows the threshold voltage shift towards the applied gate bias as a function of stress time. The origin of the shift is trapping of charge carriers.[15] The gate bias sets the total accumulated charge density. With time carriers are getting trapped, the density of free carriers decreases and the current drops. At infinite time all carriers are trapped, leading to a negligible current and a threshold voltage equal to the applied gate bias.

The change in current or threshold voltage with time depends on the NO_2 concentration. Hence a field-effect transistor can in theory be used as an NO_2 sensor. At room temperature however the charge trapping is irreversible. The time scale for release of charge carriers, or recovery, is larger than days. In other words, at room temperature the transistor is not a sensor but an integrator as it monitors the accumulation of trapped charge carriers. The response of a sensor to an analyte should be reversible, which implies that the time scales for trapping and release of charge carriers should be

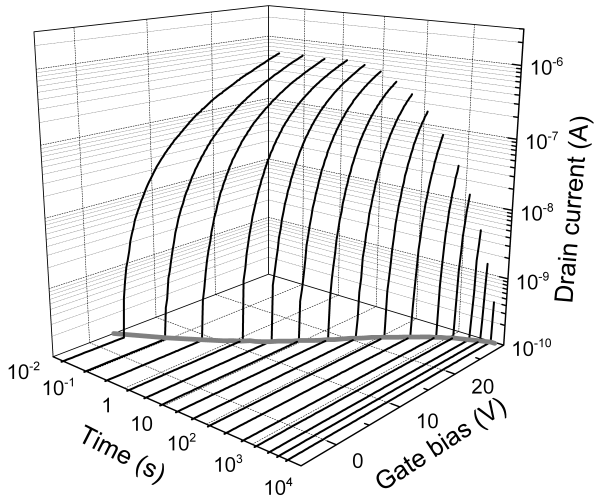

Figure 6.1: Transfer curves of a ZnO transistor exposed to 320 ppb NO_2, as a function of time under a continuously applied gate bias of 30 V. The linear transfer curves, represented by the black lines, were measured at a source-drain bias of 2 V. The grey line presents the threshold voltage as a function of stress time. The threshold voltage is empirically taken as the onset of current flow. The threshold voltage starts at about 0 V and shifts with time towards the applied gate bias of 30 V.

comparable. In this chapter, the dynamics of charge trapping and recovery as a function of temperature are investigated. At each temperature, the threshold voltage shifts follow a stretched-exponential time dependence. The relaxation times are thermally activated. The activation energies for trapping and release are independent of the NO_2 content and determined as 0.1 eV and 1.2 eV, respectively. The values for the corresponding attempt-to-escape frequencies and characteristic temperatures are discussed. The activation energy for charge release is also determined by thermally stimulated current (TSC) measurements, yielding a value of approximately 1 eV. The good agreement confirms that charge carrier trapping is the responsible mechanism of the threshold voltage shift.

6.2 ZnO transistor fabrication and characterization

The fabrication of unipolar *n*-type ZnO field-effect transistors has been described in detail in Chapter 2. The ZnO was applied using spray pyrolysis in ambient atmosphere.[17] XRD and AFM measurements showed that the 10 nm thick ZnO layers exhibited a microcrystalline morphology. To reduce the surface conductivity of the ZnO layer, a self-

assembled monolayer (SAM) of *n*-octadecyl phosphonic acid was applied from a 3 mM ethanol solution. The SAM was tested to have no effect on the sensitivity towards NO_2. The passivated ZnO transistors had a field-effect mobility of 0.1-2 cm^2/Vs and showed negligible hysteresis and high stability under gate bias stress.

The sensor's response to NO_2 was tested in the flow system described in Section 2.4. Gate bias stress measurements were carried out using a Keithley 2602A System Source Meter controlled by an in-house developed Labview program. To reduce charge trapping during the probing of the threshold voltage, the transfer curves were measured in less than a second by implementing a compliance stop at 100 nA. The ZnO transistors were annealed in vacuum at 150 °C in order to set the threshold voltage at 0 V before each measurement. As the threshold voltage, the gate bias at which the source drain current is 1 nA was taken. The TSC measurements were conducted in sampling mode with an Agilent 4155B Semiconductor Parameter Analyzer using an integration time of 0.5 seconds.

6.3 Temperature dependence of the threshold voltage dynamics

To investigate the trapping dynamics in a ZnO field-effect transistor in NO_2, stress and recovery measurements were performed as a function of temperature. The partial NO_2 pressure was fixed at approximately 1.1 ppm. Figure 6.2a shows the threshold voltage as a function of time during stress with a continuous applied gate bias at various temperatures. The solid lines are fits of the data to a stretched-exponential time dependence:

$$\Delta V_{\mathrm{th}}(t) = V_0 \left\{ 1 - \exp\left[-\left(\frac{t}{\tau} \right)^{\beta} \right] \right\} \tag{6.1}$$

where τ is a relaxation time, the dispersion parameter β equals to T/T_0, and $V_0 = V_{\mathrm{G}} - V_{\mathrm{th0}}$, where V_{G} is the applied gate bias and V_{th0} is the threshold voltage at the start of the experiment. A good agreement between measured data and the fits is obtained. The inset in Figure 6.2a shows the extracted dispersion parameter β as a function of temperature. A linear dependence is obtained with a characteristic temperature T_0 of 950 $\pm$ 75 K. The charge trapping hardly depends on temperature. The relaxation time for charge trapping, τ, is presented in Figure 6.3 as a function of reciprocal temperature (black). A straight line is obtained, showing that the relaxation time is thermally activated as:

$$\tau = \nu^{-1} \exp\left(\frac{E_{\mathrm{a}}}{k_{\mathrm{B}} T} \right) \tag{6.2}$$

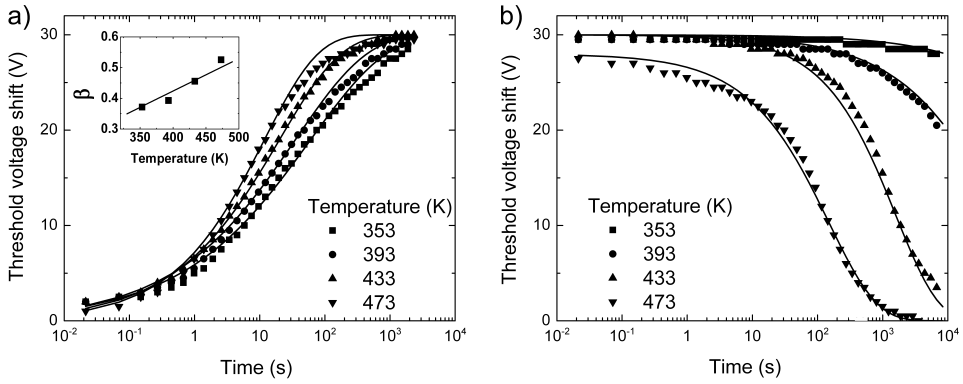

Figure 6.2: a) Threshold voltage shift of a ZnO field-effect transistor in NO_2 as a function of time under continuously applied gate bias of 30 V for several temperatures. The NO_2 concentration was approximately 1.1 ppm. The solid lines are fits with a stretched-exponential time dependence. The inset shows the dispersion parameter β as a function of temperature. b) Temperature dependence of the threshold voltage shift in recovery. The threshold voltage was first set at 30 V by applying a continuous gate bias in NO_2. With the NO_2 still present, the stressed transistors were recovered by grounding both gate and drain electrodes. The threshold voltage shift as a function of time was fitted with a stretched exponential.

with a small activation energy, E_a, of 0.10 ± 0.04 eV and an attempt-to-escape frequency, ν, of 1 ± 1 Hz. The attempt-to-escape frequency is defined as the phonon frequency multiplied by the probability of electron-phonon colocalization.[18]

The recovery of the threshold voltage was measured as a function of temperature. First the threshold voltage was set at 30 V by applying a continuous gate bias during NO_2 exposure. With the NO_2 still present, the stressed transistors were then recovered by grounding both gate and drain electrodes. The resulting threshold voltage shifts as a function of time for various temperatures are presented in Figure 6.2b. The solid lines are fits with a stretched-exponential time dependence (Equation 6.1). A good agreement is obtained. The characteristic temperature, T_0, is experimentally difficult to determine. A temperature around 750 K is estimated, comparable to the characteristic temperature extracted from the stress measurements. Figure 6.2b shows that the detrapping becomes much faster with increasing temperature. The extracted relaxation time, τ, is presented in Figure 6.3 as a function of reciprocal temperature (grey circles). The activation energy for detrapping amounts to 1.2 ± 0.1 eV and an attempt-to-escape frequency, ν, is derived of $10^{11\pm1}$ Hz.

In chapter 5, the relaxation time for charge trapping was found to be inversely proportional to the NO_2 pressure. At low NO_2 content the measurement takes hours to days. The long time scale hampers a reliable determination of the activation energy. Within

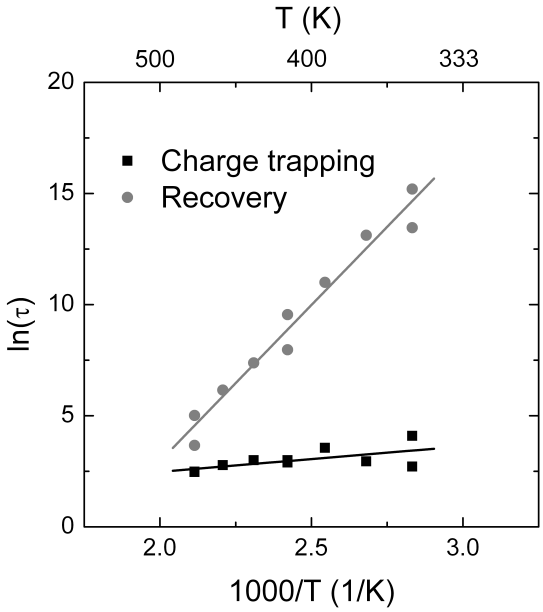

Figure 6.3: Relaxation times, τ, as a function of reciprocal temperature for charge trapping and recovery. The solid lines show that τ is thermally activated for both stress and recovery with activation energies of 0.1 eV and 1.2 eV, respectively. The attempt-to-escape frequencies are 1 Hz and 10^{11} Hz, respectively.

experimental accuracy however there is no change; the activation energy is expected to be independent on the partial NO_2 pressure. Recovery has been investigated with and without NO_2 present and furthermore in N_2 and compressed dry air. The activation energy for charge detrapping did not depend on the ambient.

In recovery the changes in threshold voltage shift due to the applied biases were investigated. For drain biases between 0 V and 20 V there was hardly any change in relaxation time. Similarly, the relaxation time was not affected by the value of the applied gate bias. Only the final threshold voltage changed; it saturated at the applied positive gate bias. Furthermore, the recovery could not be enhanced by putting the stressed transistor in deep depletion. A parameter that did influence the kinetics is the presence of light. It has been reported that the recovery properties of ZnO and SnO_2 sensors were improved remarkably by UV light irradiation.[19–21] Preliminary experiments showed that the relaxation time under UV illumination in the ZnO FET decreased by orders of magnitude.

The operational reliability of organic and inorganic field-effect transistors has been studied extensively. It has been reported that the time scale for recovery depends on the

extent of stressing.[22] In Figure 6.4 the recovery of the ZnO transistors as a function of the trapped charge density is investigated. Figure 6.4a shows the threshold voltage of a ZnO transistor in an NO_2 ambient as a function of stress time using a 30 V gate bias. After a certain stress time, varied between 1 second and 2000 seconds, the gate bias was set to 0 V and the recovery was measured. The solid lines in Figure 6.4b are fitted with a stretched-exponential time dependence. The relaxation times obtained did not depend on the history, *viz.* the trapped charge density. The reason is not yet understood.

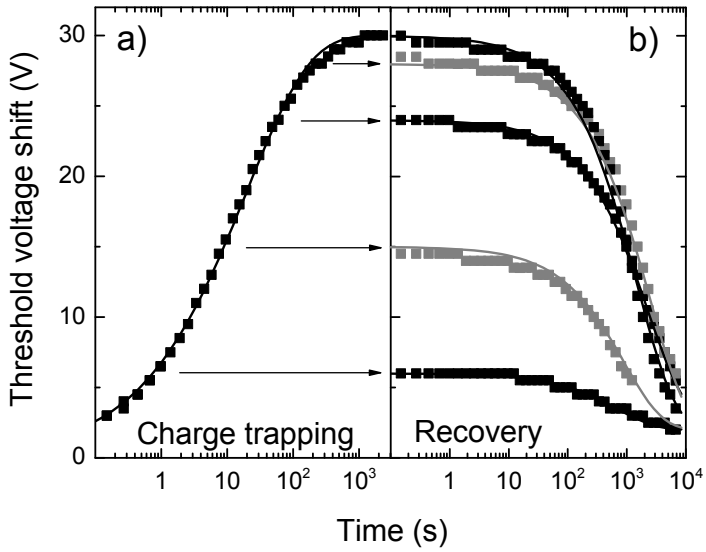

Figure 6.4: a) Threshold voltage of a ZnO field-effect transistor in NO_2 as a function of time under a continuously applied gate bias of 30 V at 433 K. b) After a certain stress time, varied between 1 second and 2000 seconds, the gate bias was set to 0 V and the recovery was measured, as indicated by the arrows. The solid lines are fitted with a stretched-exponential time dependence. The relaxation times obtained do not depend on the history.

6.4 Thermally stimulated current

To confirm the presence of trapped charge carriers and to derive the trap density and energetic depth, thermally stimulated current measurements were performed. The traps are filled by applying a bias while the temperature is such that the trapped carriers cannot be freed by the thermal energy. The temperature is then raised linearly. The liberated carriers contribute to the excess current, *i.e.* the external current minus the leakage current, until they recombine with carriers of the opposite type or join the equilibrium charge carrier distribution. This excess current, measured as function of temperature

during heating, is called the thermally stimulated current. For a single trap level, a TSC curve has one maximum whose position depends on capture cross section, heating rate and trap depth. Because detrapping currents are extremely small (pA), TSC can only be used with relatively insulating materials. Gate bias-stressed TFTs satisfy this requirement because they behave as normally-off or fully depleted TFTs. When performing TSC experiments the transistor is connected as a metal-insulator-semiconductor (MIS) capacitor.

A transistor is exposed to 1.1 ppm NO_2 and a gate bias of 30 V is applied for 1300 seconds. The transfer curve then is fully shifted to the applied gate bias; all induced accumulated carriers are trapped. The trap filling was performed at room temperature, detrapping can be disregarded (Figure 6.2b). The stressed transistor then is heated at a constant rate, $\beta_h = dT/dt$ up to 520 K. The trapped carriers are released and collected at the grounded source and drain electrodes. The temperature where a current peak occurs is related to the energetic depth of the trap state and the area under the peak is related to the trap density.

The TSC curves as a function of temperature are presented in Figure 6.5 for three linear heating rates, 0.8, 2.4 and 4.0 K/min. The TSC gradually increases with temperature until a peak maximum is observed at a particular temperature, T_m. Both the absolute value of the current and T_m increase with the heating rate as expected.

The density of filled traps, N_t, can be estimated from the time integrated TSC current as:

$$Q = eN_tA = \int Idt \tag{6.3}$$

where Q is the integrated total charge and A is the surface area between the electrodes. However, experimentally a linear dependence of the integrated current on the channel length is not observed, which indicates that the charges are extracted from an area larger than that between the electrodes. This conclusion is supported by the magnitude of the integrated current. The derived trapped charge density from the threshold voltage shift and the dielectric capacitance is 3×10^{12} charges per cm^2. From the TSC measurements an integrated total charge of 9×10^{-8} C is found. Assuming that only the area between the electrodes contributes to the TSC current, a trapped charge density of 6×10^{14} charges per cm^2 is calculated. The value is two orders of magnitude higher. The reason for this discrepancy lies in the fact that the entire substrate is coated with ZnO. Therefore, when the gate bias is applied, the entire ZnO/SiO_2 interface is charged. The charges in the vicinity of the TFT can diffuse to the contacts and the leads, where they are collected and measured in the external circuit. Based on the differences of the total amount of

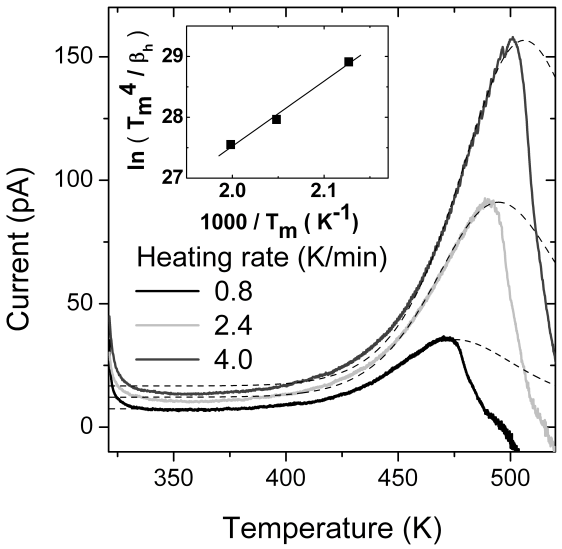

Figure 6.5: Thermally stimulated current as a function of temperature (TSC) obtained in a ZnO field-effect transistor exposed to 1.1 ppm NO_2. The traps were filled at 320 K by applying a 30 V gate bias for 1300 seconds and grounding the source and drain electrodes. After stressing, the source and drain current was measured while grounding all three electrodes. The heating rates, β_h, were 0.8, 2.4 and 4.0 K/min. The dashed lines are a fit to the data using the Cowell and Woods method. The inset presents a plot of $\ln(T_m^4/\beta_h)$ versus T_m^{-1}, where T_m is the temperature of the current maximum.

charge and the experimental device geometry, it is estimated that electrons can diffuse over distances in the order of 1 mm.

The extraction of the trap parameters from TSC measurements is not straightforward. The current temperature profile does not only depend on the density, depths and distribution of the traps, but depends also on the details of the charge transport such as charge carrier mobility and the occurrence of retrapping. The data was analyzed using several models, *viz*. the initial rise time method,[23,24] the heating rate method[25,26] and the curve fitting method by Cowell and Woods.[27,28]

The initial rise method is valid for all types of recombination kinetics and assumes that the current in the initial part of the curve, when the traps begin to empty, is exponentially dependent on temperature. This method is often used when the full TSC curve cannot be recorded or is distorted by other processes. The method only provides the trap depth and is usually less accurate than the other models. The initial TSC curves in Figure 6.5 follow a single exponential behavior with an activation energy of 0.72 eV.

A more reliable determination of the trap depth is obtained from the relation between

the heating rate, β_h, and the temperature of the peak maximum, T_m, as described by Blood and Orton in Equation 6.4:

$$\ln\left\{\frac{T_m^4}{\beta_h(T_m)}\right\} = \frac{\Delta E}{k_B T_m} + \ln\left(\frac{\Delta E}{\sigma\gamma k_B}\right) \tag{6.4}$$

in which ΔE is the trap depth, k_B is the Boltzmann constant, σ is the capture cross section and γ is a parameter depending on the effective mass. From the series of TSC scans at different heating rates in Figure 6.5, the peak temperatures are determined. The activation energy of the trap can then be obtained from a linear plot of $\ln(T_m^4/\beta_h)$ versus T_m^{-1}. The inset in Figure 6.5 shows that a straight line is obtained. The slope yields a value for the activation energy, ΔE, of 0.92 eV.

Finally, the complete TSC curves were fitted numerically using the classical approach of Cowell and Woods. The underlying assumption is monomolecular recombination of the charge carriers from a discrete set of traps with a single trapping level with a trap depth, ΔE, below the conduction band, with negligible retrapping. The current then follows from:

$$I = \frac{A\,\exp(-\Theta)}{\left(1 + B\,\exp(-\Theta)\Theta^{-2}\right)^2} + I_{off} \tag{6.5}$$

in which $A = n_t \tau e \mu \nu$, $B = \nu \Delta E/\beta_h k_B = \Theta_m^2 \exp\Theta_m$, $\Theta = \Delta E/k_B T$ and $\Theta_m = \Delta E/k_B T_m$. Here, n_t is the initial density of filled traps, τ is the average lifetime of a free carrier, μ is the mobility and ν is the attempt-to-escape frequency. The TSC curves can be fitted with four fitting parameters, T_m, A, ΔE and I_{off}. At high temperatures, when a significant number of traps is emptied, the conductivity of the TFT channel is partially restored and the associated background current severely distorts the measurements. For temperatures above the TSC peak the current cannot be treated solely as a detrapping current and the analysis is not possible. The best fits, shown in Figure 6.5 as dashed lines, show a good agreement with the measured currents. A trap depth, ΔE, of 1.0 eV is extracted comparable to the value derived by the method of Blood and Orton described above.

The apparent capture cross section, σ, given by the attempt-to-escape frequency divided by the thermal velocity, v_{th}, and the density of conduction band states, N_c, can also be estimated. When it is assumed that B equals $\nu \Delta E/\beta_h k_B$, an attempt-to-escape frequency, ν, can be derived in the order of 10^7 Hz. Using a thermal velocity of 10^7 cm/s[29] and $N_c = 10^{20}$ cm^{-3} an apparent cross section is derived in the order of 10^{-20} cm^{-2}. This small value might suggest that in order to capture a charge carrier, a repulsive barrier has to be surmounted.[25] However, the attempt-to-escape frequency

may be grossly underestimated because the fitting parameters are not independent. A more reasonable value for ν of 10^{11} Hz was obtained from the recovery measurements. By using this value the apparent cross section is estimated to be 10^{-16} cm^{-2} in line with a non-ionized, neutral trap.

6.5 Trapping mechanism

The different time constants for charge trapping and recovery can be explained by a deep trap filling process. The trap filling is essentially controlled by the number of unoccupied trap states and by the free carrier density induced by the gate bias, while the recovery is due to thermally activated emission. Initially, the transistor is not stressed. The traps are empty and the free carrier concentration is relatively high. The capture rate, c_n, is directly proportional to the free carrier concentration, n, and to the number of unoccupied states:[30]

$$c_n = n\{N_t[1 - f(E_t)]\}\,\nu_{th}\sigma \tag{6.6}$$

where N_t[1-f(Et)] gives the density of empty states, N_t is the density of filled traps, E_t is the trap depth and v_{th} the thermal velocity. As the threshold voltage shifts towards the applied gate bias, the free carrier density decreases which slows down the capture rate. Equation 6.6 shows that the capture rate is temperature independent. Only the thermal velocity depends on the square root of the absolute temperature. For the experimentally used temperature range of 300 K through 500 K, this dependence can be disregarded. In conclusion, the electron capture process is a temperature independent process, as is experimentally observed by an almost negligible activation energy of 0.1 eV.

The attempt-to-escape frequency of 1 Hz extracted from the threshold voltage dynamics upon charging is orders of magnitude lower than that of a typical phonon frequency of 10^{12} Hz. The reason is that depending on the microscopic mechanism, the extracted escape-frequency contains temperature independent prefactors. A rate determining step can be the diffusion of NO_2 at the gate dielectric-ZnO interface. In the previous chapter it was shown that the relaxation time τ is inversely proportional to the density of NO_2 at the gate dielectric-ZnO interface. This assumption explains the experimentally observed dependences of the relaxation time on NO_2 pressure and ZnO layer thickness, *viz.* $\tau \approx 1/p_{NO_2}$ and $\tau \approx \exp d_{ZnO}$.[15] Calculating a capture cross section while disregarding these prefactors leads to an unrealistically small value.

During recovery all free carriers are exhausted. Therefore, retrapping can be disregarded. The emission rate from the traps is now mostly determined by the trap depth and by the number of filled traps N_t. The emission rate is given by:[30]

$$e_n = [N_t f(E_t)]\, \nu_{th} \sigma n_i \, \exp\left(\frac{E_t - E_i}{k_B T}\right) \tag{6.7}$$

Contrary to the temperature independent charge carrier trapping, the recovery is strongly thermally activated. From the temperature dependent recovery experiments we have extracted an activation energy of 1.2 eV, in good agreement with the trap depth of 1.0 eV as derived from the TSC measurements. Detrapping can be described as a simple phonon assisted process. The value of the extracted attempt-to-escape frequency of about 10^{11} Hz is comparable to that of a typical phonon frequency and the capture cross section of 10^{-16} cm^{-2} is in line with that of a neutral trap.

6.6 Conclusions

A field-effect transitor with ZnO as a semiconductor was used to investigate the charge trapping dynamics in NO_2 ambient. The ZnO transistors are chemically stable in NO_2. The transport only changes when upon exposure to NO_2 the transistor is biased in accumulation; the threshold voltage shifts towards the applied gate bias. The origin of the shift is charge carrier trapping. The dynamics of trapping and recovery have been investigated as a function of temperature. The threshold voltage shifts for both trapping and recovery follow a stretched-exponential time dependence. The relaxation times are thermally activated. The activation energies for trapping and release are independent of the NO_2 content and have been determined as 0.1 eV and 1.2 eV, respectively. The attempt-to-escape frequency and characteristic temperature have been determined as 1 Hz and 960 K for charge trapping and 10^{11} Hz and 750 K for recovery.

To confirm the presence of trapped charge carriers and to determine the trap depth, thermally stimulated current measurements have been performed. The TSC curves have been analyzed, and a trap depth around 1 eV has been obtained. The value is in good agreement with the activation energy derived from the threshold voltage dynamics. Detrapping can be described as a simple phonon assisted process. The value of the extracted attempt-to-escape frequency of about 10^{11} Hz is comparable to that of a typical phonon frequency and the capture cross section of 10^{-16} cm^{-2} is in line with that of a neutral trap.

References

1. N. Barsan, D. Koziej, U. Weimar, *Sens. Actuators B* **2007**, *121*, 18.
2. N. Barsan, U. Weimar, *J. Electroceram.* **2001**, *7*, 143.
3. T. Inoue, K. Ohtsuka, Y. Yoshida, Y. Matsuura, Y. Kajiyama, *Sens. Actuators B* **1995**, *25*, 388.

4. L. Torsi, A. Dodabalapur, *Anal. Chem.* **2005**, *77*, 380A.
5. M. E. Roberts, A. N. Sokolov, Z. Bao, *J. Mater. Chem.* **2009**, *19*, 3351.
6. A. Das, R. Dost, T. Richardson, M. Grell, J. J. Morrison, M. L. Turner, *Adv. Mater.* **2007**, *19*, 4018.
7. F. Marinelli, A. Dell'Aquila, L. Torsi, J. Tey, G. P. Suranna, P. Mastrorilli, G. Romanazzi, C. F. Nobile, S. G. Mhaisalkar, N. Cioffi, F. Palmisano, *Sens. Actuators B* **2009**, *140*, 445.
8. G. Barillaro, A. Diligenti, A. Nannini, L. M. Strambini, E. Comini, G. Sberveglieri, *IEEE Sens. J.* **2006**, *6*, 19.
9. G. Barillaro, L. M. Strambini, *Sens. Actuators B* **2008**, *134*, 585.
10. M. C. McAlpine, H. Ahmad, D. W. Wang, J. R. Heath, *Nat. Mater.* **2007**, *6*, 379.
11. J. Kong, N. R. Franklin, C. W. Zhou, M. G. Chapline, S. Peng, K. J. Cho, H. J. Dai, *Science* **2000**, *287*, 622.
12. T. Helbling, R. Pohle, L. Durrer, C. Stampfer, C. Roman, A. Jungen, A. Fleischer, C. Hierold, *Sens. Actuators B* **2008**, *132*, 491.
13. O. Kuzmych, B. L. Allen, A. Star, *Nanotechnology* **2007**, *18*, 7.
14. D. H. Zhang, Z. Q. Liu, C. Li, T. Tang, X. L. Liu, S. Han, B. Lei, C. W. Zhou, *Nano Lett.* **2004**, *4*, 1919.
15. A. Andringa, J. R. Meijboom, E. C. P. Smits, S. G. J. Mathijssen, P. W. M. Blom, D. M. de Leeuw, *Adv. Funct. Mater.* **2011**, *21*, 100.
16. The difference between the switch–on voltage and the threshold voltage can be disregarded, since the shift of both parameters is equal.
17. A. Bashir, P. H. Wobkenberg, J. Smith, J. M. Ball, G. Adamopoulos, D. D. C. Bradley, T. D. Anthopoulos, *Adv. Mater.* **2009**, *21*, 2226.
18. D. A. Jones, J. U. Lee, *Nano Lett.* **2011**, *11*, 4176.
19. G. Y. Lu, J. Xu, J. B. Sun, Y. S. Yu, Y. Q. Zhang, F. M. Liu, *Sens. Actuators B* **2012**, *162*, 82.
20. J. D. Prades, R. Jimenez-Diaz, F. Hernandez-Ramirez, S. Barth, A. Cirera, A. Romano-Rodriguez, S. Mathur, J. R. Morante, *Sens. Actuators B* **2009**, *140*, 337.
21. E. Comini, G. Faglia, G. Sberveglieri, *Sens. Actuators B* **2001**, *78*, 73.
22. A. Sharma, S. G. J. Mathijssen, E. C. P. Smits, M. Kemerink, D. M. de Leeuw, P. A. Bobbert, *Phys. Rev. B* **2010**, *82*, 075322.
23. C. Casteleiro, H. L. Gomes, P. Stallinga, L. Bentes, R. Ayouchi, R. Schwarz, *J. Non-Cryst. Solids* **2008**, *354*, 2519.
24. R. Chen, Y. Kirsh, *Analysis of Thermally Stimulated Processes*, Pergamon Press, Oxford, 1st edition, **1981**.
25. P. Blood, J. W. Orton, *Rep. Prog. Phys.* **1978**, *41*, 157.
26. P. Blood, J. W. Orton, *The Electrical Characterization of Semiconductors: Majority Carriers and Electron States*, Academic Press, New York, **1992**.
27. M. Meier, S. Karg, K. Zuleeg, W. Brtting, M. Schwoerer, *J. Appl. Phys.* **1998**, *84*, 87.
28. T. A. T. Cowell, J. Woods, *British Journal of Applied Physics* **1967**, *18*, 1045.
29. S. Nakabayashi, A. Kira, M. Ipponmatsu, *J. Phys. Chem.* **1989**, *93*, 5543.
30. R. S. Muller, T. I. Kamins, *Device electronics for integrated circuits*, John Wiley & Sons, New York, 2nd edition, **1986**.

Chapter 7

Localizing trapped charge carriers in NO_2 sensors based on organic field-effect transistors

NO_2 detection with field-effect transistors relies on trapping of accumulated electrons, leading to a shift of the threshold voltage. To determine the location of the trapped electrons, different organic semiconductors are delaminated from the transistors with adhesive tape and the surface potential of the revealed gate dielectric is measured with scanning Kelvin probe microscopy. In this chapter, the trapped electrons are shown to be located not in the semiconductor but at the gate dielectric. The microscopic origin is discussed. Pinpointing the location paves the way to optimize the sensitivity of NO_2 field-effect transistor sensors.

Published as:
A. Andringa, W. S. C. Roelofs, M. Sommer, M. Thelakkat, M. Kemerink, D. M. de Leeuw, *Applied Physics Letters*, **2012**, *101*, 153302.

7.1 Introduction

The operating mechanism of NO_2 detection with a ZnO field-effect transistor has been examined in Chapter 5 and 6. In literature, a wide variety of semiconductors has been investigated, for example amorphous organic semiconductors,[1] carbon nanotubes,[2] and metal oxide nanowires.[3] In all cases, current changes upon NO_2 exposure have been demonstrated; *i.e.* a current decrease for *n*-type semiconductors and a current increase for *p*-type semiconductors. The current change is caused by a shift of the threshold voltage. This shift is due to fixed negative interface charges.[4] Hence, electron trapping is the generic mechanism for NO_2 detection in field-effect transistors.

An important factor for the sensing with a field-effect transistor is the gate bias, which sets the electron density. Without applying a gate bias transistors are stable in NO_2 ambient. With a positive gate bias however, electrons are accumulated that are trapped. At infinite time, all induced carriers have become immobile. Then the threshold voltage, here defined as the onset of current flow, is equal to the applied gate bias.

Despite many investigations on the mechanism of NO_2 detection with field-effect transistors the actual location of the trapped charges has remained unresolved. The electron trapping can be either in the bulk of the semiconductor or at the interface between the semiconductor and the gate dielectric. The exact location cannot easily be determined because the gate dielectric interface is buried under the semiconductor. Here, a very simple but effective technique of exfoliating the semiconductor with adhesive tape is used. The revealed gate dielectric is then accessible for characterization with scanning Kelvin probe microscopy (SKPM).[5,6] This technique was earlier successfully applied to reveal the location of trapped charges due to gate bias stress[7] and to link the threshold voltage shift in a transistor with a SAM-modified gate dielectric to charges trapped by the SAM, as described in Chapter 4.[8]

In this chapter, the exfoliation technique is applied using organic semiconductors. Organic semiconductors can be completely removed at once with adhesive tape. The transistors are charged by applying a gate bias in an NO_2 ambient. In situ measurements of the surface potential within the transistor channel are performed before and after exfoliation, using SKPM measurements. Comparison of the obtained surface potentials with and without the semiconductor present pinpoints the location of the trapped electrons at the gate dielectric interface. The location can be confirmed by using a variety of organic semiconductors.

7.2 Transistor fabrication and characterization

Field-effect transistors with a channel length of 10 μm and width of 10,000 μm were prepared as described in Chapter 2. To reduce gate bias stress and to facilitate the exfoliation process, the gate dielectric was passivated with vapor deposited hexamethyldisilazane (HMDS).

As a semiconductor N,N-dialkylsubstituted-(1,7&1,6)-dicyanoperylene-3,4:9,10-bis-(dicarboximide) derivative (Polyera ActivInk™ N1400) is used. This well-established air-stable *n*-type semiconductor exhibits charge carrier mobilities of 0.01-0.4 cm^2/Vs. The chemical structure is given as inset in Figure 7.1a. The semiconductor was blended with high molecular weight polystyrene (M_w 994,000 g/mol, Aldrich Chem. Co.). This high molecular weight polymer provides mechanical robustness to the film for improved exfoliation while the device performance is not compromised, as shown in recent studies on solution blending of organic semiconductors with organic insulating polymers.[9–13] Thin films were made by spin coating a blend containing 3.6 mg/ml of ActivInk N1400, filtered with a 5 μm filter, and 18 mg/ml polystyrene in chloroform. The perylene bisimide films were annealed in vacuum at 110 °C for one hour to remove residual water and solvents.

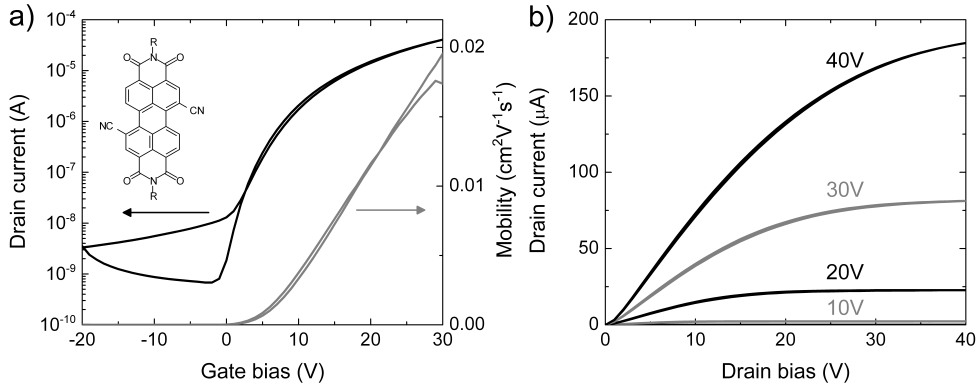

Figure 7.1: Electrical characterisation of the field-effect transistors using ActivInk N1400 blended with high molecular weight polystyrene. a) Transfer curve and mobility measured at a drain bias of 10 V. The inset shows the chemical structure of ActivInk N1400. b) Output characteristics measured at the indicated gate biases.

Electrical characterization of the blend was performed under vacuum using an HP 4155B semiconductor parameter analyzer. Figure 7.1a shows the transfer characteristics measured at a drain bias of 10 V. The extracted mobility was about 0.02 cm^2/Vs and the current modulation was over 4 decades, similar to the specifications of the pure ActivInk

N1400. In Figure 7.1b the output characteristics are shown.

Gas measurements were performed in a Teflon flow chamber equipped with feed-throughs for electrical contacting. NO_2 was supplied from a cylinder containing 3 ppm NO_2 in the carrier gas N_2 (Praxair). Additional nitrogen was used to further dilute the mixture. The concentration was regulated using two mass flow controllers.

7.3 Charge carrier trapping visualized by SKPM

First the charge trapping caused by NO_2 in perylene bisimide transistors is studied with the semiconductor still present. The pristine transistor in N_2 exhibits a 0 V threshold voltage, shown as the left transfer curve in Figure 7.2a. The transistor was then exposed to 1.5 ppm NO_2 and subjected for 60 seconds to a continuous gate bias of 5, 10, 15 or 20 V, while the source and drain electrodes were grounded. Transfer characteristics measured directly after the charge trapping are presented in Figure 7.2a. The threshold voltage has shifted completely to the applied gate bias after 60 seconds, indicating that all free charge carriers have been trapped. As a reference, a transistor was stressed without NO_2 for 60 seconds by applying a gate bias of 20 V. The resulting threshold voltage shift was then only 0.5 V. This small value rules out conventional gate bias stress as a cause for the threshold voltage shift on these time scales.

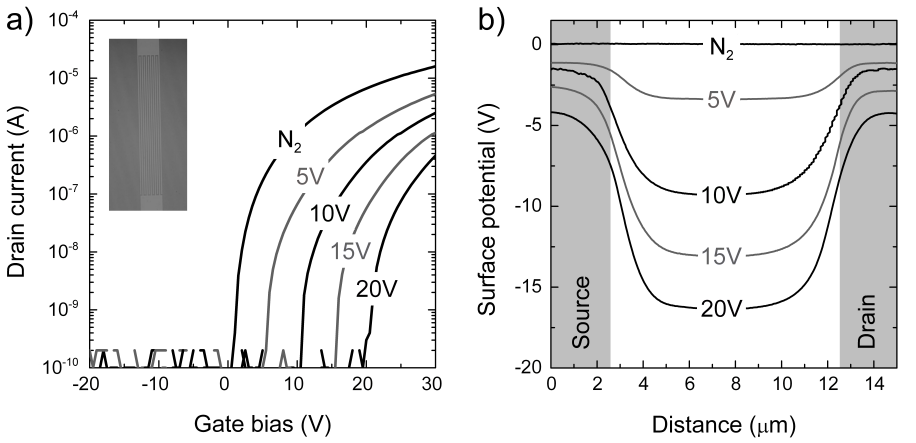

Figure 7.2: Charge carrier trapping in NO_2 ambient. a) Transfer curves of a field-effect transistor using as a semiconductor ActivInk N1400 blended with polystyrene. The gate sweep was recorded at a source-drain bias of 10 V. The left transfer curve corresponds to the pristine transistor in N_2. The transistor was then exposed to 1.5 ppm NO_2 and measured after application for 60 seconds of a positive gate bias of the indicated value. The threshold voltage shifts to the applied gate bias. The inset shows the perylene bisimide transistor. b) Potential profiles corresponding to the transfer curves of Figure 7.2a with ActivInk N1400 still present.

The charged transistors were analyzed with SKPM after measuring the transfer curves, allowing for a direct measurement of the surface potential. During the SKPM measurement, all electrodes were grounded. Perylene bisimide is a unipolar *n*-type semiconductor that does not support holes. Therefore the bulk perylene bisimide semiconductor cannot screen negative charges in the channel and SKPM can be used to visualize trapped negative charges. The local surface potentials in the channel are presented in Figure 7.2b. The pristine transistor with a 0 V threshold voltage shows a surface potential of around 0 V, which indicates that there are no immobile charges present. The values of the surface potentials measured in the channel of the charged transistors are negative and in correspondence with the value of threshold voltage. The good agreement indicates that the origin of the threshold voltage shift is trapped charges. The slight deviation originates from the finite spatial resolution of the SKPM system[14] and a decrease of the amplitude of the surface potential with time, especially in light. The nonzero potential measured on top of the source and drain contacts is again due to the spatial resolution.

7.4 Localization of trapped charge carriers

SKPM does not distinguish between electrons trapped in the bulk perylene bisimide semiconductor or at the gate dielectric interface. The experiment to find the exact location of the trapped charges is schematically depicted in Figure 7.3. The transistor with the trapped electrons exhibits a positive threshold voltage. The trapped charges are either in the semiconductor (I) or at the dielectric (II). In both cases, because there is no screening by the unipolar bulk *n*-type semiconductor, the trapped charges give rise to a negative surface potential with a magnitude equal to the value of the threshold voltage shift. A distinction can be made after exfoliation of the semiconductor. In case I, the exfoliation will remove the semiconductor including the trapped charge carriers. The resulting surface potential is then zero. In case II, the trapped charges will stay behind at the dielectric, and a negative surface potential remains.

An N1400 ActivInk transistor was exposed to NO_2 and a gate bias of 20 V was applied for 60 seconds. The surface potential, measured after charge trapping, is presented as the black curve in Figure 7.4a. The negative surface potential indicates the presence of trapped charges. To locate the charges, the experiment was repeated and the exfoliation technique was applied. The transistor was exposed to NO_2 using the same charge trapping procedure. However, then the semiconductor was delaminated after stressing using adhesive tape and tweezers, as shown in Figure 7.4b. The exposed gate dielectric was probed with SKPM. The potential profile after exfoliation is shown as the grey curve. The surface potentials are similar with and without semiconductor, which demonstrates that

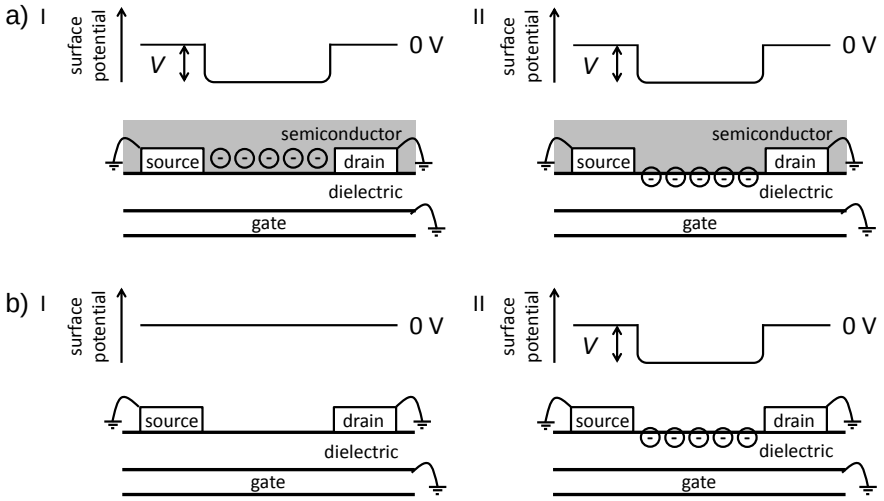

Figure 7.3: Schematic of the exfoliation experiment to localize trapped charge carriers. a) The transistor after applying a positive gate bias in NO_2. The trapped charges are either in the semiconductor (I) or at the interface with the gate dielectric (II). In both cases, when there is no screening, the trapped charges give rise to a negative surface potential equal to the threshold voltage shift. b) Potential profiles after the exfoliation process. In case I, the exfoliation will remove the semiconductor including the trapped charge carriers. The resulting surface potential is then zero. In case II, the trapped charges will stay behind at the gate dielectric interface and the negative surface potential remains.

the charges are not trapped in the semiconductor but trapped at the gate dielectric interface. The minor differences are due to recovery in ambient light when the semiconductor is still present.

It is well-known that exfoliation of two insulating materials can yield static charges by contact electrification or tribo-charging. However, as discussed previously in Chapter 4 the potentials measured here are not generated by the peeling process. Firstly the measured potentials are reproducible and secondly, the correspondence of the threshold voltage shift with the surface potential would be a rare coincidence.

The clear contrast in the optical photograph of Figure 7.4b shows that the exfoliation is almost complete. Investigation with AFM showed only minute residues, due to the phase separation between polystyrene and perylene bisimide.[15] The almost complete delamination is confirmed by photo-excitation experiments. With the semiconductor still present the surface potential and the threshold voltage are recovered by turning on the light of the microscope. In this case the trapped charges are released. However, after delamination the surface potential does not change. The photo-excited carriers cannot percolate to the contacts; the surface charges remain trapped.

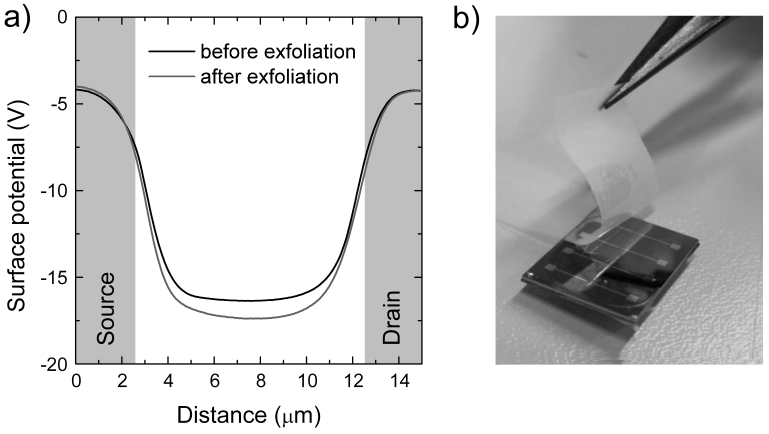

Figure 7.4: Comparison of surface potential before and after delamination. a) Surface potential profiles of an N1400 ActivInk transistor after applying a 20 V gate bias for 60 seconds in NO_2. The black curve shows the potential profile with the semiconductor still present and the grey curve shows the potential profile after delamination. The surface potentials are identical both with and without semiconductor, which demonstrates that the charges are not trapped in the semiconductor but trapped at the gate dielectric interface. b) The actual exfoliation process, using adhesive tape and tweezers.

7.5 Extension to other semiconductors

To support the assignment of trapped charges to the gate dielectric, the experiments were repeated with two other semiconductors, *viz.* poly(perylene bisimide acrylate) (PPerAcr, M_w 30,900 g/mol, PDI 1.86) and polytriarylamine (PTAA). Both semiconductors can be completely removed by delamination. The chemical structures are presented in the insets of Figure 7.5. The synthesis and properties of PPerAcr have been described previously.[16,17] Thin films were spincoated from a 5 mg/ml solution in chloroform and annealed for one hour at 210 °C. Field-effect transistors showed unipolar *n*-type characteristics with a mobility of about 4 x 10^{-4} cm^2/Vs. The threshold voltage shifted upon application of a gate bias in an NO_2 ambient. The kinetics were comparable to that of the low molecular weight perylene bisimide. The surface potentials before and after exfoliation are presented in Figure 7.5a. When the semiconductor is still present a large negative surface potential is measured. Because PPerAcr is a unipolar *n*-type semiconductor the trapped charges again cannot be screened. The surface potentials before and after exfoliation are similar confirming that the charges are trapped at the gate dielectric interface.

The experiments were repeated using PTAA, a well-established air-stable unipolar p-type semiconductor that exhibits charge carrier mobilities of 10^{-3} - 10^{-2} cm^2/Vs.[18] In

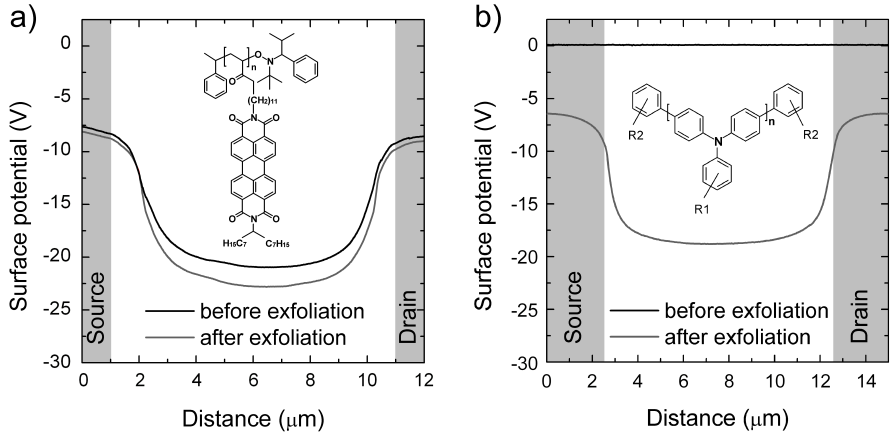

Figure 7.5: Exfoliation of different semiconductors. a) Surface potential profiles of *n*-type poly(perylene bisimide acrylate) (PPerAcr) field-effect transistor after applying a gate bias of 30 V for 60 seconds in NO_2. The chemical structure of PPerAcr is shown in the inset. The black curve shows the potential profile with the semiconductor still present and the grey curve shows the potential profile after delamination. b) Surface potential profiles of a *p*-type polytriarylamine (PTAA) field-effect transistor, after applying a gate bias of 20 V for 300 seconds in NO_2. The chemical structure of PTAA is shown in the inset. The black curve shows the potential profile with the semiconductor still present and the grey curve shows the potential profile after delamination.

an NO_2 ambient the threshold voltage of a PTAA transistor shifts towards the applied positive gate bias. The sign of the shift indicates the presence of trapped electrons. It is known that the barrier for electron injection into PTAA is too large to inject electrons within the time scale of the experiments.[19] The presence of the electrons could be due to surface conduction of the SiO_2 gate dielectric,[20] but the origin is not completely clear. Subsequently the surface potentials of the stressed transistor were measured before and after exfoliation. Figure 7.5b shows that the surface potential with the PTAA semiconductor still present is about 0 V throughout the channel. The trapped electrons didn't appear in the surface potential as they were screened by mobile holes in the *p*-type PTAA semiconductor. However, the trapped electrons were clearly visible as a large negative surface potential after peeling off the PTAA semiconductor. For both PPerAcr and PTAA AFM measurements showed that the semiconductor was completely removed by exfoliation. The magnitude of the surface potential showed a good agreement with the threshold voltage shift, pointing to electron trapping. SKPM measurements after exfoliation revealed that the trapped electrons are located at the gate dielectric.

7.6 Discussion

The microscopic mechanism of the charge trapping remains unknown. It is different from that in commercially available chemiresistors. When the resistor is exposed to NO_2, the NO_2 adsorbs on the surface of the metal oxide and redox reactions take place.[21] The extraction of electrons from the metal oxide results in an increase in the width of the depletion layer and an increase of the corresponding potential barriers at the grain boundaries. Then the resistance increases, or the current decreases. Transistors, however, are stable in NO_2 without applying a gate bias. The source-drain current only changes when a positive gate bias is applied, *i.e.* when electrons are accumulated. The origin is a shift in threshold voltage due to trapped charges at the gate dielectric and not due to a change in grain boundary resistance.

The detection mechanism in a transistor cannot simply be trapping of an electron by an isolated NO_2 molecule as might be expected from the large electronegativity of NO_2. This reduction process should take place no matter if the NO_2 molecule is in the bulk of the semiconductor or at the gate dielectric interface. However, the exfoliation experiments presented here have unambiguously shown that the trapped electrons are located at the gate dielectric. Furthermore, literature data show that the type of semiconductor does not play a role.[1–3] Current changes upon NO_2 exposure for a wide variety of semiconductors have been reported. Finally for the three semiconductors investigated here, the charge trapping dynamics are comparable. Apparently not the type of semiconductor but the nature of the gate dielectric is crucial. Here, SiO_2 passivated with HMDS is used. Preliminary experiments have shown that the trapping time may increase when the HMDS coverage increases. Experiments with organic gate dielectrics were inconclusive as the semiconductor could not selectively be delaminated. The use of various dielectrics to identify the microscopic nature of the trap is a topic of further research.

7.7 Conclusions

In summary, field-effect transistors have emerged as NO_2 sensors. When a positive gate bias is applied, electrons accumulate in the channel and they are getting trapped. At infinite time, all induced charge carriers are immobile, leading to a threshold voltage equal to the applied gate bias. To determine the location of the trapped electrons, the semiconductor was delaminated with adhesive tape and the surface potential of the revealed gate dielectric was measured with scanning Kelvin probe microscopy. The exfoliation technique can be utilized because the semiconductor is bound by weak van der Waals forces. Three different organic semiconductors have been used. The exfoliation

experiments have unambiguously shown that the trapped electrons are not located in the semiconductor but at the gate dielectric, here SiO_2. Pinpointing the location paves the way to optimize the sensitivity of NO_2 field-effect sensors.

References

1. A. Das, R. Dost, T. Richardson, M. Grell, J. J. Morrison, M. L. Turner, *Adv. Mater.* **2007**, *19*, 4018.
2. J. Kong, N. R. Franklin, C. W. Zhou, M. G. Chapline, S. Peng, K. J. Cho, H. J. Dai, *Science* **2000**, *287*, 622.
3. D. H. Zhang, Z. Q. Liu, C. Li, T. Tang, X. L. Liu, S. Han, B. Lei, C. W. Zhou, *Nano Lett.* **2004**, *4*, 1919.
4. S. M. Sze, *Physics of Semiconductor Devices*, Wiley-Interscience, New York, **1981**.
5. L. S. C. Pingree, O. G. Reid, D. S. Ginger, *Adv. Mater.* **2009**, *21*, 19.
6. V. Palermo, M. Palma, P. Samori, *Adv. Mater.* **2006**, *18*, 145.
7. S. G. J. Mathijssen, M. Spijkman, A. Andringa, P. A. van Hal, I. McCulloch, M. Kemerink, R. A. J. Janssen, D. M. de Leeuw, *Adv. Mater.* **2010**, *22*, 5105.
8. F. Gholamrezaie, A. Andringa, W. S. C. Roelofs, A. Neuhold, M. Kemerink, P. W. M. Blom, D. M. de Leeuw, *Small* **2012**, *8*, 241.
9. N. Stingelin-Stutzmann, E. C. P. Smits, H. Wondergem, C. Tanase, P. W. M. Blom, P. Smith, D. M. de Leeuw, *Nat. Mater.* **2005**, *4*, 601.
10. M. Madec, P. J. Smith, A. Malandraki, N. Wang, J. G. Korvink, S. G. Yeates, *J. Mater. Chem.* **2010**, *20*, 9155.
11. M. B. Madec, J. J. Morrison, V. Sanchez-Romaguera, M. L. Turner, S. G. Yeates, *J. Mater. Chem.* **2009**, *19*, 6750.
12. T. A. M. Ferenczi, C. Müller, D. D. C. Bradley, P. Smith, J. Nelson, N. Stingelin, *Adv. Mater.* **2011**, *23*, 4093.
13. X. R. Li, W. T. T. Smaal, C. Kjellander, B. van der Putten, K. Gualandris, E. C. P. Smits, J. Anthony, D. J. Broer, P. W. M. Blom, J. Genoe, G. Gelinck, *Org. Electron.* **2011**, *12*, 1319.
14. D. S. H. Charrier, M. Kemerink, B. E. Smalbrugge, T. de Vries, R. A. J. Janssen, *ACS Nano* **2008**, *2*, 622.
15. J. Smith, R. Hamilton, I. McCulloch, N. Stingelin-Stutzmann, M. Heeney, D. D. C. Bradley, T. D. Anthopoulos, *J. Mater. Chem.* **2010**, *20*, 2562.
16. S. Hüttner, M. Sommer, M. Thelakkat, *Appl. Phys. Lett.* **2008**, *92*, 093302.
17. S. M. Lindner, M. Thelakkat, *Macromolecules* **2004**, *37*, 8832.
18. J. Veres, S. Ogier, G. Lloyd, D. M. de Leeuw, *Chem. Mater.* **2004**, *16*, 4543.
19. J. J. Brondijk, M. Spijkman, F. van Seijen, P. W. M. Blom, D. M. de Leeuw, *Phys. Rev. B* **2012**, *85*, 165310.
20. S. G. J. Mathijssen, M. Kemerink, A. Sharma, M. Coelle, P. A. Bobbert, R. A. J. Janssen, D. M. de Leeuw, *Adv. Mater.* **2008**, *20*, 975.
21. A. Afzal, N. Cioffi, L. Sabbatini, L. Torsi, *Sens. Actuators B* **2012**, *171-172*, 25.

Chapter 8

Analytical model for functional NO_2 sensor

In the previous chapters, the operation mechanism of NO_2 detection with field-effect transistors was studied. The change in current or threshold voltage with time depended on the NO_2 concentration. Hence a field-effect transistor can in theory be used as an NO_2 sensor. In order to make a reversible sensor, the operating temperature should be increased. Therefore, the charge trapping dynamics in a ZnO field-effect transistor were investigated by performing stress and recovery measurements as a function of temperature. Here, the obtained functional dependence is used as input for an analytical model that predicts the sensor's temporal behavior. The model is experimentally verified. The perfect agreement between predicted and measured sensor response validates the methodology developed. The analytical description can be used to optimize the driving protocol. By adjusting the operating temperature and the duration of charging and resetting, the response time can be optimized and the sensitivity can be maximized for the desired partial NO_2 pressure window.

Published as part of:
A. Andringa, N. Vlietstra, E. C. P. Smits, M. Spijkman, H. L. Gomes, J. H. Klootwijk, P. W. M. Blom, D. M. de Leeuw, *Sensors and Actuators B: Chemical*, **2012**, *171-172*, 1172.
A. Andringa, E. C. P. Smits, J. H. Klootwijk, D. M. de Leeuw, *submitted to Sensors and Actuators B: Chemical*.

8.1 Introduction

A field-effect transitor with ZnO as a semiconductor was used in the Chapter 5 to investigate the charge trapping dynamics in NO_2 ambient. The transport changed when upon exposure to NO_2 the transistor was biased in accumulation; the threshold voltage shifted towards the applied gate bias. The origin of the shift is charge carrier trapping. The change in current or threshold voltage with time depended on the NO_2 concentration. Hence a field-effect transistor can in theory be used as an NO_2 sensor.

At room temperature however the charge trapping is irreversible. The time scale for release of charge carriers, or recovery, is larger than days. In other words, at room temperature the transistor is not a sensor but an integrator as it monitors the accumulation of trapped charge carriers. The response of a sensor to an analyte should be reversible. In Chapter 6, the dynamics of charge trapping and recovery were investigated as a function of temperature.

In this chapter, the experimentally determined threshold voltage dynamics are used as input for an analytical model that predicts the sensors temporal behavior. The response of the transistor can be calculated without any additional fit constants. Additionally, it is shown that a sensor protocol can be made that allows for a dynamic read-out of the partial NO_2 pressure in real time. The model is experimentally verified and used in the next chapter where the construction of a real-time sensor is described.

8.2 Charge trapping and recovery model

The charge trapping and recovery dynamics investigated in Chapter 5 and 6 can be summarized in the following analytical description. For a given NO_2 content the threshold voltage as a function of time during charging with a continuous applied gate bias at various temperatures follows a stretched-exponential time dependence:

$$\Delta V_{\mathrm{th}}(t) = V_0 \left\{ 1 - \exp\left[-\left(\frac{t}{\tau} \right)^{\beta} \right] \right\} \tag{8.1}$$

where τ is a relaxation time, the dispersion parameter β equals T/T_0, where T_0 is a characteristic temperature, and $V_0 = V_{\mathrm{G}} - V_{\mathrm{th0}}$, where V_{G} is the applied gate bias and V_{th0} is the threshold voltage at the start of the experiment. The relaxation time is thermally activated as:

$$\tau = \nu^{-1} \exp\left(\frac{E_{\mathrm{a}}}{k_{\mathrm{B}} T} \right) \tag{8.2}$$

where E_a is an activation energy, k_B the Boltzmann constant, and ν is the so-called attempt-to-escape frequency. For a given ZnO transistor the extracted parameters ν, T_0 and E_a are fixed. Upon varying the NO_2 pressure they do not change. Only the relaxation time depends on the NO_2 pressure as:

$$\tau \approx \frac{1}{p_{NO2}} \tag{8.3}$$

To quantitatively describe the NO_2 dependence, Equation 8.2 is therefore normalized as:

$$\tau = \frac{p^*_{NO2}}{p_{NO2}} \nu^{-1} \exp\left(\frac{E_a}{k_B T}\right) \tag{8.4}$$

where the normalization constant p^*_{NO2} is the partial pressure at which the frequency factor ν has been determined. Hence the complete charging dynamics, *viz.* the time, bias, temperature and NO_2 dependence, can be described by only three parameters, ν, T_0 and E_a, that are constant for a given transistor and a normalization factor for the NO_2 concentration. The extracted values for the present transistor are 11 Hz, 960 K and 0.1 eV, respectively. The underlying physics of the charge trapping process has been presented in Chapter 6. The parameters can be extracted from a single measurement set and then be used to quantitatively predict to complete charging dynamics.

Similarly the recovery can be described by a stretched-exponential time dependence with a thermally activated relaxation time, Equations 8.1 and 8.2. The relaxation time for recovery is independent of NO_2 content. Hence, the recovery can quantitatively be described with three parameters, ν, T_0 and E_a, that are constant for a given transistor. For recovery the extracted values are 10^{11} Hz, 750 K and 1.2 eV, respectively. The underlying physics of the recovery process has been presented in Chapter 6.

8.3 Functional NO_2 sensor

The model describes the change of the threshold voltage with time during charge trapping or recovery. The threshold voltage dynamics depend on the partial NO_2 pressure. Hence it seems obvious to make an NO_2 sensor. However, development of a sensor protocol that allows for a dynamic response is not trivial.

Assume that a continuous gate bias is applied. Then the threshold voltage shifts to the applied gate bias. The time needed to reach the final state is dependent on the partial NO_2 pressure. However, the final state itself is irrespective of the partial NO_2 pressure and the temperature. Hence, with a fixed continuous gate bias a transistor cannot be used as a sensor. The gate has to be turned on intermittently. When a gate bias is applied the transistor is charged and the threshold voltage shifts. When the transistor

is turned off by applying 0 V gate bias, the transistor recovers. By optimizing the cycle time and temperature, the final threshold voltage depends on the partial NO_2 pressure, yielding a real-time NO_2 sensor.

At room temperature a practical sensor cannot be realized. Figure 6.2b in Chapter 6 shows that the time to recover is then in the order of months. Because there is no relaxation, the sensor can only be used once and has to be reset into the pristine state after each measurement. For a dynamic read out the time scales for charging and recovery should be comparable, which can be achieved using higher operating temperatures.

The operating temperature and the cycle times can be optimized using the model as described in Section 8.2. The model uses the temporal behavior of the threshold voltage as a function of temperature and NO_2 pressure. Now the model is adapted to the measurement protocol including the charge trapping and recovery cycles. The response of the transistor can then be calculated analytically with experimentally determined parameters, without the use of any additional fit parameters.

The operation mechanism of the sensor is elucidated in Figure 8.1. For this example the driving protocol consists of repetitive cycles of 10 seconds charging at a gate bias of 30 V followed by 10 seconds recovering at a gate bias of 0 V, as presented by the dashed lines. The calculated threshold voltage response is shown for 100 and 1000 ppb NO_2. In the calculation, the bias, V_0, is taken as the difference between the applied gate bias and the threshold voltage at the start of the pulse. Figure 8.1a shows the calculated temporal behavior at room temperature. Upon application of the first gate bias pulse the threshold voltage shifts. Upon switching off the gate bias, the threshold voltage remains unchanged. At room temperature there is no recovery. In the next charging pulse the threshold shifts further. After infinite time, the threshold voltage is the same as the applied gate bias, irrespective of the NO_2 concentration. The only difference is the time needed to reach the final stage. The transistor acts as an integrator. The threshold voltage irreversibly saturates at the maximum applied gate bias. Figure 8.1b shows that by adjusting the operation temperature, a reversible response can be obtained. The threshold voltage shifts upward and downward upon charging and recovering. The selected driving protocol yields a dynamic response where the final threshold voltage is a function of the NO_2 pressure.

The calculated temporal behavior can be understood as follows. The driving force for the change in threshold voltage is the difference between gate bias and the threshold voltage at the start of the pulse. With an increasing number of cycles, the threshold voltage shifts to the applied gate bias. The driving force for charging decreases and, at the same time, the driving force for recovery increases. Figure 8.1b shows that after a number of cycles, ΔV_{th} charging is equal to ΔV_{th} recovery and a dynamic equilibrium

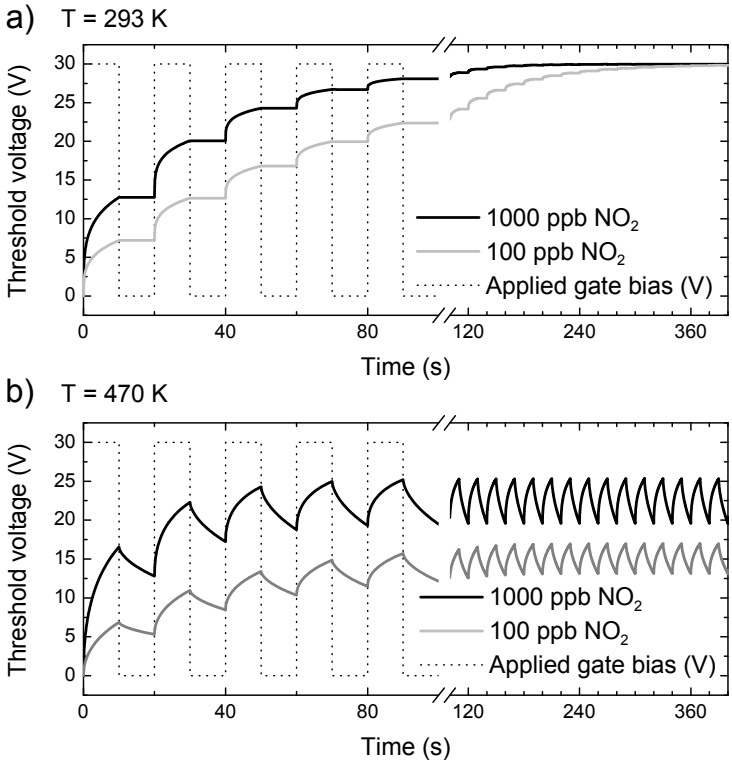

Figure 8.1: Calculated threshold voltage response to repetitive cycles of 10 seconds charging at gate bias 30 V followed by 10 seconds recovering at gate bias 0 V upon exposure to 100 and 1000 ppb NO_2. a) At room temperature there is no recovery and for every concentration the threshold voltage saturates at the maximum applied gate bias. b) At 470 K, the response is reversible and the threshold voltage shifts upward and downward upon charging and recovering. After a number of cycles, a dynamic equilibrium is reached. The maximum and minimum threshold voltages in equilibrium depend on the partial NO_2 pressure.

is reached. The maximum and minimum threshold voltages in equilibrium increase with partial NO_2 pressure. The concentration dependence follows from the fact that the rate of charging increases with NO_2 pressure while the rate of recovery remains the same.

Using this analytical description, the final threshold voltages for each driving protocol, temperature and NO_2 pressure can be calculated. As an example in Figure 8.2 the calculated maximum threshold voltages in equilibrium are presented as a function of NO_2 pressure for 420 K and 470 K. The driving protocol comprised a charge and reset time of 10 seconds each. The solid lines are calculated. The experimentally determined threshold voltages are presented by the squares. The values coincide with the calculated line. The perfect agreement verifies the methodology developed.

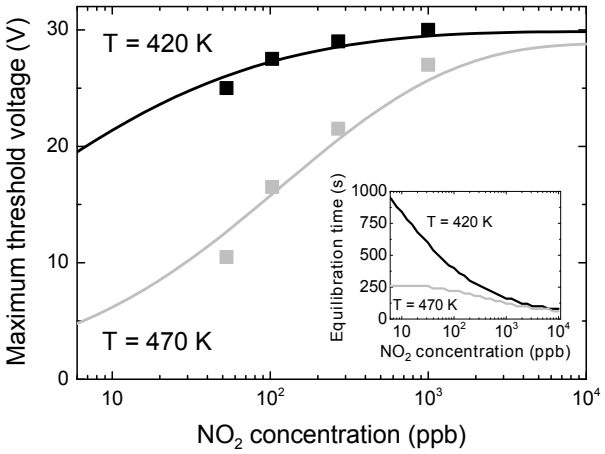

Figure 8.2: The maximum threshold voltages in equilibrium after charging as a function of NO_2 content for 420 and 470 K using the driving protocol as presented in Figure 8.1. The solid lines are calculated. The experimentally determined threshold voltages verify the calculations. In the inset the equilibration time is plotted for the specified concentration range.

The inset of Figure 8.2 shows the time calculated to reach dynamic equilibrium for the specified concentration range. The equilibrium is reached faster at higher temperatures and at higher NO_2 pressure. The reason can be that at higher pressures the rate of charging increases, leading to a faster equilibrium. The calculated equilibrium times have to be compared with those using a driving protocol with full recovery. At 470 K full recovery will take an hour which is incompatible with any practical sensor application. Here it is shown that full recovery is not needed to achieve an NO_2 concentration dependent response. A functional NO_2 sensor can be made by intermittently addressing the gate bias.

A practical sensor can only be obtained by measuring in real sensors working conditions; changing background conditions should not affect the sensor performance.[1] In the next chapter this topic will be addressed.

The analytical description can be used to optimize the driving protocol. The input parameters follow from the threshold voltage dynamics. Without any fit constants the sensor response can be predicted. By adjusting the driving protocol and operating temperature, the response time can be optimized and the sensitivity can be maximized for the desired partial NO_2 concentration window.

8.4 Conclusions

To predict the response of the ZnO field-effect transistors in NO_2, an analytical model has been made based on a charge trapping process. Using this phenomenological model, a sensor protocol has been developed for a functional NO_2 sensor that monitors the partial NO_2 pressure in real time. The gate bias is turned on intermittently for repetitive cycles of charging and resetting. To obtain comparable time scales for trapping and detrapping, higher operating temperatures are used. The threshold voltage shifts upward and downward upon charging and recovering. A dynamic equilibrium is reached where the final threshold voltage is a function of the partial NO_2 pressure. The operating temperature and the driving protocol were optimized using the analytically calculated temporal behavior of the threshold voltage. Only the experimentally determined parameters from the charging and recovery measurements were used as input. The methodology has been verified by comparing the calculated values with experimentally determining values. The perfect agreement validates the methodology developed.

References

1. N. Barsan, D. Koziej, U. Weimar, *Sens. Actuators B* **2007**, *121*, 18.

Chapter 9

Real-time NO_2 detection at ppb level with ZnO field-effect transistors

A functional real-time NO_2 sensor based on a ZnO field-effect transistor is presented. The dynamic response of the sensor is calculated using the analytical model described in Chapter 8. Only the experimentally determined parameters are used, there are no additional fit parameters. This phenomenological model based on charge trapping is implemented in the sensor protocol to create a hardware demonstrator sensor. The partial NO_2 pressure in ambient air can be monitored in real-time for concentrations as low as 40 ppb. The response is verified by simultaneously measuring the NO_2 content with a calibrated reference sensor. A perfect agreement between the measured and reference data is obtained, which validates the methodology. The sensor can be fabricated using standard IC technology, which can easily be miniaturized and used in handheld applications.

Published as part of:
A. Andringa, E. C. P. Smits, J. H. Klootwijk, D. M. de Leeuw, *submitted to Sensors and Actuators B: Chemical*.

9.1 Introduction

NO_2 sensors are required to monitor the air quality. An overview of the state-of-the-art performance of NO_2 sensing with chemiresistors based on metal oxides has recently been reported.[1] The operating temperature is typically around 200 °C, the response time is around 1 minute, the detection range in the order of 1-100 ppm NO_2, and the gas response as relative resistance change is around 10-100 % per ppm NO_2. Issues are long term stability, reliability and cross sensitivity for other gases especially oxygen, although the lack of selectivity can be overcome by using differential reading of multi sensor arrays.

In this chapter, a real-time NO_2 sensor is constructed based on a ZnO field-effect transistor (FET). In a FET, the current through the semiconductor can be altered over orders of magnitude. Hence, a sensor based on a FET is intrinsically more sensitive than a chemiresistor. In Chapter 5 it has been shown that the electrical transport does not change when the transistor is exposed to NO_2. However, the transport changes in an NO_2 ambient when a continuous gate bias is applied. This change can be monitored by shortly interrupting the continuous gate bias and measuring a transfer curve. As shown schematically in Figure 9.1a the transfer curve then shifts with time to the applied gate bias. The shape remains the same. The only change is the threshold voltage, here empirically taken as the onset of current modulation. The mechanism is due to gate bias controlled charge trapping of electrons at the gate dielectric ZnO interface.[2,3]

When the gate bias is turned off, the trapped electrons are thermally released and the threshold voltage recovers to its original value as schematically depicted in Figure 9.1b. The time constants for charging and recovery depend on temperature and partial NO_2 pressure. By intermittently turning the gate bias on and off, the threshold voltage shifts up and down and a dynamic equilibrium of the threshold voltage is reached. The gate bias pulse sequence and temperature can be chosen in such a way that the dynamic equilibrium of the threshold voltage depends on the partial NO_2 pressure, as depicted in Figure 9.1c. The field-effect transistor then functions as a dynamic real-time sensor.

In Chapter 8, the temporal behavior of the threshold voltage was modeled to set the operating temperature and cycle time to obtain a reversible sensor. The model uses as input the threshold voltage dynamics as a function of temperature and NO_2 pressure as measured in Chapter 6 for both charging and recovery. The response of the transistor can then be calculated with experimentally determined parameters, without the use of any additional fit parameters. Here, the phenomenological model is implemented into a hardware demonstrator sensor. The sensor is able to monitor the partial NO_2 pressure in air in real time. Concentrations as low as 40 ppb have been detected. The measurements are verified by comparing the sensor response with a calibrated commercial NO_2 detector.

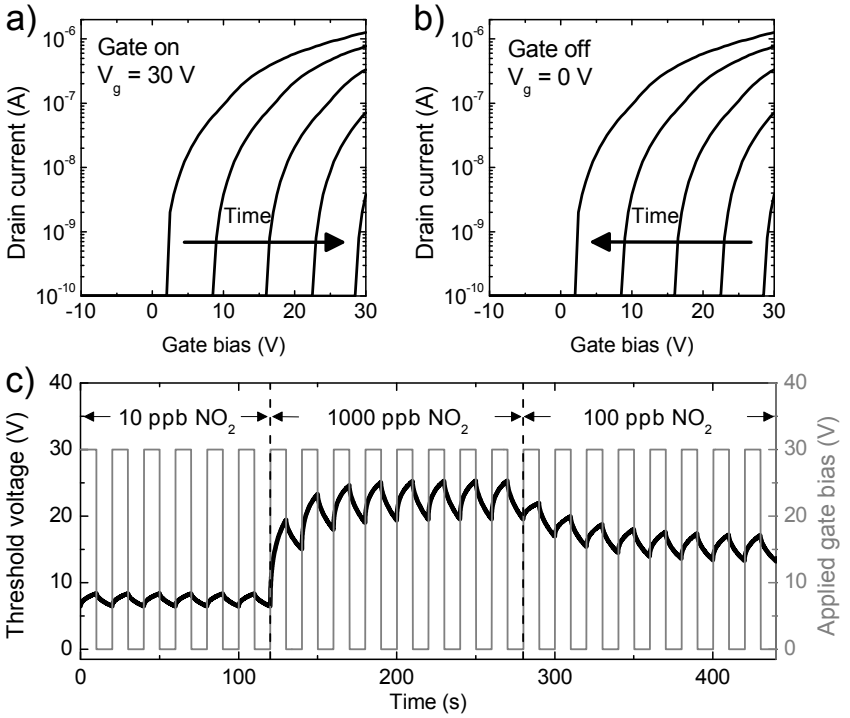

Figure 9.1: NO_2 sensing principle with a field-effect transistor. a) Schematically depicted transfer curves of a field-effect transistor in an NO_2 ambient upon charging. When a continuous gate bias of 30 V is applied, the transfer curve shifts with time, as indicated by the arrow. The threshold voltage starts at 0 V and saturates at the applied gate bias of 30 V. b) Recovery. When a zero V gate bias is applied, the threshold voltage shifts back with time to its original value. The temperature is set to obtain comparable time constants for trapping and recovery. c) Analytically calculated threshold voltage response as a function of time under intermittently applying a gate bias. The pulse profile is indicated in grey. The threshold voltage shifts up and downwards under charging and recovery. The dynamic equilibrium value is reached that depends on the partial NO_2 pressure. The NO_2 content is varied with time as indicated.

9.2 Sensor fabrication

The fabrication of unipolar *n*-type ZnO field-effect transistors has been described in detail in Chapter 2. Test substrates have been used as depicted on the photograph in Figure 2.1 of the same chapter. The ZnO was applied using spray pyrolysis in ambient atmosphere.[4] A solution of zinc acetate in methanol was nebulized and deposited on top of the transistor substrate, heated at 400 °C. XRD and AFM measurements showed that the 10 nm thick ZnO layers exhibited a microcrystalline morphology. To reduce the surface conductivity of the ZnO layer, a self-assembled-monolayer (SAM) of *n*-octadecyl

phosphonic acid was applied from a 3 mM ethanol solution. The SAM was tested to have no effect on the sensitivity towards NO_2. The passivated ZnO transistors had a field-effect mobility of 0.1-2 cm^2/Vs and showed negligible hysteresis and high stability under gate bias stress in inert atmosphere.

The sensor cell was fabricated from Teflon and equipped with feed-throughs for the electrical source, drain and gate contacts. For demonstration purposes a large box of 0.4 L was used. A photograph is presented in Figure 9.2a. The transistor was placed on to a ceramic plateau, fitting around a UHV Substrate Heater (HeatWave Labs, Inc.) and contacted. The temperature of the heater, electrically insulated from the transistor substrate by a locally thin ceramic sheet, was regulated using a Eurotherm 2416 controller and a Delta power supply. To maintain visibility of the sensor but to prevent UV irradiation from distorting the measurement, the polycarbonate lid of the flow cell was covered with an orange foil filtering UV light.

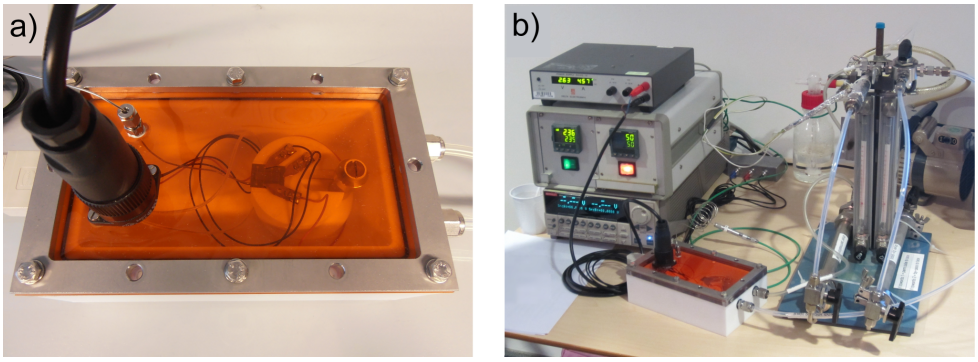

Figure 9.2: Sensor cell and system. a) Photograph of the Teflon sensor cell containing a ZnO field-effect transistor mounted on a heater. For demonstration purposes a large box was used. The lid of the flow cell was covered with an orange foil filtering UV light. b) Photograph of the complete sensor system containing the sensor cell, Teflon tubings, additional flow meters, NO_2 permeation tube, molsieves moisture filters, vacuum pump and peripheral electronics.

A block diagram of the gas flow system is depicted in Figure 9.3. Air flow was achieved by using a diaphragm vacuum pump. Teflon tubings were used. Ambient air was dried with molsieves (Type 3A, 8-12 mesh beads, Janssen Chimica). No other precautions were taken. The humidity of the exhausted air was measured to be 40 ppm, 0.2 % of the original humidity. As NO_2 source, a permeation tube was chosen with a calibrated emission rate of 369 ng/min at 45 °C and 200 sccm (Kin-Tek). The temperature of the permeation tube was regulated with a Eurotherm 2216e controller. A 4-port 2-way valve was applied to switch the NO_2 flow from the sensor cell to the bypass, while ensuring continuous flow over the permeation tube. Two mass flow controllers were

used to regulate the flow speeds through the sensor cell and the bypass. For calibrated measurements, the exhausted flow from the sensor cell was redirected to a commercial reference sensor based on chemiluminescence, an Eco Physics CLD 88p NO analyser. A gas converter (series CG, M&C TechGroup) was used to convert NO_2 catalytically to NO at 330 °C with a carbon molybdenum mixture. Electrical measurements were carried out using a Keithley 2602 System Source Meter controlled by an in-house developed Labview program as described in the next section. A photograph of the complete sensor system is presented in Figure 9.2b.

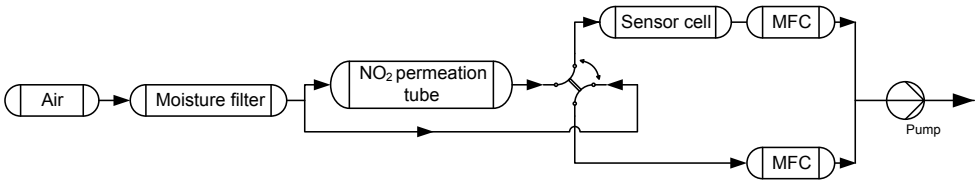

Figure 9.3: Block diagram of the gas flow system. An air flow was achieved by using a diaphragm vacuum pump. Ambient air was dried with molsieves. As an NO_2 source a permeation tube was used. A 4-port 2-way valve was applied to switch the NO_2 flow from the sensor cell to the bypass, while ensuring continuous flow over the permeation tube. With two mass flow controllers (MFC) the flow speeds were regulated through the sensor cell and the bypass.

9.3 Methodology and implementation

The complete sensor response as a function of time, bias, temperature and NO_2 can be described by the model for the temporal behavior of the threshold voltage that is described in Chapter 8. Only three parameters for charging and three parameters for recovery are used, ν, T_0 and E_a, and a normalization factor for the NO_2 concentration. To extract these input parameters for the model, charging and recovery measurements have been performed previously on ZnO field-effect transistors as a function of temperature and NO_2 pressure in Chapter 5 and 6. The parameters are constant for a given transistor. The extracted values for ν, T_0 and E_a for the present transistor are 11 Hz, 960 K and 0.1 eV for charging and 10^{11} Hz, 750 K and 1.2 eV for recovery. The measurement protocol, including the operating temperature, pulse time and duty cycle, was set using the sensor model in order to obtain a reversible sensor.

In the measurement protocol, the gate is intermittently turned on and off. The gate bias as a function of time is depicted as the grey block diagram, as shown in Figure 9.1c. The NO_2 concentration is varied with time from 10 ppb for the first 120 seconds, then 1000 ppb for the next 160 seconds and finally 300 ppb for 160 seconds. The black curve represents the threshold voltage as a function of time, calculated using Equations 8.1 and

8.2 or 8.4 for recovery or charging, respectively, given in Chapter 8. When a gate bias is applied the transistor is charged and the threshold voltage shifts. When the transistor is turned off, the transistor recovers. By pulsing the gate, the threshold voltage oscillates between a maximum voltage after charging and a minimum voltage after recovery. After a number of cycles, equilibrium is reached, in which the threshold voltage at the end of the charging pulse corresponds to the NO_2 concentration.

The flow chart to determine the NO_2 partial pressure from the dynamic electrical measurement of the sensor is presented in Figure 9.4. First a look up table is created. The three parameters describing the charging dynamics and the three parameters describing the recovery are used as input. Then the gate bias, the measurement protocol and temperature are set. For a given NO_2 pressure the threshold voltage is calculated as a function of time using Equations 8.1 and 8.2 or 8.4 for recovery or charging, respectively. In the calculation, a correction for probing the threshold voltage is implemented by taking into account the average charging and recovery time of the transfer curve measurement. The calculations are continued until convergence is reached indicating that the dynamic equilibrium has been obtained. The minimum and maximum extracted voltages are stored together with the set NO_2 pressure. The look up table is completed for the relevant NO_2 pressures and used as calibration curve.

The gate bias protocol and temperature chosen in the model are applied to the transistor. As measurement protocol we used 10 seconds gate bias pulse at 30 V for charging and 10 seconds at zero gate bias for recovery. The temperature was set at 200 °C. Based on the activation energies of charge trapping and release, experimentally determined in Chapter 6, the sensor is reversible at this temperature. The threshold voltage is experimentally extracted at the end of each charging and recovery pulse. To this end a transfer curve is recorded, by measuring the source-drain current with increasing gate bias at a low drain bias of 2 V. To reduce charge trapping during the probing of the threshold voltage, the transfer curves were measured using a short integration time and a compliance stop. The compliance stop was chosen at 100 nA, one decade above the noise of the off-current. The threshold voltage is extracted from the final gate bias by subtracting a fixed offset of 2 V. This offset was experimentally determined. The threshold voltage is translated into NO_2 concentrations using the lookup table. The discretisation of the threshold voltage sets the NO_2 concentration resolution. Finally, in the case that the transistor is sensitive to conventional gate bias stress, due to *e.g.* high back ground humidity, the look up table has to be adapted.

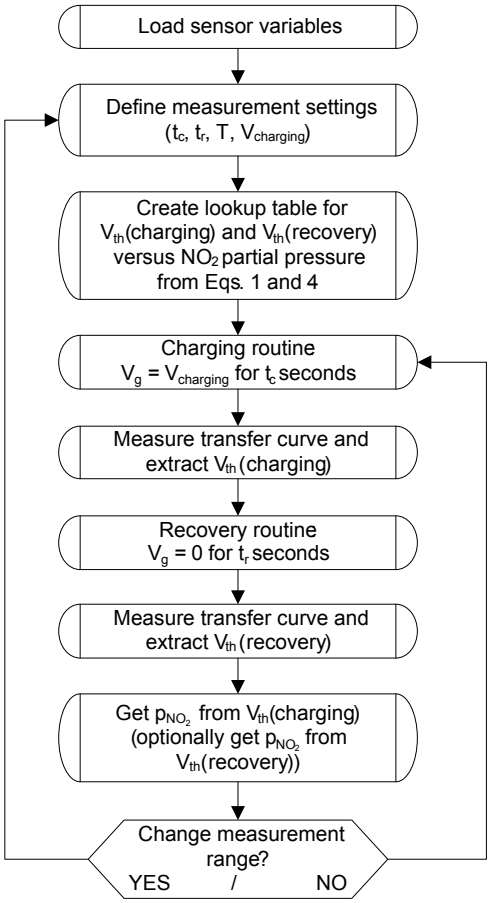

Figure 9.4: Flow chart to determine the NO_2 partial pressure from the electrical measurement of the sensor.

9.4 Sensor verification

To perform dynamic measurements a transistor was mounted in the sensor cell and the heater was set at 200 °C. The vacuum pump was turned on and the system was flushed with air for one hour. The measurement protocol was started and the permeation tube was heated to deliver a certain amount of NO_2. The signal from the sensor was processed as described above in Section 9.3 and recorded. The flow was switched intermittently from air with an air without NO_2. The NO_2 content was varied by adjusting the temperature of the permeation tube. The dynamic sensor response, the NO_2 concentration as a function of time, is presented in Figure 9.5 as the black curve.

The discretisation of the determined threshold voltage was set at 0.1 V which yields

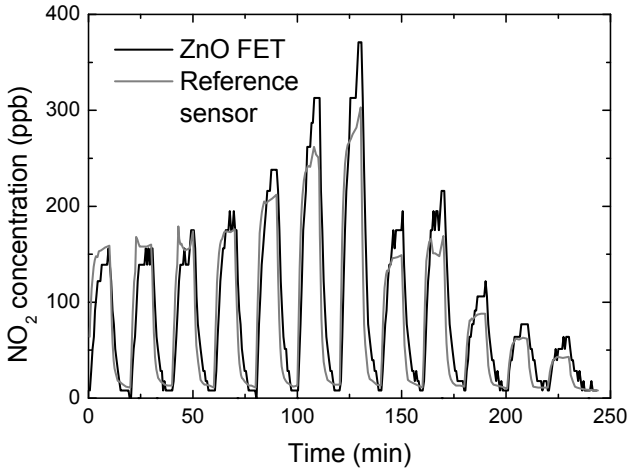

Figure 9.5: Sensor verification. The ZnO field-effect transistor sensor was heated, turned on and equilibrated. Then the NO_2 concentration was set by adjusting the temperature of the permeation tube. The flow was switched by the 4-port 2-way valve between sensor and bypass. The measured NO_2 concentration as a function of time is presented by the black line. The grey line represents the NO_2 content as simultaneously measured with a calibrated commercial reference sensor.

a resolution in NO_2 concentration of about 20 ppb. The lowest stable concentration achieved, set by the minimum quantity the permeation tube can deliver, was 40 ppb. The base line is about 10 ppb. This background is due to degassing of the Teflon walls of the sensor cell. The sensor is capable to detect these minimal changes in concentrations. The sensor was tested up to an NO_2 level of 1 ppm. Above 1 ppm, the threshold voltage is almost at the applied gate bias and the concentration can no longer be resolved. When a higher concentration range is desired, this saturation can be addressed by reducing the stress time or increasing the temperature.

The response time of the sensor at 200 °C lies between tens to hundreds of seconds. A new value of the threshold voltage is recorded every 22 seconds and compared to the calibration curve calculated in equilibrium. When the concentration in the system has changed, a new equilibrium has to be obtained by performing multiple measurement cycles. The equilibrium is reached faster at higher temperatures and higher NO_2 concentrations. The response time can be further optimized by adjusting the measurement protocol. However, there will be an inherent trade off between sensitivity and response time. In addition, the enormous dead volume of the current sensor cell prevents fast intermixing and limits the time resolution to around 100 seconds.

To verify the sensor response the NO_2 content was simultaneously measured with the Eco Physics NO sensor system. The recorded response is presented in Figure 9.5 as the grey curve. A good agreement between the measured and reference data is obtained, which validates the methodology used. Only a minor drift in the NO_2 concentration measured by the ZnO FET sensor was observed. The nature of the drift is unclear, possible reasons are slight variations in temperature or influence of the residual 40 ppm water.

The Eco Physics NO sensor is a compact expensive stand-alone system being used for environmental monitoring, industrial applications such as waste incineration, and exhaled breath analysis in hospitals. The price prohibits point of care use. Here it is shown that a similar performance can be obtained with a single field-effect transistor as NO_2 transducer. The transistor can be fabricated using standard IC technology, which can easily be miniaturized and used in a variety of handheld applications. The detection is not optical but only electrical. The implementation of the transducer can therefore lead to a major cost reduction of an NO_2 detection system.

The present sensor is sensitive to water: operating the sensor in wet air causes instability observed as a baseline drift. The absorption of water onto a gate dielectric such as SiO_2 in transistors causes threshold voltage shifts. Surface passivation of silanol groups by organic primers (e.g. HMDS or OTS) have been shown to strongly reduce these instabilities.[5] Optimization of the gate dielectric of the ZnO sensor might solve this problem, but experiments have not been attempted. Here molsieves were used to dry the ambient air. The water content was measured to be at most 40 ppm. This procedure is sufficient to yield a reliable sensor. Regeneration of the molsieves is needed after one week of full operation. The ZnO transistor was stable in NO. The sensor in combination with the developed measurement protocol did also not show baseline drifts in compressed dry air, indicating that the sensor is insensitive to oxygen. Although the sensor dynamics and extracted parameters were determined from measurements performed in nitrogen they could be successfully used to determine the NO_2 concentration in the ambient air dried by the molsieves. The shelf life of the sensors in ambient was found to be over a year and under dry conditions the sensor has been operated for a multiple days without any drop in performance.

9.5 Conclusions

A functional real-time NO_2 sensor based on a ZnO field-effect transistor was presented. The dynamic response of the sensor was calculated using a phenomenological charge trapping model, using only experimentally determined parameters. The parameters are

constant for a given transistor and have been determined previously. The analytical model was implemented in the sensor protocol to create a hardware demonstrator sensor. A sensor has been fabricated and tested. The NO_2 concentration was measured in real time. The response was verified by simultaneously measuring the NO_2 content with a calibrated reference sensor. The perfect agreement obtained validates the sensor and methodology.

The sensor is capable of detecting concentrations as low as 40 ppb. The sensor functions up to an NO_2 level of 1 ppm. When a different concentration range is desired, the detection protocol can be adapted. The sensor operates in ambient air. Apart from drying with molsieves, no further precautions were taken to purify the air, showing that the fabricated sensor is selective for NO_2. The real-time detection of low concentrations of NO_2 down to the ppb level sets a precedent for sensing with field-effect transistors.

Watch the movie of the sensor demonstrator on:
www.youtu.be/YAQ5vCIKP1E

References

1. A. Afzal, N. Cioffi, L. Sabbatini, L. Torsi, *Sens. Actuators B* **2012**, *171-172*, 25.
2. A. Andringa, J. R. Meijboom, E. C. P. Smits, S. G. J. Mathijssen, P. W. M. Blom, D. M. de Leeuw, *Adv. Funct. Mater.* **2011**, *21*, 100.
3. A. Andringa, N. Vlietstra, E. C. P. Smits, M. Spijkman, H. L. Gomes, J. H. Klootwijk, P. W. M. Blom, D. M. de Leeuw, *Sens. Actuators B* **2012**, *171-172*, 1172.
4. A. Bashir, P. H. Wobkenberg, J. Smith, J. M. Ball, G. Adamopoulos, D. D. C. Bradley, T. D. Anthopoulos, *Adv. Mater.* **2009**, *21*, 2226.
5. S. G. J. Mathijssen, M. Kemerink, A. Sharma, M. Coelle, P. A. Bobbert, R. A. J. Janssen, D. M. de Leeuw, *Adv. Mater.* **2008**, *20*, 975.

Summary

Fabrication of miniaturized, low-cost electronic gas sensors is important for a broad range of applications, such as in- and outdoor air quality monitoring, medical diagnostics and food quality control. Electronic sensors have the advantage that the signal can easily be read and recorded via low-end supporting electronics. Miniaturization allows for use in handheld detection systems. The sensor can, for example, be integrated in a mobile phone and be used to test the owner's breath alcohol content or bad breath.

The electronic sensor that is studied in this thesis is based on a field-effect transistor. The transistor is a key component in electronic circuits and acts as a micro-electronic switch. In a field-effect transistor the semiconductor is contacted by two electrodes, the source and the drain. The third electrode, the gate, is electrically insulated from the semiconductor by a dielectric layer. The current through the semiconductor can be modulated by orders of magnitude by adjusting the bias applied to the gate. Due to this current modulation, a sensor based on a field-effect transistor is intrinsically more sensitive than commercially available resistive sensors. The key device parameters of the field-effect transistor, such as the mobility and the threshold voltage, can be used to characterize the sensor response.

An interesting application area for field-effect transistor based sensors is the detection of nitrogen oxides, NO_x. Nitrogen oxides are released by the combustion of fossil fuels, for example by cars, trucks, buses and power plants. These environmental pollutants play a major role in the formation of ozone, acid rain and smog. Nitrogen dioxide, NO_2, is used as the indicator for the larger group of NO_x and is the component of greatest concern. Inhalation of NO_2 has been linked to adverse respiratory effects such as airway inflammations. Real-time monitoring of NO_2 is therefore of utmost importance

for public health and environmental safety. In this thesis, the operational mechanism of NO_2 detection with field-effect transistors is investigated and the obtained insights are used to develop a sensitive, real-time NO_2 sensor.

Detection of nitric oxide, NO, in exhaled breath can be used to identify an infection of lung tissue. The NO level in exhaled breath increases three to fivefold a few days before an asthma attack. In Chapter 3, an NO sensor is described based on a self-assembled monolayer field-effect transistor (SAMFET). A SAMFET based sensor is highly sensitive because the analyte and the active channel are separated by only one monolayer. The sensor is functionalized for direct NO detection using iron porphyrin receptors. Upon exposure to NO, a threshold voltage shift towards positive gate biases is observed. It is argued that the threshold voltage shift is due to trapping of charges. The sensor response is examined as a function of NO concentration. Extremely high sensitivity is demonstrated by detection of concentrations NO in the low parts per billion range.

A change of the threshold voltage is observed as well in organic field-effect transistors with a specific self-assembled monolayer (SAM) on the gate dielectric. The sign of the threshold voltage depends on the chemical nature of the SAM. In Chapter 4, scanning Kelvin probe microscopy in combination with exfoliation of the semiconductor is used to investigate the origin of the threshold voltage shift. The surface potentials of the revealed SAMs are shown to perfectly agree with the threshold voltages measured before delamination. This demonstrates that the threshold voltage shift is due to charge trapping at the SAM.

In Chapter 5, zinc oxide field-effect transistors are investigated as NO_2 sensors. It is shown that upon application of a positive gate bias during NO_2 exposure, the threshold voltage shifts towards that applied gate bias. The dynamics of the shift under prolonged gate bias are evaluated at room temperature as a function of the NO_2 concentration and ZnO layer thickness. The temporal behavior can be described by a stretched-exponential relaxation. A mechanism for NO_2 detection involving charge carrier trapping is proposed. The generic nature of the detection mechanism is illustrated by demonstrating similar sensor responses using different semiconductors.

A requisite for a real-time sensor is reversibility. During NO_2 exposure, the threshold voltage shifts due to gate bias induced electron trapping. When the gate bias is turned off, the trapped electrons can be thermally released. In Chapter 6, the dynamics of charge trapping and recovery are presented as a function of temperature. The complete charging and recovery dynamics can be described by a stretched-exponential time dependence with three parameters for each process: an activation energy, an attempt-to-escape frequency and a characteristic temperature. The extracted activation energy for recovery points to deep traps around 1.2 eV. The presence of trapped charge carriers and the trap depth

are verified with thermally stimulated current measurements.

The location of the trapped electrons in NO_2 sensors based on organic field-effect transistors is studied in Chapter 7. Three different organic semiconductors are used. Surface potential measurements before and after exfoliation of the semiconductor reveal that the charges are not in the semiconductor but at the gate dielectric, here SiO_2. Pinpointing the location paves the way to optimize the sensitivity of NO_2 field-effect transistor sensors.

In Chapter 8, the obtained fundamental insights into the detection mechanism are translated to an analytical model that is used to calculate the dynamic response of the sensor. Only the three experimentally determined parameters are used, there are no additional fit parameters. Based on this phenomenological model, a sensor protocol is developed for a functional NO_2 sensor that monitors the NO_2 concentration in real time. The gate bias is turned on intermittently at elevated operating temperatures in order to make the sensor reversible. The model is experimentally verified and can be used as a tool to optimize the sensor. By for example adjusting the operating temperature or the duration of charging and recovery, the response time can be optimized and the sensitivity can be maximized for the desired NO_2 concentration range.

Finally, we developed a sensitive, real-time and functional NO_2 sensor prototype based on a ZnO field-effect transistor, as presented in Chapter 9. The analytical model is implemented into the sensor protocol. The NO_2 concentration in dried ambient air is monitored for concentrations down to 10 ppb. The response is verified by simultaneously measuring the NO_2 concentration with a calibrated reference sensor. A good agreement between the measured and reference data is obtained, which validates the sensors performance and methodology. The sensor can be fabricated using standard IC technology, which can easily be industrialized and used in handheld applications.

Samenvatting

Kleine en goedkope elektronische gassensoren kunnen worden ingezet voor allerlei toepassingen, zoals het meten van de luchtkwaliteit in de binnen- of buitenlucht, het stellen van medische diagnoses of het bewaken van de voedselkwaliteit. Een elektronische sensor heeft als voordeel dat de meetresultaten elektrisch kunnen worden uitgelezen. Bovendien zijn ze, dankzij hun kleine formaat, uitermate geschikt voor draagbare detectiesystemen. Zo kan de sensor bijvoorbeeld geïntegreerd worden in een smartphone en gebruikt worden om een alcohol promillage te bepalen of op slechte adem te testen.

De elektronische sensor die onderzocht wordt in dit proefschrift is gebaseerd op een veld-effect transistor. De transistor is een belangrijk element in elektronische circuits en gedraagt zich als een schakelaar. Twee elektrodes van de veld-effect transistor, de 'source' en de 'drain', staan in direct contact met de halfgeleider. De derde elektrode, de 'gate', is elektrisch geïsoleerd van de halfgeleider door een diëlektricum. De stroom door de halfgeleider kan aan en uit worden gezet door de spanning op de gate aan te passen. Doordat het verschil in stroom tussen 'aan' en 'uit' groot is, is een sensor die gemaakt is van een veld-effect transistor veel gevoeliger dan bestaande weerstandsensoren.

Een interessante toepassing voor op veld-effect transistor gebaseerde sensoren is de detectie van stikstofoxiden, NO_x. Stikstofoxiden komen vrij bij de verbranding van fossiele brandstoffen, bijvoorbeeld in auto's, bussen en elektriciteitscentrales. Ze spelen een belangrijke rol bij luchtvervuiling: ze zijn mede de veroorzakers van zure regen en smog. Stikstofdioxide, NO_2, wordt gebruikt als indicator voor de grotere groep NO_x en is de meest schadelijke component. Inademen van NO_2 is schadelijk voor de luchtwegen, niet alleen voor mensen, maar ook voor dieren. Daarom is het enorm belangrijk om de NO_2 concentratie goed te kunnen meten. In dit proefschrift wordt bestudeerd hoe

NO_2 detectie met veld-effect transistoren werkt. De uitkomsten van dit fundamentele onderzoek worden gebruikt om een gevoelige, realtime NO_2 sensor te ontwikkelen.

Het analyseren van de samenstelling van uitgeademde lucht geeft informatie over de gezondheid van de betreffende persoon. Het meten van een verhoogde concentratie stikstofmonoxide, NO, in uitgeademde lucht kan duiden op een luchtweginfectie zoals astma. In Hoofdstuk 3 wordt een NO sensor gepresenteerd die gemaakt is van een zelfgeassembleerde monolaag veld-effect transistor (SAMFET). Een SAMFET sensor is extreem gevoelig omdat het gas en het geleidende kanaal slechts één monolaag van elkaar verwijderd zijn. Om NO detectie mogelijk te maken is de sensor gefunctionaliseerd met een extra laag porfyrinereceptoren. Bij blootstelling aan NO schuift de drempelspanning naar positieve waarden. Deze drempelspanningsverschuiving wordt veroorzaakt door vastgezette lading. Het kunnen detecteren van extreem lage concentraties NO laat zien dat de gevoeligheid van de sensor inderdaad hoog is.

Een drempelspanningsverschuiving wordt ook gemeten in organische veld-effect transistoren met een zelfgeassembleerde monolaag (SAM) op het gatediëlektricum. De richting van de verschuiving wordt bepaald door de chemische compositie van de SAM. In Hoofdstuk 4 wordt met scanning Kelvin probe microscopy (SKPM) en een techniek om de halfgeleider van het diëelektricum af te halen de oorzaak van de drempelspanningsverschuiving onderzocht. De gemeten oppervlaktepotentiaal van het blootgestelde SAM-gemodificeerde diëlektricum is precies gelijk aan de drempelspanning bepaald voor het afpellen. Dit toont aan dat de drempelspanningsverschuiving wordt veroorzaakt door vastzittende lading in de SAM.

In Hoofdstuk 5 wordt NO_2 detectie met zinkoxide veld-effect transistoren bestudeerd. Wanneer de transistor wordt blootgesteld aan NO_2 en een positieve gatespanning wordt aangelegd, dan schuift de drempelspanning naar die aangelegde gatespanning. De dynamica van de verschuiving wordt op kamertemperatuur geanalyseerd als een functie van de NO_2 concentratie en de zinkoxide laagdikte. De tijdsafhankelijkheid kan worden beschreven met een gestrekte exponentiële formule. Een mechanisme voor NO_2 detectie wordt voorgesteld waarin NO_2 zorgt voor het immobiliseren van de elektronen. Dit mechanisme geldt niet alleen bij gebruik van zinkoxide maar ook bij gebruik van andere halfgeleiders.

Een vereiste voor een realtime sensor is reversibiliteit. Bij blootstelling aan NO_2 verschuift de drempelspanning als gevolg van het vastzetten van de mobiele elektronen die worden geïnduceerd door de gatespanning. Als de gatespanning wordt uitgezet kunnen de vastzittende elektronen door voldoende thermische energie weer ontsnappen. In Hoofdstuk 6 wordt de dynamica van het vastzetten en weer losmaken van lading bestudeerd als een functie van de temperatuur. De complete dynamica kan worden beschreven met een gestrekte exponentiële tijdsafhankelijkheid met drie parameters voor het invangen

van de elektronen en drie parameters voor het ontsnappen van de elektronen, te weten: een activeringsenergie, een karakteristieke frequentie en een karakteristieke temperatuur. De gevonden activeringsenergie voor het ontsnappen van een elektron is 1.2 eV, wat duidt op een energetisch diepe val. Met een andere techniek, thermisch gestimuleerde stroommetingen, wordt bevestigd dat de elektronen vastzitten op een energie niveau met een diepte van deze waarde.

De locatie van de vastzittende elektronen die zijn gecreëerd bij de NO_2 experimenten wordt onderzocht in Hoofdstuk 7 met organische veld-effect transistoren. Drie verschillende organische halfgeleiders worden gebruikt. Oppervlaktepotentiaalmetingen voor en na het verwijderen van de halfgeleider laten zien dat de ladingen niet in de halfgeleider zitten maar op het gate diëlektricum. Deze informatie geeft mogelijkheden om de gevoeligheid van de NO_2 veld-effect transistor sensoren te optimaliseren.

In Hoofdstuk 8 worden de verkregen fundamentele inzichten in het detectiemechanisme vertaald naar een analytisch model dat gebruikt wordt om de dynamische respons van de sensor te berekenen. Slechts drie experimenteel bepaalde parameters zijn nodig, er worden geen extra fit parameters gebruikt. Het model vormt de basis voor een sensorprotocol, waarmee de veld-effect transistor sensor de NO_2 concentratie in real time kan meten. Om de sensor reversibel te maken wordt op hoge temperatuur de gatespanning telkens aan en uit gezet. De voor een bepaalde concentratie berekende sensorrespons komt overeen met de gemeten respons bij die concentratie. Het model kan daarnaast gebruikt worden om de sensor verder te optimaliseren. Zo kan bijvoorbeeld berekend worden welke gevolgen een aanpassing van de temperatuur of de tijdsduur van de gatespanningspuls heeft op de gevoeligheid of de responstijd.

Tenslotte wordt in Hoofdstuk 9 een gevoelige, functionele, realtime NO_2 sensor prototype gepresenteerd. Met de zinkoxide veld-effect transistor kan de NO_2 concentratie worden gemeten in gedroogde lucht voor concentraties zo laag als 10 ppb. De respons van de zinkoxide veld-effect transistor is gecontroleerd met een gekalibreerde en commercieel verkrijgbare referentiesensor. De transistor sensor meet dezelfde concentraties met een vergelijkbare gevoeligheid. Bovendien kan de in dit proefschrift ontwikkelde sensor worden gefabriceerd met standaard IC technologie en daardoor gemakkelijk worden geïndustrialiseerd.

Publications

The work presented in Chapters 3-9 is based on the following publications:

1. *Gas sensing with self-assembled monolayer field-effect transistors*,
   A. Andringa, M. Spijkman, E. C. P. Smits, S. G. J. Mathijssen, P. A. van Hal, S. Setayesh, N. P. Willard, O. V. Borschev, S. A. Ponomarenko, P. W. M. Blom, D. M. de Leeuw, *Organic Electronics*, **2010**, *11*, 895.

2. *Gate-bias controlled charge trapping as a mechanism for NO_2 detection with field-effect transistors*,
   A. Andringa, J. R. Meijboom, E. C. P. Smits, S. G. J. Mathijssen, P. W. M. Blom, D. M. de Leeuw, *Advanced Functional Materials*, **2011**, *21*, 100.

3. *Charge trapping by self-assembled monolayers as the origin of the threshold voltage shift in organic field-effect transistors*,
   F. Gholamrezaie, A. Andringa, W. S. C. Roelofs, A. Neuhold, M. Kemerink, P. W. M. Blom, D. M. de Leeuw, *Small*, **2012**, *8*, 241.

4. *Dynamics of charge carrier trapping in NO_2 sensors based on ZnO field-effect transistors*,
   A. Andringa, N. Vlietstra, E. C. P. Smits, M. Spijkman, H. L. Gomes, J. H. Klootwijk, P. W. M. Blom, D. M. de Leeuw, *Sensors and Actuators B: Chemical*, **2012**, *171-172*, 1172.

5. *Localizing trapped charge carriers in NO_2 sensors based on organic field-effect transistors*,
   A. Andringa, W. S. C. Roelofs, M. Sommer, M. Thelakkat, M. Kemerink, D. M. de Leeuw, *Applied Physics Letters*, **2012**, *101*, 153302.

6. *Real-time NO_2 detection at ppb level with ZnO field-effect transistors*,
   A. Andringa, E. C. P. Smits, J. H. Klootwijk, D. M. de Leeuw, *submitted to Sensors and Actuators B: Chemical*.

Other publications:

7. *Ordered arrays of ferroelectric nanoparticles by pulsed laser deposition on PS-b-P4VP-(PDP) supramolecule-based templates*,
   W. van Zoelen, A. H. G. Vlooswijk, A. Ferri, A. Andringa, B. Noheda, G. ten Brinke, *Chemistry of Materials*, **2009**, *21*, 4719.

8. *Revealing buried interfaces to understand the origins of threshold voltage shifts in organic field-effect transistors*,
   S. G. J. Mathijssen, M. Spijkman, A. Andringa, P. A. van Hal, I. McCulloch, M. Kemerink, R. A. J. Janssen, D. M. de Leeuw, *Advanced Materials*, **2010**, *22*, 5105.

Dankwoord / Acknowledgements

Vier jaar transistors contacteren, mass flow controllers instellen, slepen met Bahco's... En dan weer metingen uitwerken, artikelen schrijven, presentaties voorbereiden... Als ik dit in mijn eentje had gedaan, dan waren alle vooroordelen over saaie promotieonderzoeken waar geweest. Maar gelukkig heb ik een heleboel leuke mensen leren kennen, die het een leerzame, boeiende en aangename tijd hebben gemaakt. Ik maak graag van deze gelegenheid gebruik om iedereen te bedanken.

Voor mijn eerste promotor, Dago de Leeuw, heb ik maar één woord: uniek. Uniek dat je in het lab komt om met ons metingen doen. Uniek dat je altijd een artikel tevoorschijn tovert waarin het antwoord op onze lastigste vragen al staat. Uniek dat je al rokend en koffiedrinkend de tijd neemt om samen een artikel te schrijven. Uniek dat je bij Philips Research (en ver daarbuiten) zo'n staat van dienst hebt opgebouwd, dat ons cluster een zelfde vrijheid had als op de universiteit. Uniek dat je twee jaar lang elke vrijdag naar Groningen bent gereden om daar de aio's te begeleiden. Uniek dat ik nu een glas wijn zit te drinken door jouw tip over hoe ik het beste een dankwoord kan schrijven. Ik heb ontzettend veel waardering voor jou en heel veel van je geleerd. Bedankt voor het vertrouwen dat je mij hebt gegeven.

Mijn tweede promotor, Bert de Boer, heeft mij aangestoken in zijn enthousiasme voor de organische elektronica. Hij heeft mij voor mijn stage in contact gebracht met Dago en later mijn promotiecontract binnen de groep Physics of Organic Semiconductors geregeld. Zijn plotselinge overlijden was een groot verlies voor onze groep. Ik weet zeker dat iedereen die met hem gewerkt heeft een sprankje van zijn enthousiasme en sociale betrokkenheid met zich meedraagt. Daarnaast wil ik onze groepsleider, Paul Blom, bedanken voor de mogelijkheid om in zijn groep te promoveren. Hoewel je geen directe

begeleider was, stond je altijd op de achtergrond klaar om te helpen. Ongelofelijk hoe je vriendelijk doch overtuigend de editor van mijn artikel duidelijk had gemaakt dat mijn artikel er eentje was die niet afgewezen kon worden.

I would like to thank prof. Henrique Gomes, prof. Erik Bakkers and prof. Paul Blom for their willingness to be a member of my reading committee and for judging the scientific quality of my thesis. Henrique, I enjoyed our cooperation, when we struggled with the interpretation of the TSC measurements at the university in Faro or at the beach. Thanks for your hospitality and for showing me around in the Algarve. Erik, bedankt voor het beschikbaar stellen van de flow-opstelling. It is also an honor that Johan Klootwijk, Nicolae Barsan and Martijn Kemerink are willing to take place in my thesis defense committee. Johan, bedankt voor de ondersteuning bij het maken van de demo. Na het bespreken van de uitdagingen kon ik altijd vol goede moed weer verder. Nicolae, thanks for the nice discussions and a glance in the lab with your gas detection setups in Tübingen. I will never forget the Diplomatenkiller... Martijn, bedankt voor de gastvrijheid in het SKPM lab op de TU/e, zelfs toen ik met gascilinders kwam. Deze samenwerking heeft hele mooie resultaten opgeleverd.

Mijn onderzoek heb ik uitgevoerd in het cluster organische elektronica bij Philips Research. De levendige discussies, het met zijn allen komen kijken als iemand een interessante meting doet, het vieren van een goed resultaat of een publicatie in het Grand Café: het maakte dat ik met plezier naar de High Tech Campus kwam. Ik wil graag iedereen in het cluster bedanken voor de stimulerende werksfeer en goede samenwerking. Ook de gezelligheid tijdens de Bommel-etentjes, de pubquiz-avonden en de volleybaltoernooitjes zal ik nooit vergeten. Een speciaal woord van dank gaat naar Mark-Jan; ik kon altijd bij je langslopen en je was altijd bereid om te helpen. Ook bedankt voor de tientallen keren dat ik met je mee kon rijden van en naar het noorden. Edsger, bedankt voor al je ideeën en de succesvolle samenwerking. Het steeds maar uitbreiden van jouw Labview-programma heeft ervoor gezorgd dat we een sensorprototype konden maken, waarmee we samen op de open dag van Philips hebben gestaan. Fatemeh, in our office we always talked about everything. Thank you for sharing so much with me. You made Paul B. dance with you at your PhD-party, so you can achieve anything! Paul van Hal, ik vond het echt gaaf dat je kaartjes geregeld had voor een voetbalwedstrijd van FC Barcelona tijdens een ONE-P meeting. Jouw levendigheid en enthousiasme werken enorm motiverend. Simon en Christian, bedankt voor de vele discussies en jullie inzet bij de SKPM-experimenten. I also would like to thank Mengyuan, Kamal, Patrick, Frank and Sepas in our cluster.

In het gassensoronderzoek mochten we twee studenten welkom heten: Juliaan en Nynke. Jullie hebben allebei bergen werk verzet. Juliaan, het automatiseren van de

gegevensverwerking heeft, naast het voorkomen van RSI, mij geïntroduceerd in de voordelen van programmeren. Daar heb ik nu al veel profijt van gehad, bedankt. Nynke, voor jouw komst naar Philips kreeg ik je CV te lezen. De gelijkenissen tussen ons waren groot: een vrouw in de wetenschap, Fries, ondernemend, sportief en trompet spelend. Er was meteen een goede klik en je kon gelijk mee naar mijn fanfareorkest. Tijdens je stage mocht ik van je geen Fries met je praten, maar nu grijp ik mijn kans: Tige tank foar de geweldige gearwurking en in soad súkses mei dyn eigen promoasje.

Buiten het cluster wil ik ook iedereen uit de groep Photonic Materials and Devices bij Philips Research bedanken voor de goede sfeer op het werk. In het bijzonder zijn dat Rein en Harm als mede-aio's en Anja Welvaarts en Pauline Deuning als geweldige secretaresses. De groepsleiders Eric Meulenkamp en later Hans van Sprang wil ik bedanken voor de mogelijkheid om te promoveren in deze omgeving. I also appreciated the pleasant company in the lab of the Holst Centre guys, especially Xiaoran, Gari and Juan Diego.

De ondersteuning van de mensen van Philips Innovation Services was onmisbaar in mijn onderzoek. Zo heeft Tom Geuns de transistor-testsubstraten geprocessed en Henk Verberne heeft de meest geavanceerde meetopstellingen ontworpen en in elkaar gezet (de foto's zijn te bewonderen in Hoofdstuk 2). John Giller, Ton Swinkels en Paul Verschueren wil ik bedanken voor het installeren van de gascilinders en leidingen. Bij analyse dank ik Paul Krusemann voor de hulp bij de demo-opstelling, Harry Wondergem voor de XRD en Cees van der Marel voor XPS. Ook wil ik een aantal mensen van Philips Research bedanken voor hun bijdrage: Hans van Kesteren voor het beschikbaar stellen van de Eco Physics referentiesensor, Nico Willard voor het delen van zijn kennis over porfyrinen en astma en collega-gassensoronderzoekers Ben Giesbers en Marco de Wild voor het delen van hun ervaring.

The majority of organic semiconductors used in this thesis were provided by our collaborators. The alternative, buying 'low cost' semiconductors at a certain chemical company, was not an option after a shocking email: In the quote for 25 grams of PTAA the salesman made a 'genuine' mistake; the price was not 5,000 but 50,000 euros. Therefore I would like to thank Iain McCulloch and Steven Tierney for providing the PTAA within the European projects. I also would like to thank Sergei Ponomarenko and Oleg Borschev for the synthesis of the SAMFET molecule and Michael Sommer and Mukundan Thelakkat for providing the *n*-type polymer PPerAcr. Finally, I want to thank Alfred Neuhold in the group of Roland Resel for analyzing the X-ray reflection data.

Once every six months, we travelled with a delegation of Philips and the RuG to ONE-P project meetings all over Europe. The smileys of Yves Geerts and the company of the other PhD-students and postdocs made the meetings always a big success. I especially want to mention the nice weekend trips to Barcelona and Bologna with Renee

Kroon and his Swedish colleagues.

Ook wil ik de collega's van de MEPOS-groep bedanken voor de bijzondere sfeer en gezelligheid. De werkgerelateerde bezoeken aan Groningen draaiden geregeld uit op feestjes. Dankzij jullie heb ik erg genoten van de groepsuitjes, Vlieland meetings, werkweken en promoties. Na de geslaagde feestjes stond er een bed klaar bij Auke en Christa, al dan niet met ontbijt, en later bij Johan en Bernadette. Heel erg bedankt daarvoor. Een bijzondere ervaring voor mij was tijdens de werkweek op de camping in Baarle-Nassau, waar Johan gitaar speelde en ik zong. Hylke zijn opmerking, dat als ik dit durfde, dat ik dan alles durfde, heeft misschien wel geleid tot een poster- en presentatieprijs. Many thanks as well to all the other members of the MEPOS-group: Alex, Arne, Claudia, Date, Davide, Davood, Dorota, Eek, Francesco, Frans, Femke, voor de culinaire afspraakjes in Eindhoven, Gert-Jan, Herman, Ilias, Irina, Jan, Jan Anton, Jan Derk, Jolt, Jia, Jurjen, Kriszty, Marianna, Martijn Kuik, Martijn Lenes, Milo, Niels, Paul de Bruyn, Reeuwerd and Yuan. En een speciaal bedankje voor Renate voor de supergoede administratieve ondersteuning.

Naast collega's zorgden vrienden voor de nodige ontspanning. Het is lastig om iedereen op te noemen, ik hoop dat jullie wel weten dat jullie gezelschap heel waardevol voor mij is. Harmke en Judith met gezin, jullie zijn twee geweldige vriendinnen. Auke, als mijn KISS papa maakte je meteen duidelijk dat wetenschappers ook cool kunnen zijn. En Christa, bij het introkamp bespraken we al ons liefdesleven en daar zijn we nooit meer mee gestopt. Nu tien jaar later ben ik heel blij dat je mijn paranimf wilt zijn. Verder wil ik mijn oud-CBestuursgenootjes en andere mensen van scheikunde in Groningen en van de TU/e bedanken voor de vriendschappen. Ook heb ik erg genoten van de sportieve, sociale en culinaire activiteiten met D5/D6 bij studentenvolleybalvereniging Hajraa en de muzikale uitdagingen bij muziekvereniging Wilhelmina Eindhoven.

As lêste wol ik myn famylje tank sizze foar de stipe en belangstelling. Maaike, do snapst alles fan my. It is dan ek in ear datst myn paranimf wêze wolst. Pablo, bedankt voor je oprechtheid en het schitterende ontwerp van de cover. Gerryt, as grutte broer bin ik altyd grutsk op dy west. Ik hoopje datst dat ek in bytsje op my bist. Heit en mem, ik wit dat jimme der altyd foar my binne. Tank foar jim leafde, stipe en fertrouwen.

Anne-Marije